METEOR-Berichte

Gulf of Corinth Groundwater - Is the deep offshore freshened groundwater body within the Gulf of Corinth actively recharging?

Cruise No. M196

5.12.2023 – 27.12.2023,
Piraeus (Greece) – Limassol (Cyprus)
GoCW

Dr. Marion Jegen, Dr. Amir Haroon, Dr. Katrin Schwalenberg, Dr. Thomas Müller, Dr. Mark Schmidt, Bruna Pandolpho, Dr. Monica Bucci, Dr. Senay Horozal and Dr. Dimitris Sakkelariou

Chief Scientist: Dr. Marion Jegen
GEOMAR Helmholtz Centre of Ocean Reseach Kiel

2024

Table of Contents

1 Cruise Summary

1.1 Summary in English

The quality of groundwater is deteriorating globally, leading to an increase in pressure on water resources, particularly in coastal regions. In the quest for mitigating water scarcity under changing climatic conditions, alternative water sources such as offshore freshened groundwater (OFG) have come into scientific focus. Estimates suggest that globally the freshwater volume within OFGs amounts to half a million cubic kilometres. This volume corresponds to more than one century's worth of freshened water assuming present-day consumption rates.

Despite the global significance of OFGs, our understanding of their spatial dimensions, volumes, and geological controls beneath the seafloor remains limited. Discoveries have largely been serendipitous, occurring during borehole drilling. Few studies have effectively integrated point-scale ground-truthing data from boreholes with regional measurements to accurately delineate the extent of OFGs. Furthermore, questions persist regarding the connectivity of OFGs to terrestrial aquifers.

On this cruise, we investigated a newly-discovered OFG site within the Gulf of Corinth, Greece. We acquired electromagnetic and geochemical data to derive the spatial extent of the Gulf of Corinth OFG to understand if this low-salinity anomaly is due to present-day recharge through an onshore aquifer system or, alternatively, a remnant of past sea-level low stands.

1.2 Zusammenfassung

Die Qualität des Grundwassers verschlechtert sich weltweit, was zu einer zunehmenden Einschränkung der Wasserressourcen führt, insbesondere in den Küstenregionen. In dem Bestreben, die Wasserknappheit unter den sich ändernden klimatischen Bedingungen abzumildern, sind alternative Wasserquellen wie das Offshore-Grundwasser (OFG) in den wissenschaftlichen Fokus gerückt. Schätzungen gehen davon aus, dass sich das Süßwasservolumen in OFGs weltweit auf eine halbe Million Kubikkilometer beläuft. Dieses Volumen entspricht dem Frischwasserverbrauch der globalen Bevölkerung von mehr als einem Jahrhundert, wenn man vom heutigen Verbrauchstand ausgeht.

Trotz der globalen Bedeutung der OFGs ist unser Verständnis ihrer räumlichen Ausdehnung, ihres Volumens und ihrer geologischen Kontrolle unter dem Meeresboden nach wie vor begrenzt. Entdeckungen waren größtenteils Zufallsfunde gemacht wurden, die bei Bohrungen gemacht wurden. Nur wenige Studien haben punktuelle Bodenuntersuchungsdaten aus Bohrlöchern mit regionalen Messungen kombiniert, um das Ausmaß der OFGs genau abzugrenzen. Darüber hinaus bestehen weiterhin Fragen hinsichtlich der Verbindung von OFGs zu terrestrischen Aquiferen.

Auf dieser Fahrt untersuchten wir einen neu entdeckten OFG-Standort im Golf von Korinth, Griechenland. Wir sammelten elektromagnetische und geochemische Daten, um die räumliche Ausdehnung des OFG im Golf von Korinth zu bestimmen und herauszufinden, ob der OFG ein Überbleibsel früherer Meeresspiegeltiefstände ist oder auf die Anreicherung durch ein küstennahes Aquifersystems zurückzuführen ist.

2 Participants

2.1 Principal Investigators

Name	Institution
Dr. Amir Haroon	GEOMAR/now University of Hawaii
Dr. Thomas Müller	GEOMAR
Dr. Dimitris Sakellariou	Hellenic Center for Marine Research

2.2 Scientific Party

Name	Discipline	Institution
Dr. Marion Jegen-Kulcsar	Fahrtleiter / *Chief Scientist*	GEOMAR
Dr. Amir Haroon	PI Electromagnetics	U of H
Dr. Thomas Müller	PI Geochemistry	GEOMAR
Dr. Dimitris Sakellariou	PI Geology	HCMR
Bruna Panolpho	PhD Student / PI Hydro-Acoustics	GEOMAR
Dr. Monica Bucci	Co-PI Hydro-Acoustics	U of M
Dr. Dionisis Patiris	Physicist	HCMR
Dr. Mark Schmidt	Geochemistry	GEOMAR
Dr. Dimitrios Christodoulou	Geologist	U of P
Dr. Ariel Thomas	Electromagnetics	U of M
Dr. Senay Horozal	Acoustics / Electromagnetics	U of M
Dr. Anna Pastoressa	Electromagnetics	U of M
Dr. Katrin Schwalenberg	Electromagnetics	BGR
Merrit Kahler	Electromagnetics	GEOMAR
Julia Schätzel	Acoustics / Electromagnetics/	GEOMAR
Lea Eggensberger	Student	GEOMAR
Paula Lürßen	Student	GEOMAR
Paul Moser Röggla	PhD Student / Geochemistry	ETH
Spyridoula Roumelioti	PhD Student / Geochemistry	HCMR
Bettina Domeyer	Technician / Geochemistry	GEOMAR
Regina Surberg	Technician / Geochemistry	GEOMAR
Martin Wollatz-Vogt	Technician / Electromagnetics	GEOMAR
Sergiy Cherednichenko	Technician / Geochemistry	GEOMAR
Jan Fleer	Technician / Electromagnetics	GEOMAR
Jannis Usinger	Technician / Geochemistry	GEOMAR
Hannes Schuler	Film Maker	

2.3 Participating Institutions

GEOMAR: GEOMAR Helmholtz Centre for Ocean Research Kiel

U of H: University of Hawaii

HCMR: Hellenic Centre for Marine Research

U of M: University of Malta
BGR: Federal German Institute for Geosciences and Natural Resources
ETH: Swiss Federal Institute of Technology Zurich
U of P: University of Patras

3 Research Program

3.1 Description of the Work Area

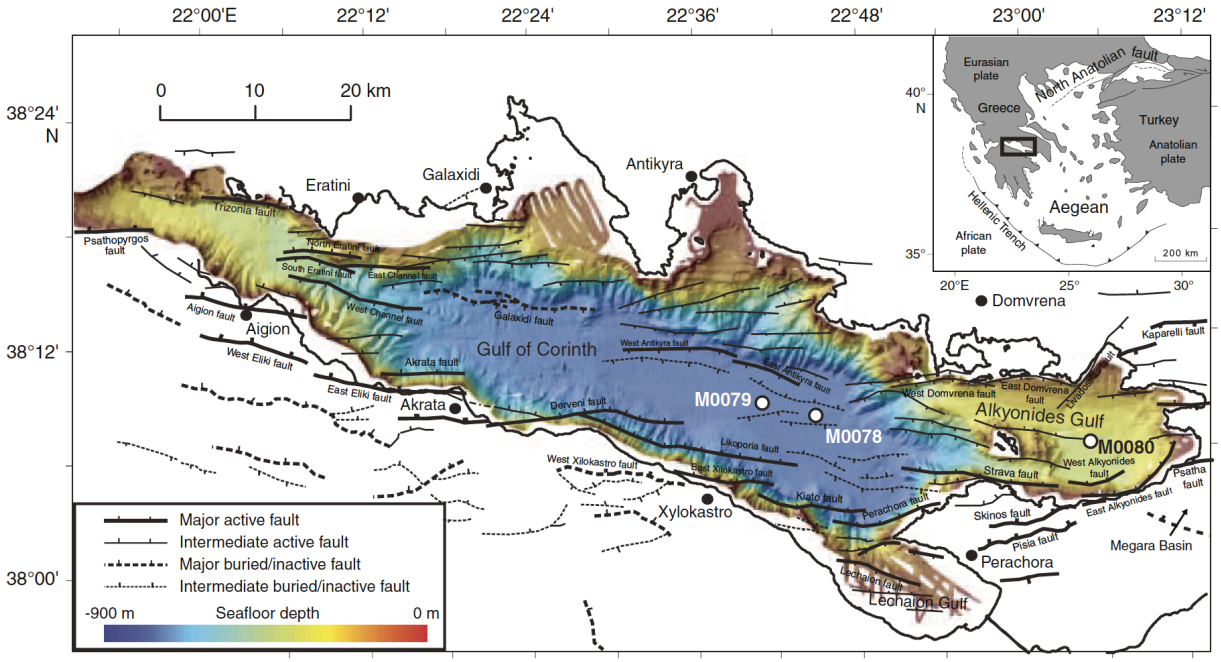

Fig. 3.1.1 Corinth rift with primary rift-related faults (both active and currently inactive), multibeam bathymetry of the gulf, and Expedition 381 drill sites. Offshore fault traces are derived from Nixon et al. (2016), building on Bell et al. (2009) and Taylor et al. (2011). Onshore fault traces are derived from Ford et al. (2008, 2013) and Skourtsos and Kranis (2009). Bathymetry data was provided by the Hellenic Centre for Marine Research and collected for RV Aegaeo cruises (Sakellariou et al., 2007). Inset: tectonic setting of Corinth rift in the Aegean region, Eastern Mediterranean Sea. M0078, M0079 and M0080 mark the positions of the boreholes during IODP expedition 381 (MacNeil et al., 2019).

The Gulf of Corinth is a young, small-scale, sedimented ocean basin produced by continental rifting which is still in its early stage (Figure 3.1.1). On its western side, it is connected to the Ionian Sea by the narrow, 60-62 m deep Rion Strait and is bounded on the eastern side by the Isthmus of Corinth. North-South extension and rifting started here at around 5 My ago and current extension rates with values of 10-15 mm/year are some of the highest in the world (e.g. Clarke et al., 1998 and Bernard et al., 2006). Due to its unique setting, the eastern part of the Gulf of Corinth was drilled during the IODP 381 expedition to resolve at high temporal and spatial resolution how rift faults initiate and link and how strain is distributed over time (MacNeil et al., 2019).

The rifting process is divided into three phases. In the initial Pliocene phase, sedimentary deposits are mainly of continental origin, consisting of preferred alluvial sediments in the west to lacustrine sediments in the east (e.g. Ford et al., 2013). The second phase is marked by a transition to increased subsidence rate and sediment supply (Figure 3.1.2). The time of transition to phase 2 occurred at different times along the Gulf, at around 2.2 Ma in the eastern, around 3 Ma in the central and around 1.8 Ma in the western region (Leeder et al., 2012, Ford et al., 2013). During this phase, sediment deposition is associated with large marginal fan deltas (named unit 1 in the lithostratigraphic nomenclature of the IODP drilling). At approximately 0.6 Ma year, the Gulf of

Corinth system transitioned into phase three, characterized by alternate phases of marine and none-marine (isolated/semi-isolated) stages associated with interglacial and glacial eustatic sea level changes (Figure 3.1.2). Sediment packages deposited in this phase are named unit 2 in the litho-stratigraphic nomenclature of the IODP drilling. The alternating lacustrine (fresh to brackish water) and marine (saline water) cycles (Figure 3.1.3) likely intersected by catastrophic flooding events, which is well documented within the sediment stratigraphy (Perissoratis et al. 2000; Moretti et al. 2004; McNeil et al. 2019). From piston core analysis and geophysical data, it has been documented that the Gulf of Corinth was essentially a fresh to brackish water lake, disconnected from the marine environment during periods of low sea-level stands (Heezen et al. 1966; Perissoratis et al. 2000). As a result, the low salinity anomaly documented within the IODP boreholes is likely also a remnant of previous lake-type fresh to brackish water conditions. However, the salinity anomalies documented by McNeil et al. (2019) are not confined to only the lacustrine sediments but extend across both lacustrine and marine horizons, which raises the question of how the deep systems can host and maintain freshened pore fluid of such low salinities (3 – 10 PSU) within a present-day saltwater environment?

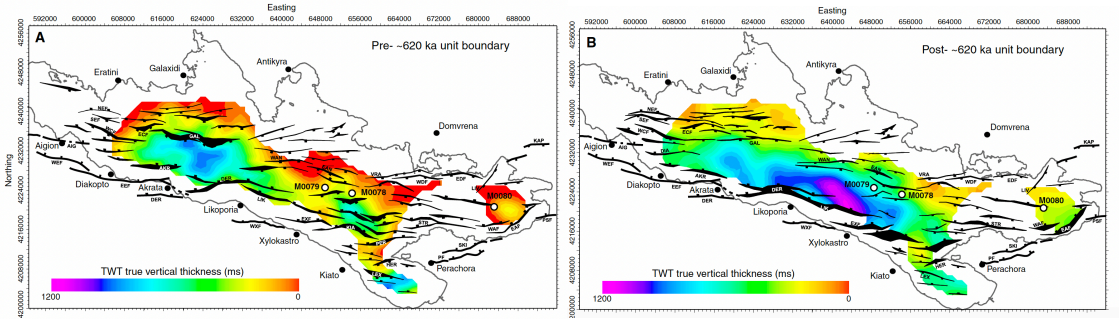

Fig. 3.1.2 Isochore maps for the two primary stratigraphic units of the offshore syn-rift succession with Expedition 381 sites. These two units are separated by a regional unit boundary or unconformity (compiled by Bell et al., 2009; Taylor et al., 2011; Nixon et al., 2016). A. Seismic Unit 1 (pre-regional unit boundary or unconformity, likely equivalent to onshore Middle Group, with an estimated age older than ~0.62 Ma). B. Seismic Unit 2 (post-regional unit boundary or unconformity, likely equivalent to onshore Upper Group, with an estimated age younger than ~0.62 Ma). Represented faults are mainly those active during the time period shown. Age estimates are predrilling and based on seismic stratigraphic interpretations only. NEF = North Eratini fault, SEF = South Eratini fault, WCF = West Channel fault, ECF = East Channel fault,
AIG = Aigion fault, GAL = Galaxidi fault, WEF = West Eliki fault, EEF = East Eliki fault, AKR = Akrata fault, DER = Derveni fault, WAN = West Antikyra fault, LIK = Likoporia fault, WXF = West Xylokastro fault, EXF = East Xylokastro fault, EAN = East Antikyra fault, KIA = Kiato fault, VRA = Vroma fault, PER = Perachora fault, LEX = Lechaion fault, HER = Heraion fault, WDF = West Domvrena fault, STR = Strava fault, PF = Pisia fault, EDF = East Domvrena fault, SKI = Skinos fault, LIV = Livadostras fault, WAF = West Alkyonides fault, EAF = East Alkyonides fault, KAP = Kaparelli fault, PSF = Psatha fault. TWT = two-way traveltime. From MacNeil et al., 2019.

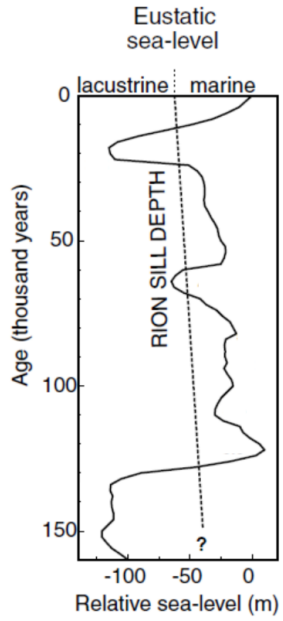

Fig. 3.1.3 Eustatic sea-level curve for the GoC. Modified after Perissoratis et al. (2000).

3.2 Aims of the Cruise

The scientific programme has been designed to achieve the following objectives:

O1: Characterize the spatial extent of OFG in the Gulf of Corinth using geophysical tools and integrate these with in-situ data from IODP boreholes.

Electrical resistivity mapping is key in OFG research since it is the only physical rock parameter, which changes with pore water salinity in sediments. In conjunction with already existing seismic data constraining porosity variations of the sediments, resistivity sections can be transformed into pore water salinity estimates.

The objective O1 is therefore addressed through high-resolution, controlled source electromagnetic (CSEM) and deeply penetrating, low-resolution passive magnetotelluric (MT) measurements, which will result in electrical resistivity sections along various transects within the Gulf of Corinth. The obtained resistivity models will be calibrated against physical property measurements at the IODP borehole 381, which is crossed by the CSEM transects. To collect 2D CSEM data, we use a seafloor-towed electric dipole-dipole system consisting of a 100-m long horizontal dipole transmitter antenna and multiple receiver dipoles towed at increasing offsets from 150 m to ~1000 m from the transmitter. MT data are acquired at 6 seafloor stations distributed along a central transect along the Gulf of Corinth.

O2: Characterize the seafloor groundwater discharge locations using CSEM data and geochemical data. Determine the origin of the water and deduce how / whether SGD is linked to the onshore aquifers.

Sub-bottom profiler and water column imaging data are used to define areas of interest in terms of water/gas seepage at the seafloor, which is further investigated using Video-CTD. The Video-CTD, equipped with temperature, conductivity-, pressure sensors, and additional in situ sensors (i.e., pH, CH4, CO2, O2, turbidity) is towed at 1-2 m above the seafloor to investigate the water column and the ambient bottom water. Niskin water samplers are triggered frequently when sensor

data indicate freshwater seepage. We also planned to use an in-situ gamma-ray spectrometer of the Hellenic Centre for Marine Research (HCMR) installed on the Video-CTD towed system for radon emanation mapping indicating groundwater seeps along the transects. Unfortunately, the system broke on a previous cruise and could not be repaired in time for M196 such that we had to omit these measurements.

Porewater, sediment, and headspace gas of the retrieved sediment cores are sampled directly onboard at a resolution of 25 cm. Porewater composition is analysed partly onboard and subsequently on land to determine diffusive/advective fluxes within the sediment (0-15 m).

O3: Characterize seeping groundwater and porewater to correlate with geophysical data and to indicate different origins of water and secondary water/sediment interaction.

Newly detected and known shallow SGDs in the basin are sampled as a reference to link shallow SGD with pore waters in the deep part of the basin. Gravity coring provides pore water data which will be used in transport-reaction modelling to investigate temporal pore water fluid flow. The measurement of major and minor constituents, elements and isotopes of the water/porewater samples allows us to determine the origin of water and constrain diagenetic processes.

3.3 Agenda of the Cruise

We departed the port of Piraeus as planned on Dec 5th. To ensure a sufficient length of magnetotelluric time series, the OBEMs were deployed first and recovered last. Geochemical data acquisition consisted of gravity coring and Video-CTDs. During the first part of the cruise, the geochemical data acquisition focused on gravity coring. Altogether twelve cores with core lengths between 200 and 850 cm were acquired. Half of the core sites were in the vicinity of IODP boreholes M1078 and M1079 in the eastern part of the basin, three cores along the central basin and another 3 cores within bays along the northern coast of the Gulf of Corinth. Video-CTD stations in the form of 5 hydro casts along the entire central basin were collected within the second week of the cruise. Within the last week, 3 Video-CTDs profiles at a 1.5 m distance to the seafloor were collected in the vicinity of the Egion Fault in the southwestern region of the Gulf of Corinth, where our acquired bathymetric data indicated pockmarks. Homogeneous temperature and salinity values were recorded along most of the tracks. However, salinity drops indicative of freshened pore water seep sites were noticed and sampled at two specific sites, a reef structure and a pockmark around the Egion Fault.

Altogether three CSEM profiles, one 40 km long profile through the entire center of the Gulf of Corinth basin, a second 30 km long SE to NW profile and a third 20 km long high-resolution profile in the eastern section of the basin were acquired. All profiles crossed the IODP boreholes. Before the acquisition of the third profile, 2 of the OBEMs in the western section of the Golf were redeployed in the eastern section to record additional CSEM signals. Unfortunately, on the second profile, the array encountered an obstacle (probably carbonate block) on the seafloor at the beginning of the profile, which tore off the last receiver of the array. Due to the temporary increase in tension along the entire array, the other receiver failed as well, such that no receiver data was acquired on profile 2.

In between geochemical and electromagnetic data acquisitions, we acquired both EM122 and EM710 bathymetric, backscatter and water column data concurrent with parasound data. The hydroacoustic data were recorded for pre-investigation of the core sites and Video-CTDs, along the CSEM profiles and also mapped the eastern and western ends of the Gulf of Corinth for which no high-resolution data yet existed. An overview of all M196 stations is shown in Figure 3.3.1.

We fully complied with the research permission granted by the Greek government. No acoustic data acquisition was performed that are deemed to be harmful to mammals. All OBMT stations were recovered such that no moorings were left on the seafloor.

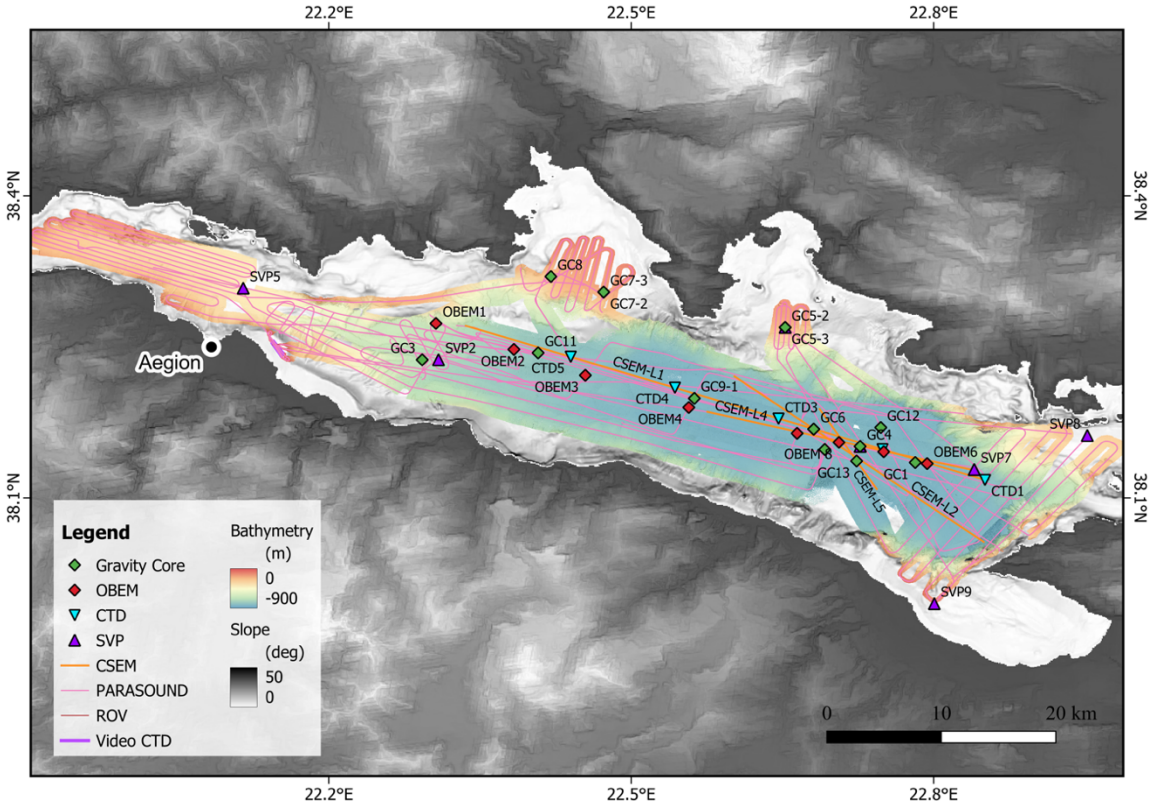

Fig. 3.3.1 Overview of M196 stations. Bathymetric data acquired on M196 is shown as a colour map, cruise track as orange lines.

4 Narrative of the Cruise

December 5th,2023:

The snow chaos in Germany made for an exciting and long journey for the participants from Germany due to flight cancellations and re-bookings. By 20:00 UTC in the evening, however, the last scientist was on board with her luggage so that we were able to set sail as planned and in good weather on the morning of December 5. Most participants watched excitedly from various decks as RV METEOR left the pier and headed out into the Aegean Sea. Before lunchtime, most participants had settled down in the different laboratories, unpacking boxes, setting up equipment and internet connections and arranging lashing systems for the equipment. Much of the afternoon was used up for an introductory presentation on life, etiquette and safety at sea followed by the fire drill. To streamline onboard scientific operations, we appointed three group leaders: Dr Amir

Haroon for the electromagnetic experiments, Dr Thomas Müller for the geochemical experiments and Bruna Pandolpho / Dr Monika Bucci for hydro acoustics.

December 6th,2023:
Most of the day was dedicated to programming, testing and preparing our ocean-bottom electromagnetic stations (OBEMs) for deployment. In preparation for the controlled source electromagnetic (CSEM) seafloor towed experiment, the Toronto winch (used to deploy the CSEM streamer) and Werner winch with fiber-optical cable (used to tow the transmitter at the head of the streamer and to communicate to the transmitter electronics) were tested and connected. In parallel, the different lengths of ropes between the receiver dipoles were measured carefully and wound up on the Toronto winch, and the receiver loggers were programmed and prepared. The geochemistry group prepared the laboratory for chemical analysis and all facilities needed for analyzing the cores. In the evening we passed underneath the beautiful bridge of Patras when entering the Gulf of Corinth (GoC). Our first activity in the western end of our working area on the evening of St Nicholas' Day was a releaser test combined with sound velocity measurements of the water column. The deployment of our ensembled system to the sea via a winch wire aroused the curiosity of a large number of dolphins. To our surprise, on recovery of our releaser test ensemble, only a torn rope was hanging where the sound velocity probe was attached to the winch wire. It is not possible to reconstruct what happened to the probe, but a briefly increased load on the wire while the equipment was in the water, led to speculation that a dolphin or even a large shark that occurs at greater depths might have taken a too great interest in our silver-coloured device.

Later in the night, we rigged a Posidonia pinger with a weight and a releaser system to deploy it stationary on the seafloor in order to calibrate the USBL system. Unfortunately, no signal was received from the pinger, prompting us to abort the calibration and retrieve the system back on deck. However, a spare velocity probe also attached to the wire, was this time successfully recovered yielding our first velocity profile of the water column.

December 7th,2023:
In the morning we started with a velocity profile in the eastern section of the GoC. At 09:00 UTC we were ready for our first gravity core (GC1) near borehole M0078 of IODP leg 381. The IODP borehole indicates freshened groundwater below a seafloor depth of 5m to 6m. Unfortunately, the gravity corer only penetrated 3.5 m, probably due to the presence of a turbidite layer, and the first pore water analysis of the core did not show any pore water salinity anomaly. At lunch time we commenced to set out 5 OBEMs at distances of 5nm from each other starting from the eastern end of GoC. We first tried to deploy the system on a wire Posidonia pinger and release it 50m above the seafloor, such that we could have an exact position of the OBEM stations on the seafloor. However, the first and third OBEM did not release properly from the wire, such that we deployed the remaining stations free-falling and left the determination of the exact position to acoustic ranging to the releaser on the OBEM frame at a later stage of the cruise. Using the frame of the 6th OBEM, we deployed the Posidonia beacon and successfully calibrated the USBL system, reducing the error in positioning by a factor of 2.

December 8th, 2023:
We started with the deployment of the last OBEM and a velocity profile for bathymetry at the western section of GoC. We then deployed the gravity corer at the western end of GoC (GC3), unfortunately again only penetrating less than 4 m, with no sign of a pore water salinity anomaly. Our first deployment of the CSEM receiver streamer started at 16:00 UTC using the Toronto winch. As always, it was a bit tricky to deploy since receiver dipoles and loggers are assembled into the ropes spooled off the Toronto winch during the deployment. After connecting the receiver streamer to the head of the streamer consisting of a depressor that houses the transmitter electronics, the depressor, which we call a pig, was deployed over the Werner winch. After the successful deployment, we started our CSEM Line 1 along the center of the entire deep basin of the GoC from east to west. Strong winds with changing directions due to the particular topography of the GoC posed a challenge for the bridge to keep the ship and streamer aligned during the first mile of the profile. In the evening though, the wind died down and turned back towards steady westerlies, such that we had a smooth ride with 0.7 kn to 1 kn along the profile during the night.

December 9th, 2023:
A quiet day for everybody but the electromagnetic group, who kept watch over the data acquisition along CSEM profile 1.

December 10th,2023:
At 04:00 UTC we started heaving the CSEM streamer and recovery was completed without problems by 08:00 UTC. Unfortunately, we noticed some damage to the system. The cables of the first two receiver electrodes were torn. On the positive side, the transmitter functioned perfectly, and the data on the two furthest positions along the streamer was good enough for further analysis. We then transit to the location of gravity core 4 in the vicinity of the IODP borehole. Gravity core 4 showed the first pore water salinity anomaly, i.e. a decrease of pore water salinity over its 3.2 length. During the night we acquired bathymetric and parasound data in the eastern area of the GoC.

December 11th, 2023
The morning was used to acquire 3 cores at gravity core location 5, situated close to the northern coast of the GoC. As in gravity core 4, a pore water salinity gradient was detected. After a velocity profile at the core location, the remainder of the day, between about 12:00 and 19:00 UTC, was used to measure salinity and conductivity profiles along CSEM profile 1. These data are required for the inversion of the CSEM data into seafloor electrical resistivity models. However, the salinity and electrical conductivity profiles of the water column did not vary significantly along the entire basin, such that we decided that there was no need for further water column conductivity profile acquisition. During the remainder of the night until the next morning, we acquired bathymetric and parasound data at the northern coast of the Gulf of Corinth around Itea Bay in preparation for gravity core 7 planned for the 14th of December.

December 12th, 2023
West of IODP, we acquired 3 cores at gravity core 6 locations. As in some of the previous cores, we observed again a pore water salinity decrease with depth, indicating that the offshore

groundwater extends westwards of the IODP locations. The deployment of the CSEM system took place at the southern end of CSEM Line 2, which stretches from the southeast towards the northwest in the western part of GoC.

December 13th, 2023
This day proved to be rather disappointing for the electromagnetic group. After recovery of the streamer at around 20:00 UTC, we noticed that the last receiver dipole was missing. A quick analysis of the data of the remaining dipole showed, that the other receivers failed to record. We attribute the loss of data to a short increase in tension on the streamer observed at the beginning of the profile, probably because we hit an obstacle on the seafloor. During the night we transferred to the west of the GoC to acquire bathymetric and parasound data in the western section of the GoC, where up to now high-resolution data did not exist.

December 14th, 2023
The day started, as often, with coring. Within Itea Bay, 3 cores were recovered at the gravity core 7 location. Again, a porewater salinity decrease with depth was observed. While acquiring bathymetric and parasound data around GC 3 area, where there was a problem with data quality on the previous acquisition, and within the center of the GoC, we celebrated the Bergfest with a BBQ.

December 15th, 2023
The first action of the day was the acquisition of gravity core 8, which was also located in Itea Bay, approximately 2.5 nm northwest of gravity core 7. The next action point on the list was the ranging of the four western OBEMs (OBEM1 to OBEM4) to determine the exact position on the seafloor and their subsequent recovery. The plan was to redeploy the OBEMs between OBEM5 and OBEM 6 which straddle the IODP borehole locations to have a higher density of receivers for a calibration CSEM profile planned for Dec 18th. While the OBEM3 responded to the acoustic ranging signals and released without failure, we had trouble finding it at the sea surface due to a failure of the radio beacon and flash. Rain and nightfall made the search for the OBEM a suspense. OBEM4 gave no acoustic reply to our interrogation signal. We found out the next morning after a call from the port authority that a fisherman had dredged the system up while fishing and had recovered it onto his fishing vessel. OBEM2 answered, yet when we tried to release it, it sent the message that it could not be released since the OBEM was not stationed properly on the seafloor. We concluded that it most likely has been dredged as well and tipped over and feared for the remaining OBEMs on the seafloor. Yet OBEM1 answered and released, but it was again difficult to find due to a failure of the radio beacon and flasher. All together it was a long hard night.

December 16th, 2023
The day was used for two gravity coring stations, gravity cores 10 and 11, along the center axis of the GoC basin, and completed the bathymetric survey in the western area of GoC.

December 17th, 2023
In the early morning, bathymetric and parasound data were acquired in an area of known seafloor groundwater discharge sites on the southeastern shore of GoC in preparation for a planned Video-

CTD investigation in the area. Based on the bathymetric data, new pockmarks were identified, and the subsequent Video-CTD measurements identified freshwater seepage in two areas. In the evening we deployed and subsequently ranged two OBEM stations (OBEM7 and OBEM8 station) in preparation for the planned CSEM calibration profile.

Dec 18th, 2023
In the morning the work boat Meteorite was let in the water to be used as a platform to deploy Mini-ROV to investigate further the shallow water groundwater discharge on the seafloor. Unfortunately, while the wind was down, the waves were still too high to efficiently work, such that we abandoned the survey at lunchtime. Instead, we went to the eastern section of the Gulf to meet the fishermen and transferred OBEM4 to the ship. In the evening, after another velocity profile, we deployed the CSEM streamer and started a high-density data acquisition along CSEM L4 crossing the IODP boreholes.

Dec 19th, 2023
The recovery of the CSEM streamer in the morning was smooth, such that we had sufficient time to acquire two more gravity cores, GC 12 and GC13 south and north of the IODP drilling sites, at lunchtime. During the late afternoon until twilight, we recovered OBEM5 and OBEM8 at very calm seas. While the strobe and lights were functioning at the calm seas, we deferred the recovery of the remaining two stations in the eastern section to the following morning. Over the night we filled up the remaining lines in the bathymetric and parasound survey in the eastern section of the GoC as well as acquired velocity profile soundings to improve the processing of bathymetric data.

Dec 20th, 2023
Recovery of OBEM6 was smooth, however, OBEM7 did not answer to our interrogation and release signal, indicating that it was dredged again from its deployment location. Yet fortunately the radio on the system worked this time and while on a search pattern and we received a radio signal and could recover OBEM7 4 nm north of its original position. We then tackled the recovery of OBEM2, which answered but had not released on December 15th. When we arrived at the ranged position, the system did not answer our acoustic interrogation, indicating that it was probably dredged again. We nevertheless deployed a video camera attached to the MUC frame, which was also equipped with a hook, and dived to see whether we could locate it. Yet, visibility was very bad due to sediment flares close to the seafloor. Just about when we lost hope to recover OBEM2 we received a phone call from our fishermen, who had spotted the instrument floating on the surface approximately 5 nm west of our current location. So, after the adventurous hunt for our OBEMs, we were happy to report on the evening of Dec 20th that all of them were back on deck. Nighttime was used to complete our bathymetric survey in the west to a full grid.

Dec 21st, 2023
The morning of December 21st was used to also complete the Mini-ROV survey around the seep areas. While the mini-ROV sensor online data did show a salinity anomaly, changes in Flora and fauna suggest seepage of groundwater. By 12:15 UTC we ended our scientific data acquisition to have sufficient time for data backups, preparing all boxes for shipping and cleaning up the labs on our short transit to Patras.

Dec 22nd, 20023
At 5:00 UTC we passed the bridge in Patras leaving the GoC and tied to the pier of the Port of Patras shortly after 6:00 UTC, where the agent awaited us. All scientists, except the chief scientist and two further members of the scientific crew, left the ship to travel home for Christmas and we started our transit over the Christmas holidays to Limassol, our final port, at 13:30 UTC.

5 Preliminary Results

5.1 Electromagnetic Investigations

(Amir Haroon, Katrin Schwalenberg, Marion Jegen and Shipboard Scientific Party)

Marine controlled source electromagnetic (CSEM) is a geophysical exploration method used to derive the electrical properties, that is resistivity, of the seafloor. Electrical conduction in seafloor sediments occurs through ions in pore fluids, and therefore the conductivity (1/resistivity) of seafloor sediments depends mainly on the sediment porosity, pore space connectivity and the conductivity (ion content) of the pore fluid. An important source of ions is the amount of salt in the pore fluid, which is why the conductivity of the pore fluid depends strongly on its salinity.

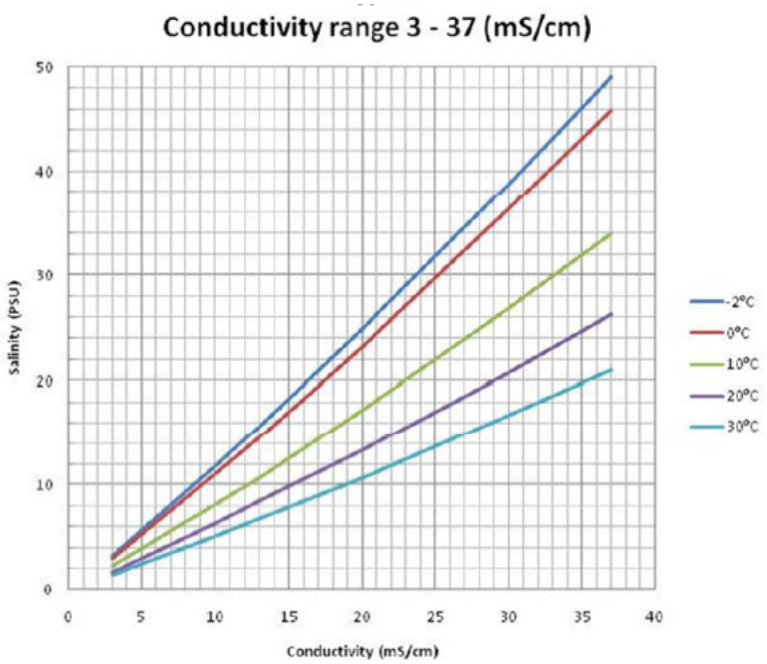

Fig. 5.1.1 Pore fluid conductivity for different salinity values and temperatures.

Figure 5.1.1 shows the relationship between salinity and pore fluid conductivity for different temperature values. The relationship between the bulk resistivity of sediment (ρ_{bulk}), porosity (ϕ) and pore fluid resistivity (ρ_{fluid}) may be described by the experimentally derived Archie's Law:

$$\rho_{bulk} = a\, \phi^{-m}\, S^{-n}\, \rho_{fluid}$$

Where F is the porosity, S denotes the pore fluid saturation, and a, m and n are constants, which range between 0.5-1.5, 1.8-2.4 and ~2 respectively in marine sediments. Rocks containing large amounts of clay have a resistivity lower than predicted by Archie's law due to conductive pathways along the surface of negatively charged clay particles.

Typical seawater resistivity varies between 0.3 Ωm to 0.5 Ωm depending on seawater salinity and shallow marine sediments typically have a bulk resistivity of around 1 Ωm. Freshwater resistivity ranges between 1 and 10 Ωm, thus the bulk resistivity increases by a factor of 3 to 30 for freshwater-saturated sediments.

The measurement of bulk electrical resistivity of marine sediments requires an electromagnetic source generating an electromagnetic wave, and electromagnetic receivers. For M196 we employed electromagnetic methods using naturally varying low-frequency magnetic field variations as a source (Magnetotellurics - MT) for low-resolution deep resistivity models as well as a method that employs a man-made electromagnetic transmitter supplying higher frequency variations (controlled source electromagnetics - CSEM) for high-resolution shallow studies.

The low-frequency variations of electrical fields in both horizontal and magnetic fields in three directions, i.e. the MT signal, are continuously logged by ocean bottom electromagnetic stations (OBEM) anchored on the seafloor at 100 Hz sampling rate. The MT signal will allow a derivation of electrical resistivity models down to a depth of approximately 5 km, yet at a rather low resolution. If the transmitter is within about 0.5 nm of the OBEM, the system additionally records the higher frequency CSEM signal, allowing for an estimate of a higher resolution electrical resistivity model between the transmitter and OBEM down to a depth of a few hundred meters.

The controlled source electromagnetic system used in the GoC consists of a dipole transmitter which is towed in line with 4 receiver dipoles at different distances behind the transmitter dipole. The deep-towed transmitter electronics were supplied by BGR since the deep-tow GEOMAR transmitter was not available due to an overlapping cruise. As receiver dipoles, we used four CSEM HYDRA IV units, that are part of the newly developed surface towed SWAN system developed during the SMART project. From the CSEM data, we expect to be able to estimate a resistivity model at 10s of meter resolution down to a depth of approximately 300 m to 400 m.

5.1.1 Instrumentation

The seafloor-towed controlled source electromagnetic system (Figure 5.1.2) was used to collect inline time domain electric field data along profiles. The system consists of a ~100 m long electric transmitter dipole followed by four receiver units (Figure 5.1.3) that are connected by Kevlar ropes at offsets between ~150 m and 725 m behind the transmitter dipole. Each receiver unit consists of an electric dipole with a length of nearly 10 m with Silvion CCS1 electrodes mounted at each end. Each dipole is connected to an autonomous, battery-powered three-channel data logger developed by Magson GmbH. The inline electric field components are recorded at 10 kHz with different gain settings on each of the three channels. Electronic boards and batteries reside in titanium pressure cylinders, which are protected by torpedo-shaped POM housings. The configuration has been successfully used in various projects for the exploration of submarine gas hydrates, shallow gas, and offshore freshened groundwater.

The receivers used during this survey are part of the SWAN system, a surface-towed CSEM system developed by GEOMAR, the University of Malta and Texas A&M University for shallow water CSEM applications (up to 100 m of water depth).

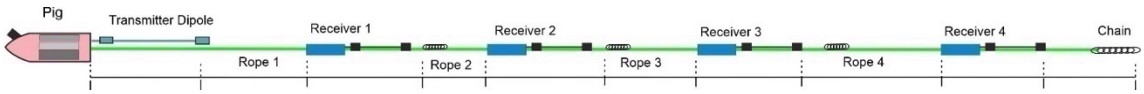

Fig. 5.1.2 Sketch of the seafloor-towed electric dipole-dipole system (not to scale).

For the M196 cruise, the BGR signal generator and communication unit (Com-Unit) were used. The signal generator is capable of transmitting rectangular and sine waveforms with amplitudes up to 20 A. For the CSEM surveys, we used repeating sequences of 100% and 50% duty cycle rectangular waveforms at 10 A. Tests with 15 A and 18 A showed dominant ~460 Hz in the DC plateaus and overshoots of several milliseconds on the signal flanks, which are likely due to limitations of the power supply in the lab and the electrical noise environment of the vessel.

The signal generator and the Com-Unit are mounted inside the pig (Figure 5.1.4), a heavy sled towed at the front of the seafloor array, which keeps the system on the seafloor and paves the way for the subsequent receivers. The Com-Unit communicates with the ship via optical fiber. Therefore, the GEOMAR "Werner-Winch" (Figure 5.1.4) was mobilized for the cruise with its 5000 m, 11 mm fiber optical tow cable, as the METEOR is not equipped with a fiber optical cable.

Deployment of the system starts from rear to front while the ship moves forward at the same speed as the deployment procedure. The connecting ropes are drummed off the Toronto winch (Figure 5.1.4), and the ropes are stopped intermittently to integrate the receiver units. At last, the transmitter dipole is connected to the aft of the pig and the electrical connection is made to the signal generator. It is important that the mechanical load is always on the Kevlar rope segments and not on the electrical connection to the transmitter and receiver electrodes, as they are not rated for that purpose.

The exact time synchronization between the source and received signals is relevant for the data analysis. Therefore, all data loggers are equipped with high-precision clocks, which are synchronized to GPS time before and after the deployment. Also, exact transmitter-to-receiver offsets need to be known. Thus, all array segments were measured before and after the deployment to consider the lengthening of the new Kevlar ropes (see Table 5.1.1).

Once the system is deployed and in seafloor operation, communication is only possible with the telemetry unit and the signal generator inside the pig. There is no connection to the receiver units, since these are connected by rope to the head of the streamer. Data communication with the receiver units has been tested at previous surveys using a similar setup (Schwalenberg et al., 2020), but proved to be challenging as electrical cable connections are prone to ground loops and noise. However, towing the receivers without communication to the ship as takes the risk of overseeing failures during the deployments or surveying.An acoustic USBL (Posidonia) transponder provided by METEOR was attached to the pig and used to monitor the pig's position during the surveys.

The towed controlled source electromagnetic measurements were augmented by stationary OBEMs, which measure the two horizontal electric and three-axis magnetic field variations. When the electromagnetic transmitter is within 0.5 nm of the OBEM station, the controlled source electromagnetic wave is recorded by the OBEM. If no transmitter signal is present or in the vicinity, the OBEM records the electromagnetic response of the Earth to the naturally varying magnetic field variations, a methodology called magnetotellurics (MT). To capture the controlled source as well as naturally varying fields, the electric and magnetic fields were sampled at the maximum sampling frequency of the OBEM, which is 100 Hz.

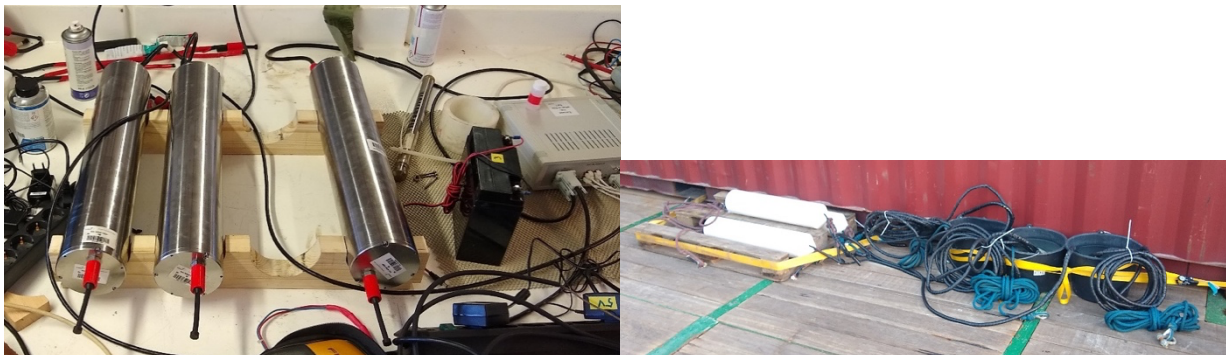

Fig. 5.1.3 Left: HYDRA IV 3 channel data loggers sampling at 10kHz. Right: Each data logger is housed in a POM vessel (white cylinders) and records voltage differences between 2 electrodes connected by a black cable at 10 m distance.

Fig. 5.1.4 Left: Depressor (pig) housing the transmitter electronics. Right: Werner Winch (dark blue winch towards the back of deck) with fiber-optical cable, that connects the transmitter electronics within the depressor to a control unit on the ship and also serves as a tow cable. The Toronto winch (light blue) is used to deploy and recover the receiver streamer.

Figure 5.1.5 shows the OBEM instrument. The instrument carrier consists of a titanium frame on which syntactic foam elements are mounted to give the frame a positive buoyancy. For deployment, a magnetically neutral concrete anchor slab is attached to the frame by a releaser. The frame is equipped with a titanium cylinder containing the battery pack, a smaller titanium cylinder containing the 3-component fluxgate magnetometer (with a precision of 10 pT/sqrt (Hz)) and a data logger (both built by Magson GmbH, Berlin). The latter records magnetic and electric field variations, tilt variations, temperature and time. Timing of the measurement is kept via a Seascan clock equipped with a temperature-controlled crystal which is synchronized to GPS before deployment (typical drift < 500 ms/year). The logged data is stored on a removable SMD card. Orthogonal horizontal electric field measurements are performed through voltage difference

measurements between non-polarizable silver-silver chloride electrodes from Silvion, separated by plastic pipes which are mounted between frame and anchor to span a 10 m electric dipole. To facilitate recovery, the OBEMs are equipped with a strobe, radio, flag and a swimming line consisting of a rope with approximately 6 m lengths attached to a small flotation device.

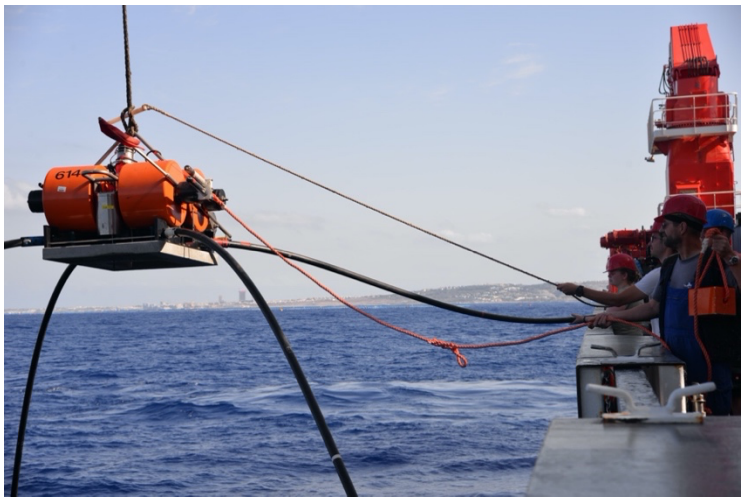

Fig. 5.1.5 GEOMAR OBEM station.

5.1.2 Data Acquisition

CSEM Deployments

During M196, we towed the CSEM system along three profiles (Figure 5.1.6).

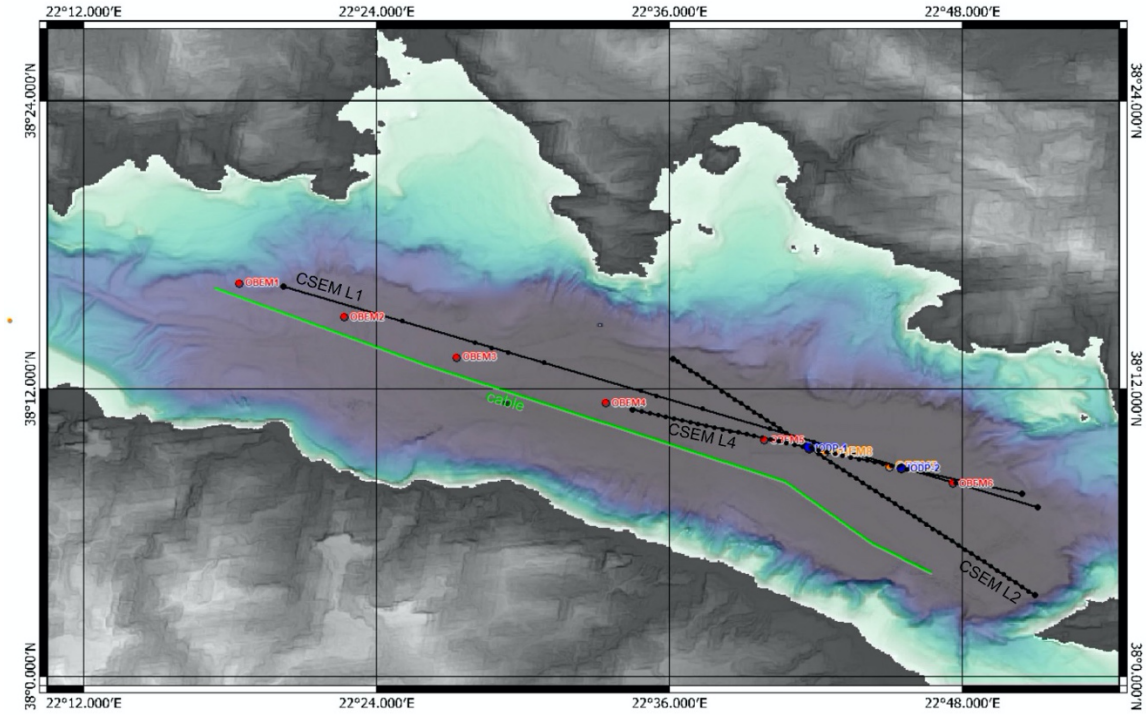

Fig. 5.1.6 Bathymetric map of the Gulf of Corinth with CSEM lines (black), OBEM nodes (red and orange) and IODP positions (blue). Black dots along the lines mark waypoints (stationary CSEM measurements), which were sporadically along Line 1 and systematically every 500m along Lines 2 and 4. For Line 4 the two western OBEM1 and OBEM2 were moved to the orange positions near the two IODP sites. The green line marks the position of an existing seafloor cable.

CSEM Line 1, 08. - 10.12.2023

The first CSEM deployment with the seafloor towed CSEM system was about 40 km in length in SEE to NWW direction along the entire basin axis (CSEM-L1 in Figure 5.1.6). We used the pig with the GEOMAR transmitter and 4 receivers. Two meter-length iron chains have been interconnected to the ropes to add weight to the otherwise light and partly buoyant parts of the array. It has been decided to tow the seafloor array at a slow speed of 0.5 – 0.7 kn with only occasional stops for stationary measurements. Useful data have been previously recorded while the array was towed, however stationary data generally provide a higher data quality but slow down the survey speed considerably.

The Hydra system was safely retrieved on deck after a 36h deployment. However, several problems occurred:

- The spherical transmitter electrodes imploded as they were at the limit of their depth rating of 800 m water depth. Nevertheless, the metal parts still functioned as current electrodes.

- The receiver dipole of the front two receivers (R1 and R2) broke at the rear splices to the Silvion electrodes. This likely happened during the deployment procedure when the dipoles were stretched at the vessel's curb. This was avoided by using a nautical block at subsequent deployments. No useful data are available for receivers R1 and R2.

- The last receiver R4 lost time synchronization when the unit was deployed. This could happen due to a short mechanical disconnection of the battery packs, which caused a restart of the logger board. The exact timing must be determined in postprocessing.

- At least for the last two receivers (R3 and R4) the data quality was poor when the array was towed and only the data sequences when the array was occasionally stopped shall be used (see data examples in Figure xx). Therefore, regular stops every 500 m have been performed in the following deployments.

Nevertheless, the transmitter signal, which was sent during the entire survey, also served as a CSEM source for the nearby OBEM receivers.

CSEM Line 2, 12. - 13.12.2023

The second CSEM deployment along Line 2 started in the southeast of the Corinth basin and was along a 25 km profile in the northwest direction across the western IODP borehole and near OBEM sites 5 and 6. The GEOMAR transmitter dipole was replaced by the BGR transmitter dipole which uses 1 m long copper pipes as current electrodes. The broken cables to the receiving dipoles were repaired and measures were taken to avoid unnecessary stretching on the cables. For example, we removed the interconnecting chains and used a nautical block to lift the receivers and dipoles in the water.

The second deployment unfortunately did not provide any useful data and loss of the last receiver unit R4. The survey started too close to shore where the array likely got stuck on the steep slope. This caused the connecting rope between R3 and R4 to rip due to the high tension on the

rope. Unfortunately, this episode caused the front three receiver dipoles to tear. At least the front 3 receivers could be recovered safely.

CSEM Line 4, 18. - 19.12.2023

The third and last CSEM deployment along Line 4 was in E-W directions close to the eastern part of Line 1, but closer to the IODP boreholes and to 4 OBEM receivers of which the two OBEM receivers 7 and 8 in the middle were moved from their previous location OBEM 1 and OBEM 3. The towed CSEM array consists of the BGR transmitter dipole and three receivers. Deployment, survey and recovery went smoothly and without noticeable complications. However, data inspection and subsequent array inspection again revealed a broken receiver dipole cable of receiver units 2 and 3. Only receiver unit 1 recorded high-quality data when the array was moving and stationary every 500 m. The remaining ship time did not allow for the repair of the broken cables.

Table 5.1.1 Overview of CSEM Deployment details.

	Line 1	**Line 2**	**Line 4**
Profile description and set up	40km long E to W profile over IODP and OBEMs covering the entire basin. 4 receivers, Geomar dipole, profile with 15 stops	SE to NW profile across IODP boreholes. 3 receivers (R4 lost), BGR dipole, profile with 49 stops every 500m	Eastern part of Line 1 over IODP boreholes und newly deployed OBEMs. 3 receivers, BGR dipole, profile with 32 stops every 500m
Start – End Time (in and out of water)	08.12.2023 18:00 – 10.12.2023 06:30	12.12.2023 15:50 – 13.12.2023 20:00	18.12.2023 17:30 – 19.12.2023 09:30
Receiver IDs / TX-RX offsets *	R1 - #162 / 166.05 m R2 - #161 / 306.21 m R3 - #160 / 496.72 m** R4 - #159 / 724.77 m**	R1 - #160 / 151.55 m R2 - #162 / 289.27 m R3 - #159 / 477. 68 m R4 - #161 / 703.78 m	R1 - #159 / 151.55 m** R2 - #160 / 289.27 m R3 - #162 / 477.68 m
Notes	TX sphere electrodes imploded, depth rating was to 800m water depth Dipole splices broke at rear electrodes of R1 and R2; R4 lost sync during deployment. Useful data at R3 and probably R4 on waypoints	Survey started too close to shore, R4 got stuck and lost, whole array was stretched, caused failure of all receiver dipoles. No useful data	Receiver dipoles of R2 and R3 broke at newly made splice to pigtail due to tension on the cable. High quality data at R1.

**center TX to center RX, ** receiver with useful data; offset calculations include estimates of the length of connecting shackles.*

OBEM Deployments

Altogether 6 OBEMs were available for the cruise. The internal settings of each OBEM were identical and are shown in Figure 5.1.7. Sampling was set to 100 Hz to allow for the capturing of the transmitter signal when the CSEM system was operating close by.

---

rem ID = 0: BFSEFHK_divider (1-256) Divider for base frequency of 100Hz
rem ID = 1: BFSEFHK_format file format (0=ASCII, 1=binary)
rem ID = 2: BFSEFHK_recording recording slow mode (0=off, 1=on)
rem ID = 3: BFSEFHK_record_raw scaling of data (0=scaled, 1=raw)

```
rem ID = 4: EF_mode                    select E-field electronics (0=slow, 1=fast)

rem ID = 5: FEF_recording              recording fast mode (0=off, 1=on)

rem ID = 6: SEF_autorange              select auto ranging for slow E-fields (0=off, 1=on)
rem ID = 7: SEF_gain_x                 gain for slow Ex (1,2,4,8,16,32,64)
rem ID = 8: SEF_gain_y                 gain for slow Ey (1,2,4,8,16,32,64)
rem ID = 9: SEF_gain_z                 gain for slow Ez (1,2,4,8,16,32,64)

print "Starting OBEM with initial settings in MT mode"
        call("set_OBM_setting", 0, 1)
        call("set_OBM_setting", 1, 1)
        call("set_OBM_setting", 2, 1)
        call("set_OBM_setting", 3, 0)
        call("set_OBM_setting", 4, 0)
        call("set_OBM_setting", 5, 0)
        call("set_OBM_setting", 6, 0)
        call("set_OBM_setting", 7, 16)
        call("set_OBM_setting", 8, 16)
        call("set_OBM_setting", 9, 1)
end
```

Fig. 5.1.7 Internal recording settings of the OBEM recordings.

The 6 stations were initially deployed on a profile along the central basin of GoC with approximately 5 nm distances along the main CSEM profile Line from December 7 until the morning of Dec 8. To ensure a higher density of OBEMs during CSEM data acquisition, OBEM1 and OBEM3 were recovered on the 16th and 15th of December respectively and redeployed on the eastern part of the profile as stations OBEM7 and OBEM8. Due to the short bottom time of stations OBEM 7 and OBEM 8, the data will not be useful for MT data. The planned recovery of OBEM2 and OBEM4 for redeployment on the eastern part of the profile failed. While the OBEM2 answered to interrogation of the releaser, it was not able to release its anchor. OBEM4 did not respond to interrogations as it had been dredged to the surface by a fisherman, who contacted us the following day. OBEM6, OBEM7 and OBEM8 were deployed via a wire and released 50m above the seafloor, while the other OBEMs were deployed from the surface. The clock of each OBEM was synchronized against a GPS signal, and the initial and final time shift relative to the GPS signal was noted. Table 5.1.2 gives an overview of the acquisition parameters of the OBEMs.

Table 5.1.2 OBEM experiment settings and deployment and recovery parameters.

Station ID	Dev ID	Dipole Length (m)	Deployment Date/Time	Deployment Coordinate N	Deployment Coordinate E	Water Depth (m)	Recovery Date/Time	Recovery Coordinate N	Recovery Coordinate E	dt (ms) depl.	dt (ms) rec.
OBEM1	59	10	08.12.2023 07:36	38 16.4	22 18.377	630	16.12.2023 00:30	38 16.596	22 18.262	-32.3	7.2
OBEM2	35	10	07.12.2023 19:46	38 14.849	22 23.022	800	20.12.2023 18:11	38 14.694	22 16.018	-313.9	-246.7
OBEM3	32	10	07.12.2023 18:35	38 13.308	22 27.271	830	15.12.2023 19:15	38 13.431	22 26.993	-778.9	-781.9
OBEM4	34	10	07.12.2023 16:14	38 11.391	22 33.428	865				-220.1	
OBEM5	26	10	07.12.2023 15:15	38 9.849	22 39.892	857	19.12.2923 15:02	38 09.862	22 40.149	-75.4	29.2
OBEM6	27	10	07.12.2023 12:21	38 08.048	22 47.618	865.2	20.12.2023 5:55	38 08.248	22 47.940	-251	-209
OBEM7	59	10	17.12.2023 22:52	38 8.752	22 45.033	853	20.12.2023 10:11	38 06.997	22 49.731	-75	62.2
OBEM8	32	10	17.12.2023 20:46	38 9.3236	22 42.3733	850	19.12.2023 14:59	38 09.3236	22 42.373	-171	-171.8

5.1.3 Preliminary Results

CSEM

Useful data for further analysis are only available for receiver 3 and partly for receiver 4 from the first deployment (Line 1) and for receiver 1 from the third and last deployment (Line 4). Figures 5.1.8 and 5.1.9 show time series data examples for Line 1 for the source signal (upper panel) and receiver 3 signal (lower panel) while the array was stationary and towed on the seafloor, respectively. The signal wave form is clearly depicted by the receiver when the array is stationary but shows a large asymmetry between negative to zero and positive-to-zero switches which is possibly caused by differences of the contact resistance of the imploded TX electrode. Note, that the TX signal is current controlled and recorded before being sent to the TX electrode, which explains the symmetry in the TX signal. Also, a long period drift is visible in the RX data.

The example when the array is towed shows noisy data, which likely cannot be used for further processing and analysis. The data example in Figure 5.1.10 shows high data quality for the first receiver of the last deployment (Line 4). At that offset, data can be used while the array is stationary as well as moving. The offset in time between transmitter and receiver data needs to be addressed in the post-processing.

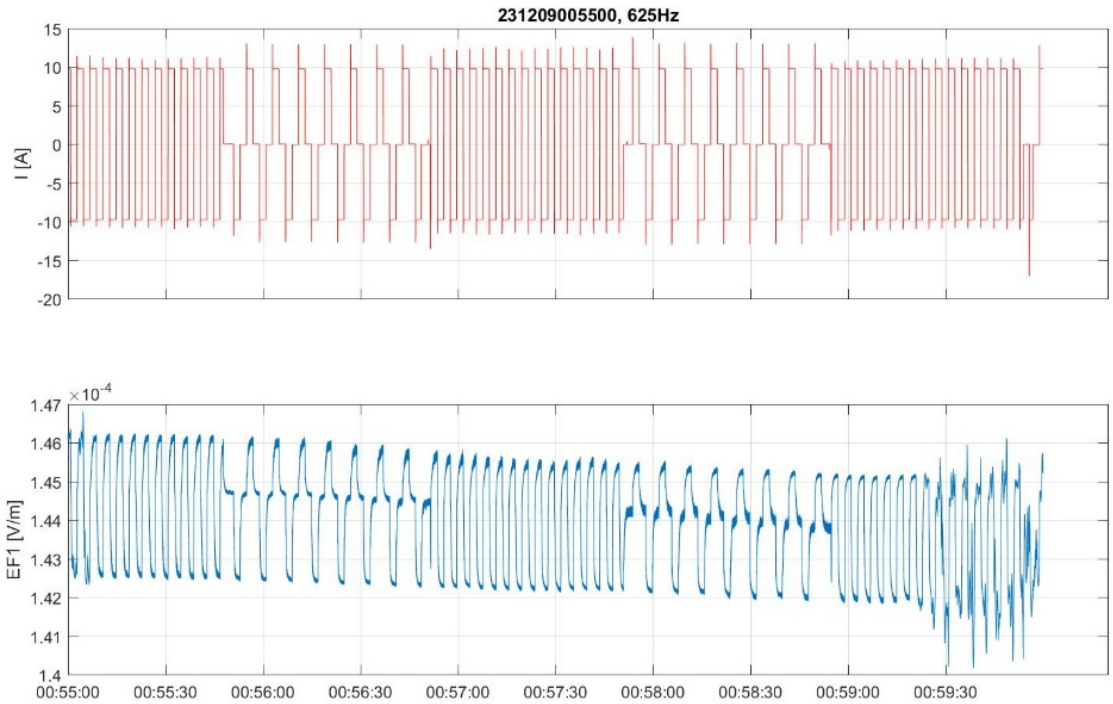

Fig. 5.1.8 5-minute time series example along Line 1. Top: transmitter signal, bottom: received signal at Receiver 3 (offset: 496.72 m) while the seafloor array was not moving until 00:59:30. Data quality is much higher when the array is stationary. Stacking of signal sequences can further improve data quality. Receiver data show drift and are asymmetric for positive and negative steps, possibly due to different characteristics of the imploded spherical transmitter electrodes.

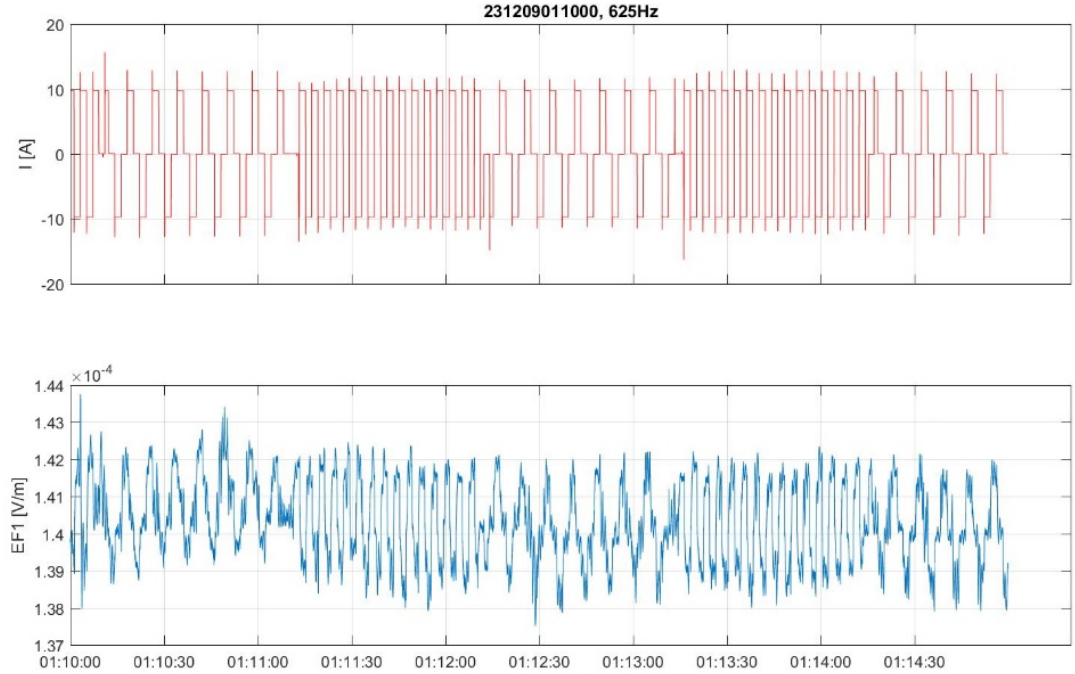

Fig. 5.1.9 5-minute time series example along Line 1. Top: transmitter signal, bottom: received signal at Receiver 3 (offset: 496.72 m) while the seafloor array was moving until 00:59:30. Data are noisy from towing on the seafloor and the small size of the signal.

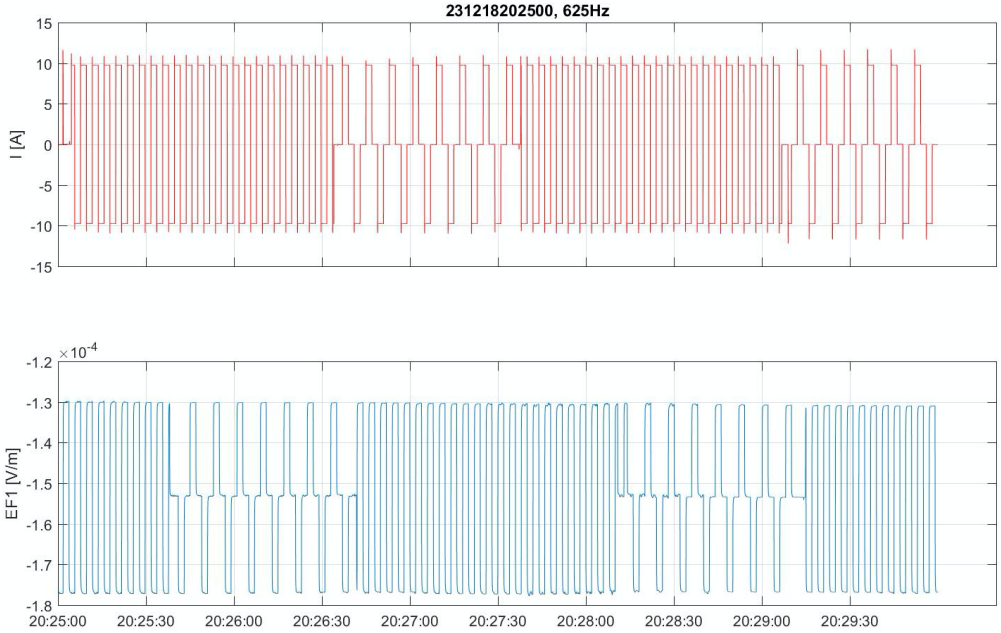

Fig. 5.1.10 5-minute time series example along Line 4. Top: transmitter signal, bottom: received signal at Receiver 1 (offset: 151.55m) while the seafloor array was not moving. Data quality is high for both, tow and stop sequences. The receiver data lost the synchronization with respect to the transmitter signal, which needs to be corrected in the post-processing.

OBEM

A close look at the data (see Figures 12.1.1 and 12.1.2 in Appendix 12.1) shows that the overall instrumental data quality of the OBEMs data acquisition is very good. All components but the Ey component of OBEM6 functioned without problem. The large jumps in the magnetic field data

observed in OBEM2 (Figure 5.1.11) and also OBEM4 and OBEM7 (Figures 12.1.1 and 12.1.2) are related to large changes in pitch and roll, which have most likely been caused by dredging of the instrument along the seafloor by fisheries.

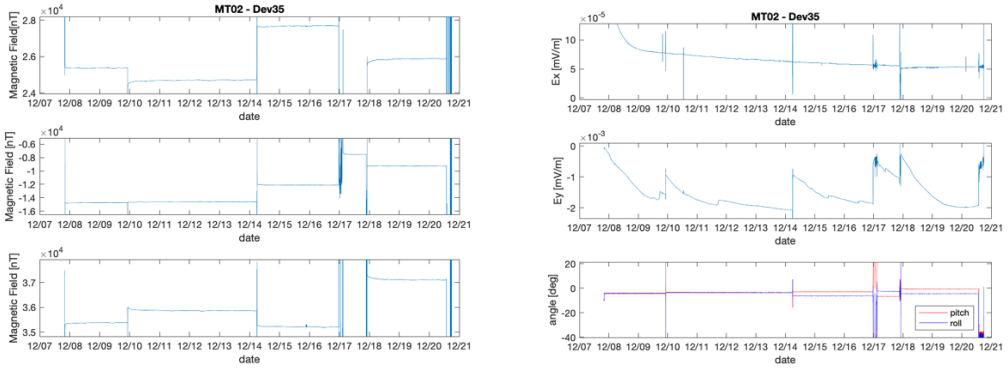

Fig. 5.1.11 Three-component magnetic field recording on station OBEM02 (left) and horizontal electric field components and pitch and roll of station (left). Abrupt changes in pitch and roll are due to dredging by fisher and are associated with large offsets in magnetic field recordings.

Figure 5.1.12 shows the total magnetic field data, which is independent of the position and changes in pitch and roll for all stations. The total fields show the expected congruency but for OBEM1 and OBEM7. For these, we observe some non-linear drift and anomalies, which we attribute to the magnetic fluxgate device 59, which was employed on these two stations. Overall, the total magnetic field variations correspond well to land geomagnetic observatory data sampled at one time a minute at Pendeli, Greece.

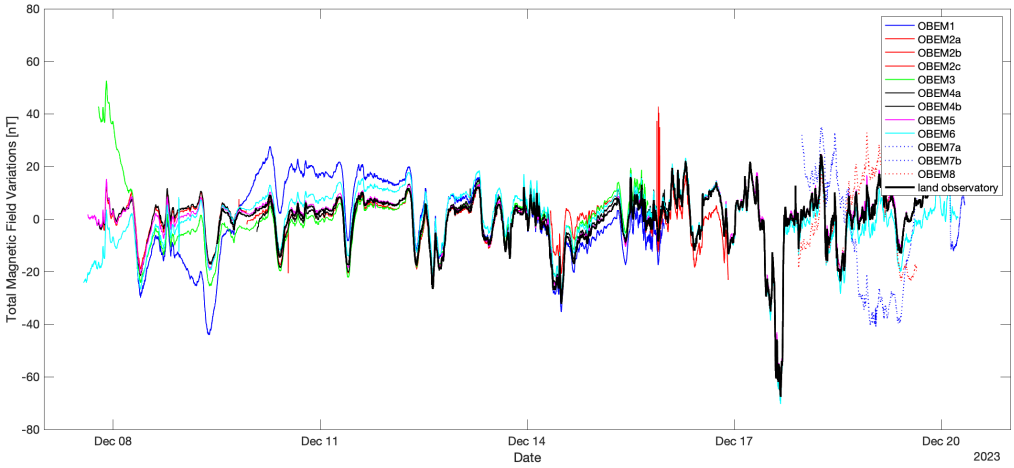

Fig. 5.1.12 Detrended Total magnetic field variations for all 8 OBEM stations. The data show the expected congruency but for OBEM1 and OBEM7, which employ the magnetometer device 59.

In the next step, we need to determine the angle of rotation towards geomagnetic north, since the OBEMs land on the seafloor in an uncontrolled fashion. The angle of rotation can be determined in different ways. One possibility is a comparison of the marine magnetic field variations to land magnetic observatory variations, where magnetic fields are measured in defined geomagnetic directions. To this purpose, the marine magnetic field variations are rotated and a coherency with the land magnetic field variations at different rotation angles are calculated. The proposed angle of rotation would then be the angle at which a maximum coherency is observed.

The coherency itself is dispersive, since the amplitudes of the marine fields change with frequency due to the strong absorption of electromagnetic fields through the ocean layer, causing a decrease in coherency with increasing frequency. Since the absorption is highest at high frequencies, the angle is best determined for coherencies at low frequencies. To this purpose, we pick 15 of the lower frequencies, determine the angle of maximum coherency for these frequencies and calculate the angle of rotation using a coherency weighted average of the angles with maximum coherency. The angle of rotation can alternatively be determined considering that the maximum horizontal magnetic field points to the north. Thus, the horizontal magnetic field measurements (full field, not variations) on the seafloor can be rotated to find the angle at which the x-component magnetic field is maximum and y-component field minimum. However, given that the battery packs in the releaser are slightly magnetic and cause an offset of the full field measurements, this approach might be slightly but systematically biased, a fact that is not reflected in the estimated error. The angles of rotations using both methodologies are summarized in Table 5.1.3 for the OBEMs.

Table 5.1.3 Angle of rotation to geomagnetic north of all OBEM stations calculated using the coherency with land and rotated seafloor variation data (upper row) and assuming that the maximum of the full horizontal field points to geomagnetic north.

	OBEM1	OBEM2	OBEM3	OBEM4	OBEM5	OBEM6	OBEM7	OBEM8
Angle to north by coherency	12±2.0	144±2.0	133±2.0	308±2.0	258±2.5	271±2.0	239±3.0	256±4.0
Angle to static north	13±1.0	149±1.0	138±1.0	311±1.0	265±1.0	278±1.0	253±1.0	268±1.0

Next to the MT data, OBEM5, OBEM7 and OBEM8 also recorded the CSEM signal (Figure 5.1.13) when the transmitter was near during the last CSEM line on December 19th. The CSEM signal is shown exemplarily for OBEM8 for the E field as well as B field recordings. The fast-changing amplitude is caused by the switching of the transmitter current, the low-frequency amplitude variation is caused by the change in distance of the transmitter relative to the receiver during the tow transect of the transmitter. The highest amplitude corresponds to the point where the source was nearest to the receiver.

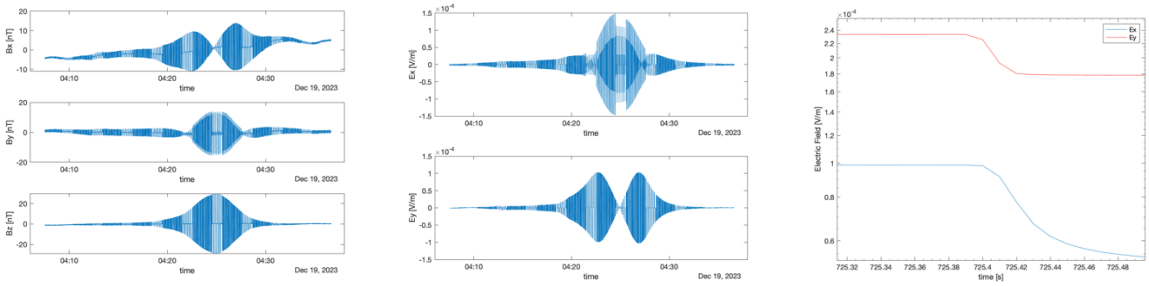

Fig. 5.1.13 CSEM signal at OBEM8 of passing transmitter tow along CSEM Line 4 recorded by OBEM fluxgate magnetometer (left) and electric field sensors (middle) and zoom-in on one electric field transient (right).

A similar signal can be observed on OBEM6 during the CSEM tow along Line 1 between 22:00 and 23:40 on December 8th.

To improve the precision of the seafloor coordinate of the OBEMs on the seafloor, the instruments were ranged from the METEOR at three different positions when the vessel was close by the stations. The ranging is done using a transponder, which is hung mid-ship on the starboard side into the water column at a depth of 15 m relative to the sea surface, and a releaser box. The releaser box measures the time between sending out an interrogation pulse from the transponder until the answer by the transponder on the OBEM's releaser is received. This two-way travel time is then transformed internally in the releaser box to a distance between the transponder and OBEM using a standard acoustic velocity of seawater. Since with these measurements we only obtain a distance but not a direction, the ranging procedure is repeated at 3 different ship positions around the OBEM. The true position of the OBEM is then assumed to be at the intersecting point of the three circles on the seafloor centered below the transponder position and a radius derived from the respective ranging values. The recorded ranging values are shown in Table 5.1.4.
Before we can calculate the new position on the seafloor, we need to take various systematic errors into account. These are a) an offset between the transponder in the water column and the GPS antenna indicating the ship's position, which is dependent on the heading of the ship. b) the depth of the transponder in the water column and c) an increased acoustic velocity relative to the assumed standard velocity used for internal calculations in the releaser box. For the offset correction we determine that for a north-heading ship 10 m Easting has to be added and 12 m Northing subtracted from the ship's GPS position to map onto the position of the transponder. The ship's heading information at the time of ranging has been extracted from D-ship data. In the triangulation, we also assumed a depth position of the transponder relative to the sea surface of 15 m as a depth correction. To account for an increase in acoustic velocity due to the high salinity of 39 PSU and high temperature of 17 °C relative to the standard velocity used in the releaser box, we apply a 3% increase to the ranging values represented as a ranging fudge factor of 1.03. The updated position of the OBEM and correction factors used are summarized in Table 5.1.5.

Table 5.1.4 Ranging values for each OBEM station. Columns 2 and 3 show the date and time of each ranging, and columns 4 and 5 the recorded ship position at the deployment of OBEM. Columns 6 and 7 denote the 3 ship positions during the ranging of each OBEM according to the hand protocol, columns 8 to 10 the 3 ranging values at each of 3 ship positions, column 11 the depth of the seafloor, column 12 the heading of the ship at the time of ranging according to D-Ship and column 13 and 14 the ship position at the time of ranging according to D-ship.

											D-ship		
Name	Date	Time (UTC)	Deployment Lat N°	Deployment Lon E°	Ship's position Lat °N	Ship's position Lon °E	Range 1	Range 2	Range 3	Depth	Heading	Lat Dec min	Lon Dec min
OBEM1	15/12/2023	22:56:00	38°16.400	22°18.377	38°16.109	22°18.527	897	894	893	630	63	16.107	18.5308
OBEM1	15/12/2023	23:14:00			38°16.711	22°18.510	751	752	754	630	91	16.7108	18.5073
OBEM1	15/12/2023	23:35:00			38°16.265	22°17.913	996	1045	954	630	85	16.2655	17.9124
OBEM2	15/12/2023	19:59:00	38°14.849	22°23.022	38°14.922	22°23.314	1100	1098	1096	800	87	14.922	23.3193
OBEM2	15/12/2023	20:32:00			38°14.610	22°22.944	945	948	948	800	90	14.6144	22.947
OBEM2	15/12/2023	20:57:00			38°15.034	22°22.756	823	824	822	800	75	15.0339	22.7578
OBEM3	15/12/2023	16:58:00	38°13.308	22°27.271	38°13.384	22°26.885	888	909	989	830	112	13.3837	26.8856
OBEM3	15/12/2023	16:09:00			38°13.533	22°27.566	993	993	993	830	116	13.5333	27.5687
OBEM3	15/12/2023	17:35:00			38°12.989	22°27.315	945	993	993	830	196	12.9888	27.3156
OBEM5	15/12/2023	13:40:00	38°09.852	22°39.883	38°09.571	22°40.114	1030	1030	954	857	293	9.5709	40.1166
OBEM5	15/12/2023	14:05:00			38°09.715	22°39.509	1042	1041	1041	857	341	9.7149	39.5031

OBEM5	15/12/2023	14:31:00			38°10.168	22°39.927	1012	1013	1012	857	326	10.1683	39.9255
OBEM6	15/12/2023	11:34:00	38°08.048	22°47.618	38°07.884	22°47.318	1194	1191	1190	865.2	358	7.8892	47.3199
OBEM6	15/12/2023	12:05:00			38°07.875	22°47.904	944	944	944	865.2	30	7.8745	47.9036
OBEM6	15/12/2023	12:23:00			38°08.384	22°47.647	1008	1008	1008	865.2	80	8.3821	47.6486

Table 5.1.5 Resulting updated position after ranging of the OBEMs. The range fudge factor refers to an increase of acoustic velocity due to the high salinity of 39 PSU and high temperature of 17 °C relative to the standard velocity used in the releaser box for converting measured response time to distances as recorded in range columns in Table 5.1.4. Also considered in the corrections is the depth of the transponder relative to the sea surface. The error estimate is based on the overlapping area of the ranging circles centered on the seafloor below the position of the transponder at the time of ranging.

OBEM	Deployment Latitude	Deployment Longitude	True Latitude	True Longitude	Range fudge factor	Transponder depth	Estimated Error	
OBEM1	38 16.400	22 18.377	38 16.4631	22 16.4631	1.03	15	10 m	
OBEM2	38 14.849	22 23.022	38 14.8800	22 22.7580	1.03	15	10 m	
OBEM3	38 13.308	22 27.271	38 13.3200	22 27.2160	1.03	15	30 m	
OBEM5	38 9.852	22 39.883	38 9.8460	22 39.9240	1.03	15	10 m	
OBEM6	38 8.048	22 47.618	38 8.1060	22 47.8440	1.04	15	20 m	

5.2 Video-CTD Observations

(Mark Schmidt, Thomas Müller, Dimitris Christodolou, Sergiy Cherednichenko, Jan Fleer)

As the Gulf of Corinth is a semi-enclosed basin with limited water exchange to the Patras basin and the Ionian Sea in the west, water exchanges mainly through the narrow and shallow Rion Straits with a sill depth of about 65 m (e.g. Poulos et al., 1996). This sill depths probably controls the water column stratification within the gulf, which was measured by various authors (e.g. Poulos et al., 1996; Anderson and Carmack, 1973 and references given therein). Most authors postulate a strong temperature stratification with warm surface water (~0-100m) and cold bottom water (~100-800m) from spring to autumn and a mixing of water masses in winter. This assumption is based on discrete temperature and salinity data mainly measured between 1910 and 1970 (Anderson and Carmack, 1973).

The main focus while conducting Video-CTD services was to monitor bottom water chemistry and seafloor characteristics within the nearshore Egio fault area (VCTD1-3; Figure 5.2.2). The aim was to search for evidence of OFG and related submarine groundwater discharge by measuring salinity decrease in bottom water, and/or observing e.g. shimmering water and benthic community changes at the seafloor.

Moreover, several hydrocasts were conducted in the Gulf of Corinth to measure conductivity changes in the water column and determine related sound velocity to improve hydroacoustic and electromagnetic data evaluation.

5.2.1 Instrumentation

Both devices the Video-CTD (GEOMAR) and the onboard standard Seabird-CTD system were used to conduct water column studies and near-seafloor monitoring.

Video-CTD Device

The Video-CTD/water sampler rosette (Figure 5.2.1) was equipped with an HD camera system and 3 LED lights, an underwater modem/control unit and a splitter unit connecting a Seabird-CTD device (SBE 9plus, #6) according to Linke et al., 2015. The SBE underwater unit operated two pressure sensors, 2 temperature sensors, 2 oxygen sensors and 2 conductivity sensors. Furthermore, a Wetlabs sensor measuring turbidity and chlorophyll-a, and an altimeter were attached. The SBE underwater unit and Niskin bottle carousel motor were powered with 350 V via the winch's coaxial cable (diameter: 18 mm, length >10 km) by using the modem/power unit from Sea and Sun Technology (S/N 025). Modem connection between the underwater modem unit and control unit was established at 27 dB (9000 kb/s) for upstream and 13 dB (330 kb/s) for downstream broadcasting. The digital video and data telemetry system (Linke et al., 2015) providing real-time monitoring of the seafloor was also used to control the distance to the seafloor in "bottom view" mode. HD videos and HD photography were recorded on the internal memory of the camera. Low-quality streaming videos were used for onboard visual control only.

The water sampler rosette is usually equipped with 12 x 10 L Niskin bottles. However, during the M196 cruise, the Niskin bottle 4 was replaced by a 4H-Jena methane sensor (HydroC-CH4M). The external CH4 sensor was powered by 24 V battery packs, which were attached to the steel frame. Data connection to the SBE underwater unit was established via a 5V/AUX6 connection.
CTD data recording and triggering Niskin bottles were controlled with SEASAVE software (version 7.21) on an external laptop in the onboard dry lab. All CTD data were recorded at 24 Hz. GPS position data was logged in parallel to the CTD data from the NMEA-string of RV METEOR. Hydrocasts and hydrographic data from CTD tracks were processed using SBE software SBE7.22.1. Usually, data files of 1 second bins and 1-meter bins, respectively were created from raw data files and exported to ASCII.

Onboard CTD Device

The onboard water sampler rosette was equipped with a Seabird 9plus CTD, which includes temperature, pressure, conductivity, oxygen, fluorescence, turbidity, and a photosynthetically active radiation sensor (Figure 5.2.1).

The deck unit (11plus V2) supplied DC power to the 9plus CTD, decoded the serial data stream, and passed data to the integrated desktop computer. Seasave Version 7.26.7.107 was used to record and store measured sensor data plus NMEA/GPS data and to trigger water samplers (24 x 10 L).

Fig. 5.2.1 GEOMAR Video-CTD/water sampler rosette device (left) and onboard CTD Device (right).

5.2.2 Data Acquisition

The five hydrocast stations were all conducted within the central part of the Gulf of Corinth (Figure 5.2.2, Table 5.2.1) in the vicinity of the OBEM stations.

Towed Video-CTD tracks on the 17th of December were conducted parallel to the shoreline (Figure 5.2.2) and roughly perpendicular to the active Egion Fault system (e.g. Zygouri et al., 2008). Recorded video files are summarized in Table 12.2.1.

Table 5.2.1 Hydrocasts conducted along the central axis of GoC

ID	Latitude /°N	Longitude / °E	First data scan
CTD1	38.11786	22.85118	11.12.2023 11:57:16
CTD2	38.14828	22.74944	11.12.2023 13:51:45
CTD3	38.17878	22.64622	11.12.2023 15:31:24
CTD4	38.20974	22.54336	11.12.2023 17:08:18
CTD5	38.24024	22.44006	11.12.2023 18:51:00

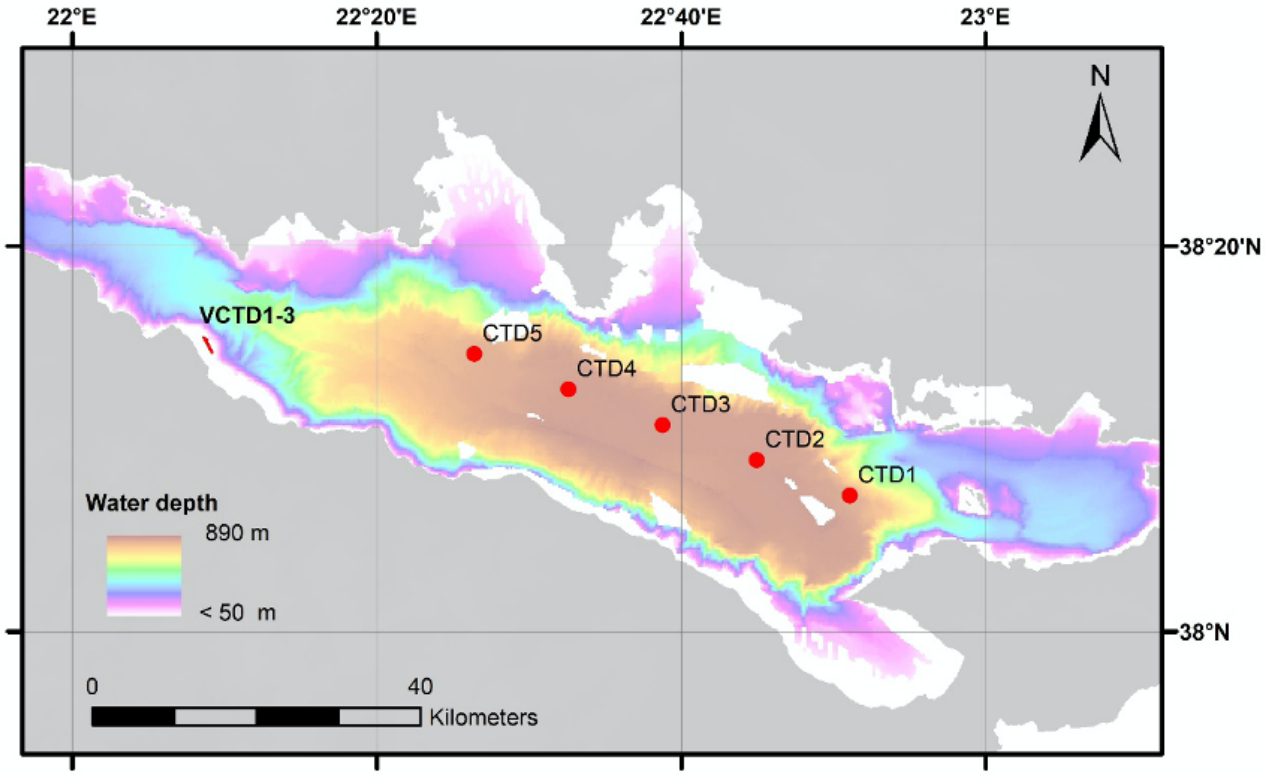

Fig. 5.2.2 Map of five hydrocasts (CTD1-5) and three Video-CTD tracks (VCTD1-3) conducted in the Gulf of Corinth.

5.2.3 Preliminary Results

During the M196 cruise surface water temperatures of 19.06°C and salinity of 39.27 were measured at five CTD stations in the central GoC (CTD1-5, Figure 5.2.2). The CTD-hydrocasts measured in December 2023 (Figure 5.2.3), principally resemble CTD-data recorded in May 1983 (Poulos et al., 1996). The comparability of May and December surface water temperatures in the GoC is also known from other sources (e.g. Rubi et al., 2022). However, our data show a much thicker surface water layer and a thermocline reaching from about 60 m (T~19.04°C) to 120 m (T~14.8°C), when compared to 20 m and a thermocline reaching 60 m as published by Poulos et al., 1996. This new finding possibly questions an effective mixing of the total water column until spring 2024 in the GoC.

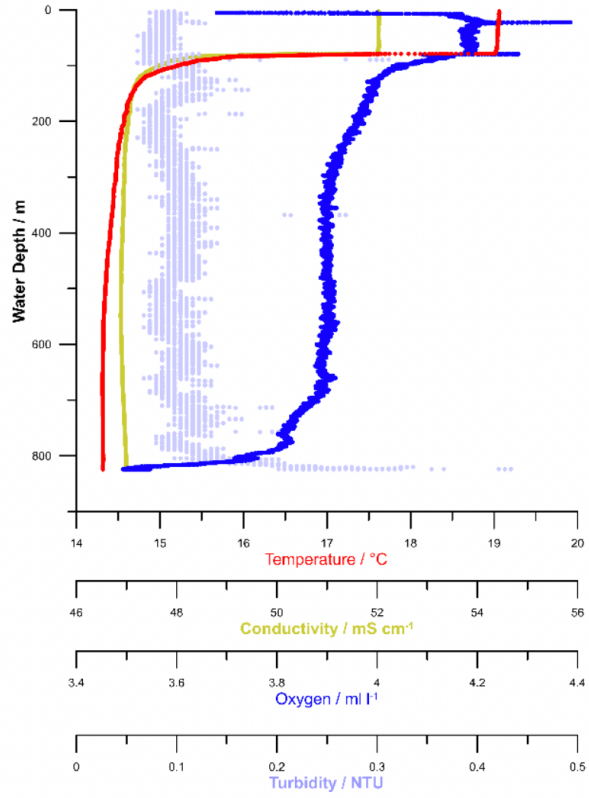
Water Depth / m
0
200
400
600
800
14 15 16 17 18 19 20
Temperature / °C
46 48 50 52 54 56
Conductivity / mS cm-1
3.4 3.6 3.8 4 4.2 4.4
Oxygen / ml l-1
0 0.1 0.2 0.3 0.4 0.5
Turbidity / NTU

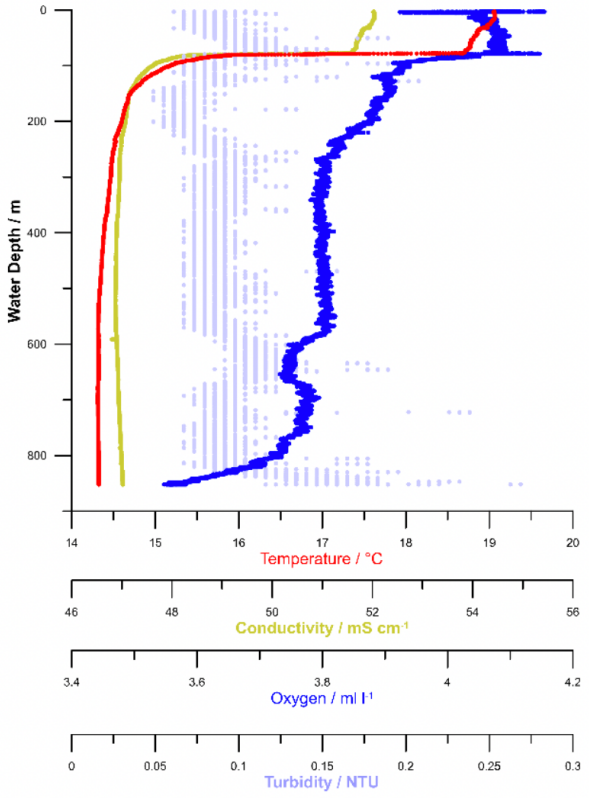
Water Depth / m
0
200
400
600
800
14 15 16 17 18 19 20
Temperature / °C
46 48 50 52 54 56
Conductivity / mS cm-1
3.4 3.6 3.8 4 4.2
Oxygen / ml l-1
0 0.05 0.1 0.15 0.2 0.25 0.3
Turbidity / NTU

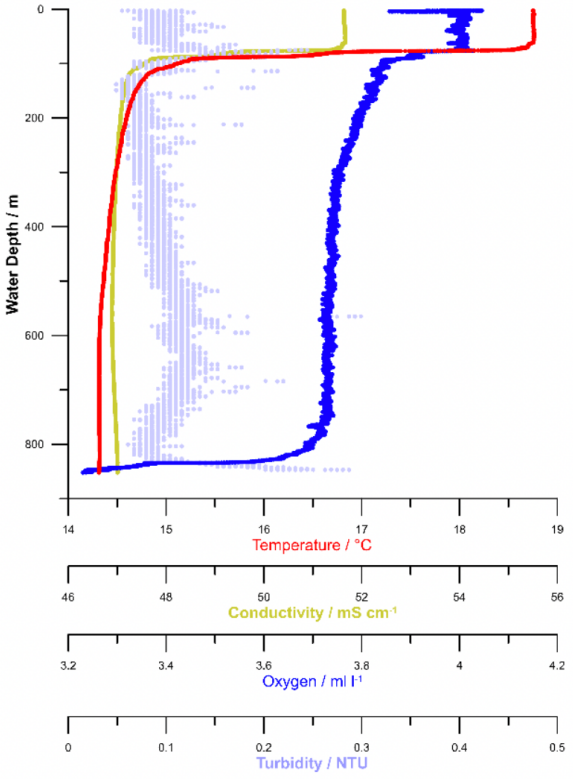
Water Depth / m
0
200
400
600
800
14 15 16 17 18 19
Temperature / °C
46 48 50 52 54 56
Conductivity / mS cm-1
3.2 3.4 3.6 3.8 4 4.2
Oxygen / ml l-1
0 0.1 0.2 0.3 0.4 0.5
Turbidity / NTU

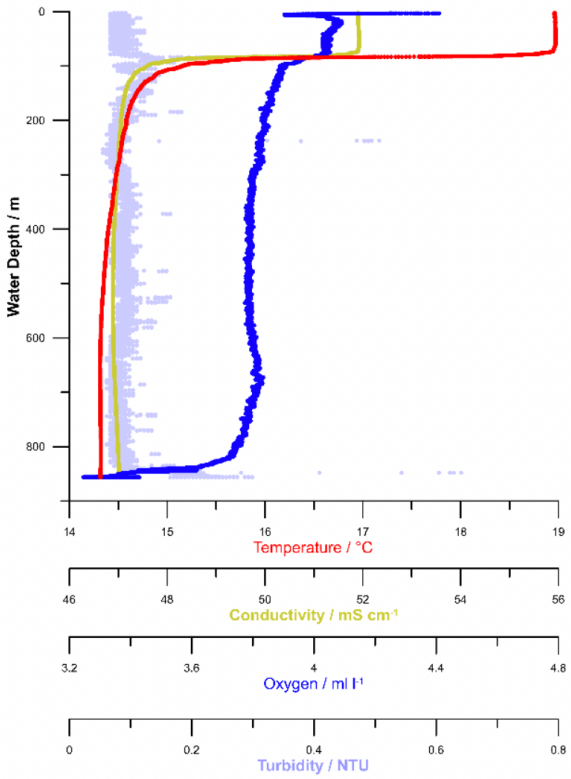
Water Depth / m
0
200
400
600
800
14 15 16 17 18 19
Temperature / °C
46 48 50 52 54 56
Conductivity / mS cm-1
3.2 3.6 4 4.4 4.8
Oxygen / ml l-1
0 0.2 0.4 0.6 0.8
Turbidity / NTU

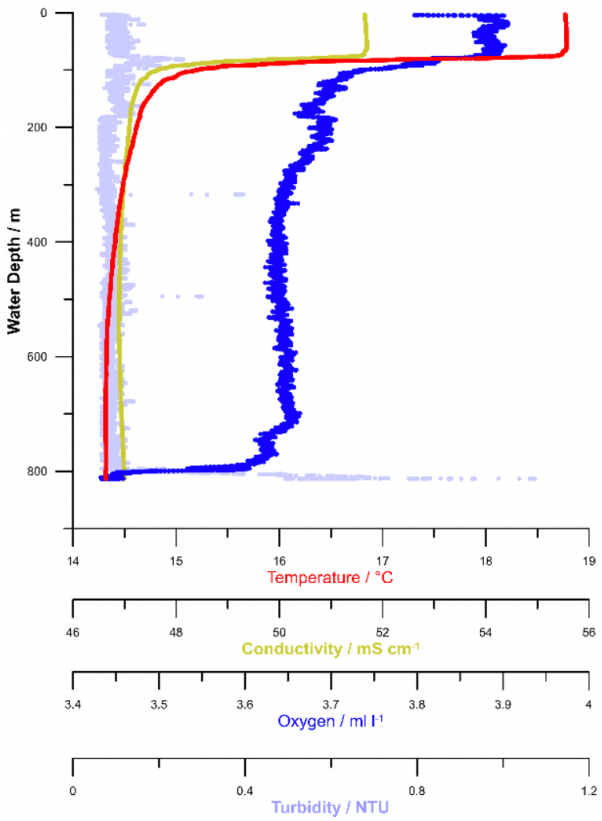

Fig. 5.2.3 Hydrocast data of CTD1-5, recorded along a central profile in the Gulf of Corinth on the 11th of December 2023 (see Figure 5.2.2 for locations).

Homogeneous temperature and salinity values were recorded most of the time when following the planned tracks at 1.5 m distance to the seafloor. However, salinity drops were noticed at two specific sites, a reef structure and a pockmark (Figures 5.2.4 and 5.2.5). The observed living and dead branched corals, sponges, and carbonate(?) hard ground structures are related to measured salinity drops. No other parallel trend was identified at the sites in CTD data, like turbidity changes, methane variations, or depth changes.

The discovered offshore benthic community is possibly comparable to the Holocene reef community described for an onshore carbonate reef (Kershaw et al., 2005). Thus, further investigations are recommended of e.g. a relation to drowned post-glacial intertidal zones (beach-rock formation?) and/or tectonic processes in the Egion Fault system inducing freshwater advection at the discovered pockmark and reef site. Therefore, a diving and sampling campaign heading for freshened fluids and carbonate crusts at shallow depths (<50 m water depth) could be useful.

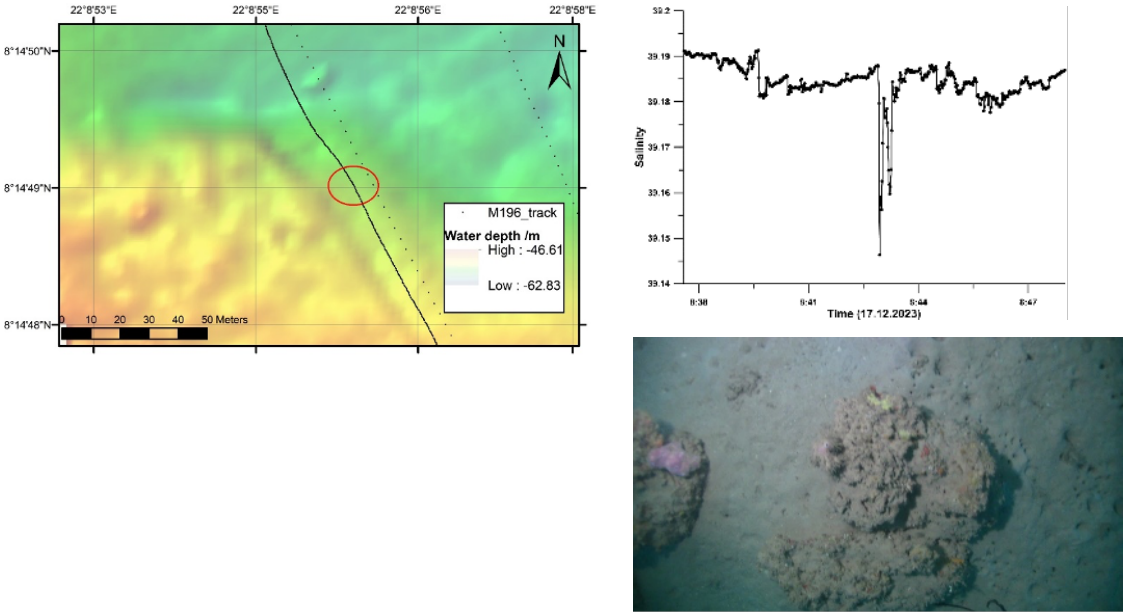

Fig. 5.2.4 Video-CTD observations at a reef structure at the southern Egion fault; Map of VCTD1 track (left); Salinity data 1.5 m above the seafloor (top right). Salinity drop was measured in the area marked by red circle on the left figure; Coral growth on reef structure (bottom right).

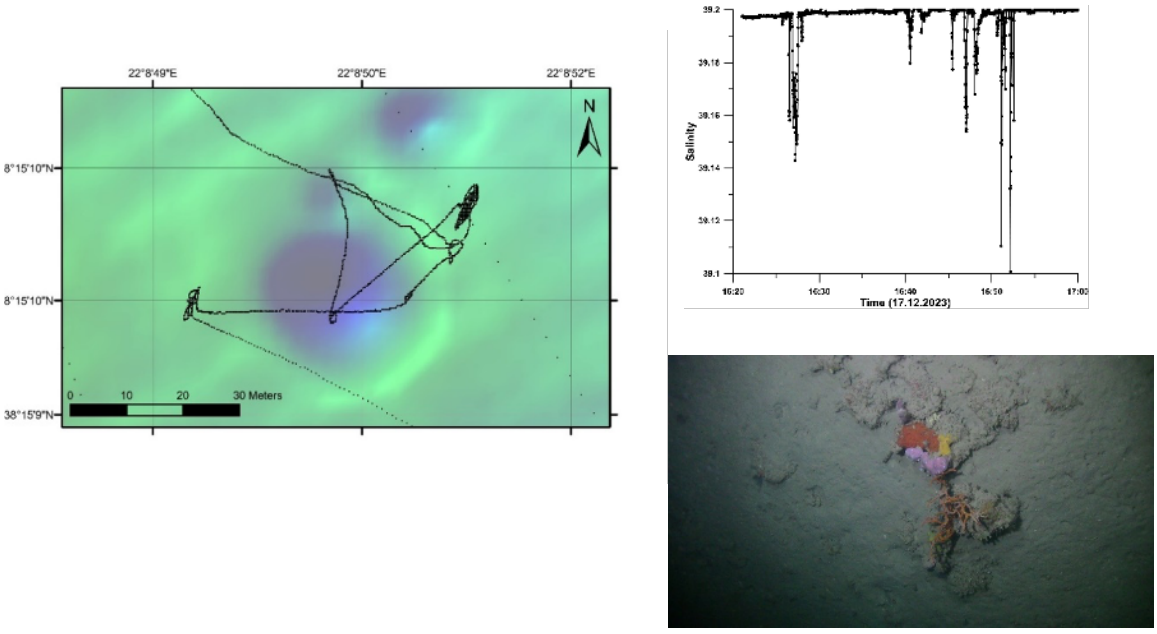

Fig. 5.2.5 Video-CTD observations at a pockmark structure within the Egion fault; Map of seafloor bathymetry and VCTD3 track (left); Salinity data recorded in the pockmark (top right); Coral growth on hard ground at the inner wall of the pockmark (bottom right).

5.3 Sediment and Pore Water Sampling

(T. Müller, D. Sakellariou, D. Christodoulou, D. Patiris, B. Domeyer, R. Surberg, J. Fleer, P. Moser-Roeggla, J. Usinger, M. Schmidt)

The main aim of the geochemical program of M196 was to find evidence for pore water freshening in the near floor sediments of the Gulf of Corinth. This was based on the results of the porewater chemistry of the boreholes of IODP expedition 381, carried out in 2018, where at all three boreholes decreasing salinity values in the upper 10 m of the sediment core were observed. For this reason, sediment cores were taken in the vicinity of the IODP boreholes M0078 and M0079. To combine geophysical and geochemical data, GC were also taken along CSEM-Line 1 which runs from east to west through the GoC, crossing the IODP boreholes. Another goal of the gravity coring was on tackling the marine-lacustrine interface which was expected to be found in the upper 3 m of the sediments in the northern bays, Itea in the west and Antikyra in the east.

The exact coordinates at each location were chosen based on sediment acoustic profiles with the Parasound echo-sounding system. Here acoustic patterns such as the shape and amplitude of the individual reflectors, the character of certain reflector packages, their spacing, and the total sub-bottom penetration were considered.

5.3.1 Instrumentation and Methodology

Gravity Coring

The main sediment coring device applied during M196 was a gravity corer (GC) shown in Figure 5.3.1, which consists of a 1.4 t head-weight and an up to 10 m long steel pipe (in 5-m-barrel increments) and an inner plastic liner.

Fig. 5.3.1 Deployment of Gravity Core during M196 with the core handling rack of the METEOR.

The speed of penetration at the seafloor was between 0.7 and 1.5 m per second. Penetration into and release from the sediments were monitored through cable tension. The device remained in the sediments for ~60 seconds to allow for penetration until it was heaved with a speed of 0.2 to 0.3

m s^{-1} out of the seafloor. The recovered sediment cores were cut in archive and working halves aboard and were subsequently processed at laboratory conditions (22°C).
Twelve GCs were taken (Figure 5.3.2), with water depths between 200 and 850 meters (Table 5.3.1). Sediment lengths from 200 cm to 450 cm have been achieved.

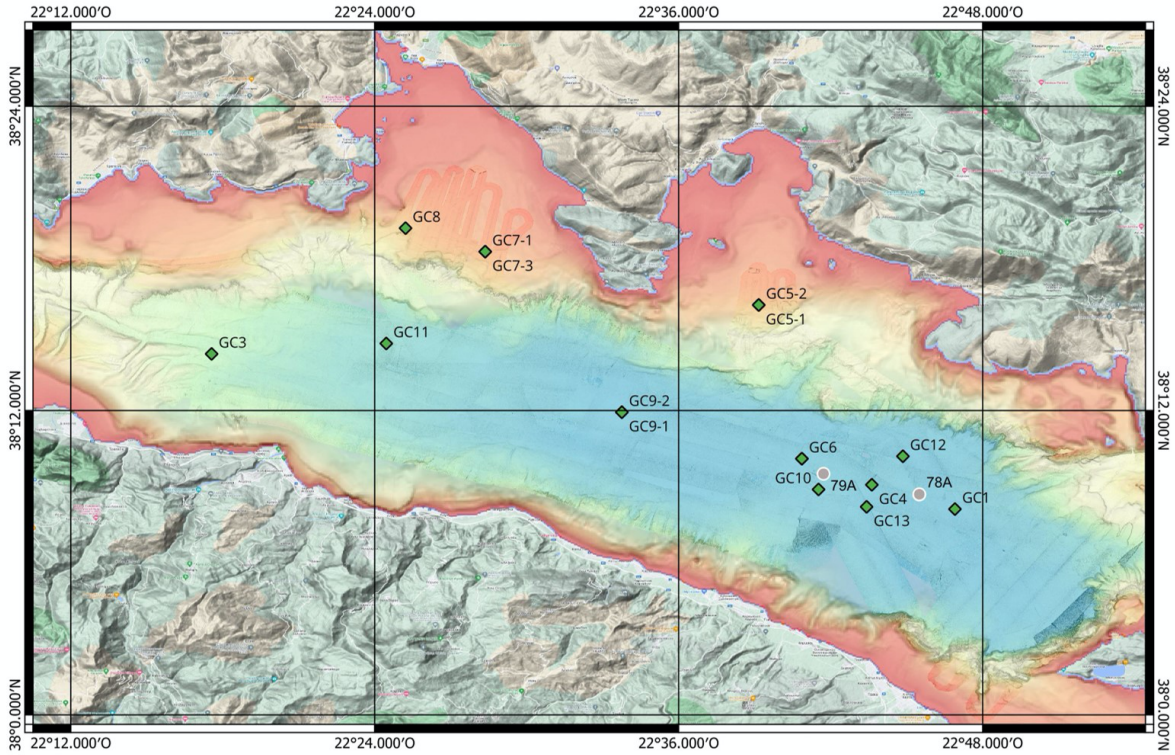

Fig. 5.3.2 GC locations during M196 in the GoC. Grey symbols mark IODP-boreholes 78A and 79A drilled in 2018.

Sediment Core Handling

After being placed on deck, the core catcher of the coring device was removed. When sufficient sediment was left in the core catcher, a Rhizone was placed in it to collect some pore water and a first salinity measurement was carried out using a refractometer (PCE-DRS 2, PCE Instruments, Germany). The 5 m-PVC-liner sections were pulled out of the steel pipes, numbered and cut into 1-m sections. Labelling of the sections and later on for the storage containers (D-tubes) included the following details (Fig 5.3.3):

- Cruise number; station number (e.g. M196 5_1)
- Label A for the archive half; label W for the working half
- Depth interval (in cm)
- Label Top/Base

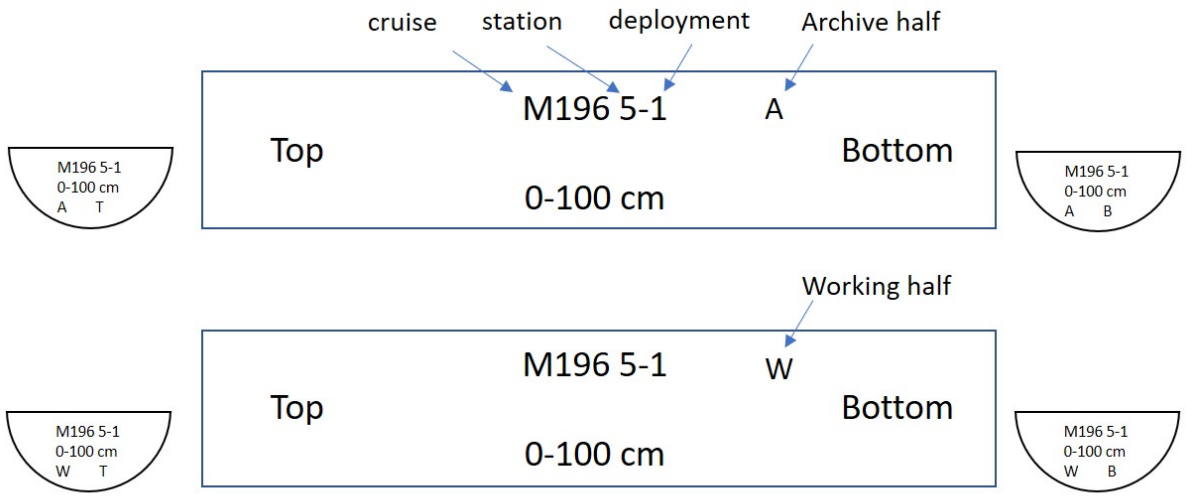

Fig. 5.3.3 Labelling scheme for liners, D-tubes and caps.

Sediment Description

The sediment sections were cut and split lengthwise into a working (W) and an archive (A) half. Once the cores were opened and split, the core sections (archive halves) were photographed and visually described. Sediment description (Figure 5.3.4) of the archive half sections included grain size, sedimentary fabric, colour, sedimentary structure, presence of fossils or fauna, disturbance and/or bioturbation. Sediment colours were determined by using the Geological Rock-Colour Chart (Munsell Color 2009 revised). One log for each gravity core was produced. Once sampling and description were done, the core sections were wrapped in transparency foil and sealed into D-tubes.

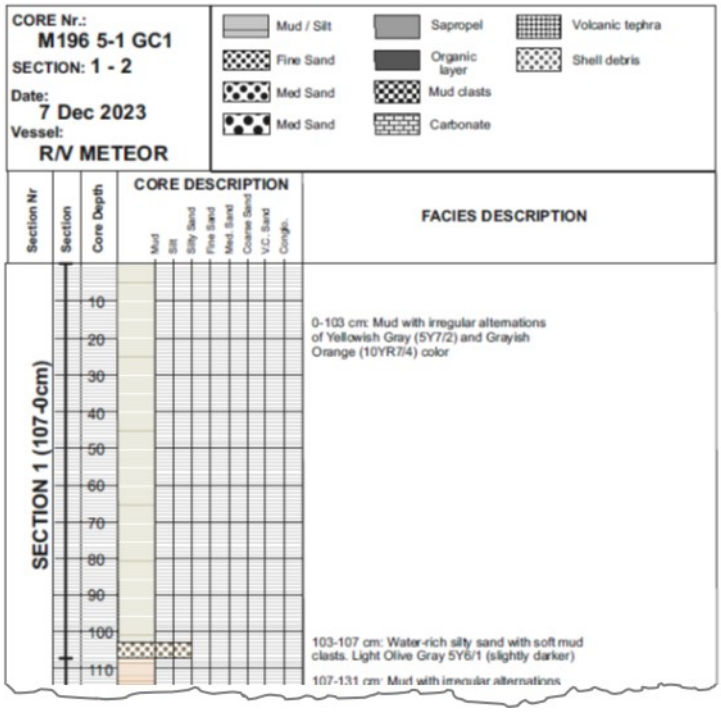

Fig. 5.3.4 Example for sedimentological description of the GCs during M196.

Wet Sediment Subsampling

About 5 ml of wet sediment was taken in approximately 20 cm intervals and were collected in small plastic cups for porosity and TCNS analyses at GEOMAR.
Three milliliters of sediment were taken by a pre-cut plastic syringe and added to 20 ml headspace vials filled with 1.5 g NaCl and 9 ml of saturated NaCl solution (Sommer et al., 2009). Vials were crimped with rubber stoppers and stored after mixing for further gas chromatographic and stable isotope measurements at GEOMAR.

Porewater Sampling

Two different methods were applied to extract pore water from split cores halves. Where the sediment allowed Rhizon-extraction the method according to Seeberg-Elverfeldt et al. (2005) was applied (Figure 5.3.5, left). If not enough pore water for subsampling could be extracted by Rhizones, wet subsamples of the sediment had to be treated by a low-pressure squeezer at an argon pressure of 1 to 7 bar (Figure 5.3.5, right). The extruded pore water was filtered through 0.2 µm Whatman cellulose acetate filters while squeezing and fluids were collected in recipient vials. Aliquots of the collected pore water were sub-sampled for various onboard and further home-based laboratory analyses. Subsamples for ICP-OES analysis were acidified with 10 µl of conc. suprapure HNO_3 per 2 ml of pore water sample (i.e., pH < 1) and ~1.8 ml subsamples for δD-, $\delta^{18}O$-H_2O were taken. All samples for home-based analyses were stored refrigerated and gas-tight.

Fig. 5.3.5 Pore water sampling by Rhizon extraction (left) and with low-pressure squeezer(right).

Chemical Titrations Aboard

Alkalinity of pore water aliquots (1 ml) was immediately determined aboard according to Grasshoff et al. (1999).

Porewater Sampling for Noble Gas Analysis

To extract information about the noble gas concentrations from sediment porewater, samples from a sediment core are taken with a mechanical press, which presses the sediment into airtight copper tubes (Figure 5.3.6). These will then be analysed and processed using the protocol outlined in the work of Tomonaga et al. (2011) and Brennwald et al. (2003) in the noble gas lab at the department of Earth Sciences at ETH Zürich. The core sites for noble gas samples were chosen based on preliminary results from bathymetry and sedimentology onboard as well as from previous results

from the IODP cruise M381 (McNeill et al., 2019). 12 sediment samples were taken at core sites GC6 and GC7.

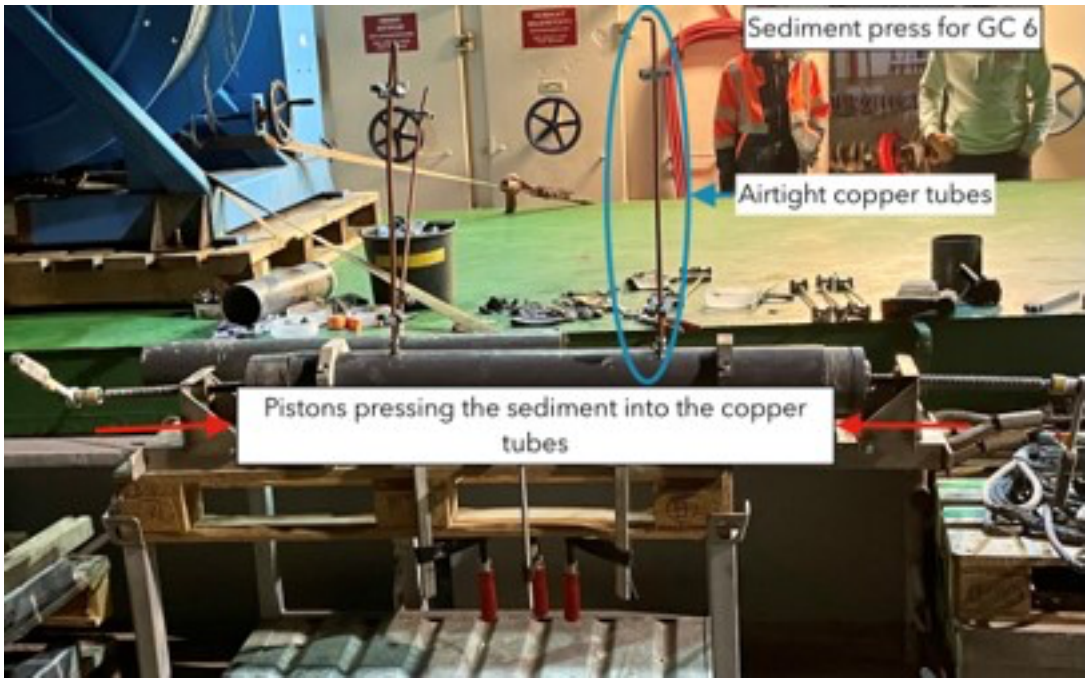

Fig. 5.3.6 Sediment sampling for noble gas analysis.

5.3.2 Data Acquisition

Altogether 20 gravity cores at 13 different sites were recovered across the GoC (Table 5.3.1). A detailed description of the cores is given in Appendix 12.3.

GC 1 - Eastern GoC

The location for GC1 was selected in close proximity to IODP borehole M0078 to confirm the gradient in the porewater (salinity) observed in boreholes M0078 and M0079. Parasound data showed that the first 10 msecs (roughly 8 m) below the seafloor display a multilayered seismic character with high amplitude reflectors alternating with acoustically transparent layers (Figure 12.3.1). This type of seismic stratigraphy reflects a depositional environment with very frequent, vertical changes in the character of the sediments, including various types mud/silt deposits and multiple layers of silty sand to fine and medium sandy layers. The latter are mass transport deposits and turbidites that are very common in the deep basin of the Gulf of Corinth. This seismic and sedimentary stratigraphy is common for all gravity cores recovered during the M196 cruise.

The goal for GC1 was to penetrate 10 m below the seafloor. However, this was proved to be not realistic. The core reached 3.53 m into the light olive gray to light brownish gray mud layers that alternate with relatively thin silty sand to fine sand layers (Figures 12.3.2 and 12.3.3).

GC 2 and GC 3 - Central to Western Part of GoC, North of Akrata

The location of GC2/ GC3 was selected in the axial channel in the western part of the Gulf, with the aim to investigate possible freshened water flow below the thalweg of the channel. The parasound profile (Figure 12.3.4) showed an upper, 1.5-2.0 m thick transparent drape underlain by a sequence of high-amplitude, sub-parallel, semi-prolonged reflectors suggesting a homogenous

muddy upper layer underlain by frequent alternations of sandy and muddy layers GC 2: No material could be collected. The location for GC3 was shifted ~50 m to the east from the location of GC2, still within the axial channel. For GC3 the tube length was changed to 5 m. A 3.67 m long sediment core was recovered at GC3. The core consists mostly of light olive gray to light brownish gray mud with thin layers of silty sand in between (Figures 12.3.5 and 12.3.6).

GC 4 - Eastern GoC, Between M0078 and M0079

The location for GC4 between the IODP boreholes M0078 and M0079 was selected to confirm the porewater gradient (salinity) observed in the upper 10 m of the IODP boreholes. The final coordinates for the GC were chosen from the parasound data (Figure 12.3.7). Sediments consists of brownish to green mud with some sandy silt layers in between. Turbidites have been found at ~90 cm and ~210 cm depth (Figures 12.3.8 and 12.3.9).

GC 5 - Bay of Antikyra

The goal of GC5 was to take a sediment core long enough to reach the marine-lacustrine interface. Based on parasound data (Figure 12.3.10) this section should be located somewhere between 1.5 and 2.0 m. Three cores have been taken at this location all with a pipe length of 5m. GC5_1 was taken with a rope speed of 1.0 m s-, GC5_2 and GC5_3 with a rope speed of 1.2 m s-1. The recovered core sections have been 2.0 m for GC5_1, 2.35 m for GC5_2 and 2.03 m for GC 5_3. GC5_1 was left in the liner and will be processed at the University of Patras. GC5_2 and GC5_3 have been sampled and described. According to the sedimentological description, the interface between the upper, marine deposits and the lower, lacustrine sediments has been found at roughly 140-150 cm below the seabed (Figures 12.3.11 and 12.3.12).

GC 6 - West of M0079

GC6 is located west of the IODP borehole 0079. As for GC1 and GC4, it was the aim to check if the salinity depletion in the porewater in the upper meters of the sediment can also be observed in this area. Based on parasound data the final location for GC6 was selected (Figure 12.3.13). A penetration depth of 364 cm was reached at GC6. Photographical and sedimentological descriptions are displayed in Figures 12.3.14 and 12.3.15.

GC 7 - Bay of Itea

Analogous to GC 5 was the target of this sediment core to reach below the marine-lacustrine interface, this time in the western Bay of Itea. Parasound data (Figure 12.3.16) showed that this interface should be located somewhere between 1.5 and 2.0 m. A penetration depth of 3.07 m was reached at GC7. Photographical and sedimentological descriptions are displayed in Figures 12.3.17 and 12.3.18.

GC 8 – Circular Depression at Bay of Itea

GC 8 has been retrieved from a circular depression found both on multibeam and parasound data (Figure 12.3.19), that was interpreted as a probable pockmark. The aim of GC8 was to investigate possible fluids in the sediments below the bottom of the "pockmark". The core penetrated 4.49 m below the seabed and it consists mostly of mudflows and slumped deposits (Figures 12.3.20 and 12.3.21).

GC 9 Central GoC

GC9 is located in the central part of the Gulf on CSEM-Line 1. Aim was to check if the salinity depletion in the porewater in the upper meters of the sediments can also be observed in the central part of the Gulf. Parasound data (Figure 12.3.22) showed a similar layering as observed at GC6 which is about 6 nm to the east. Similar sediments as in GC6 have been observed at GC9 (Figures 12.3.23 and 12.3.24).

GC 10 Central GoC, the Western End of CSEM Line 1

GC10 is located at the western end of CSEM-Line 1. Aim was to check if the salinity depletion observed in the east (around IODP boreholes M0078/ 0079) can also be observed in the western part of the Gulf. Parasound data (Figure 12.3.25) showed a similar layering as observed at GC9. Photographical and sedimentological descriptions can be found in Figures 12.3.26 and 12.3.27.

GC 11 South of M0079

GC 11 is located ~0.7 nm south of IODP borehole M0079. Parasound data (Figure 12.3.28) show an upper, 1 m thick, transparent drape underlain by multiple, high to medium amplitude, parallel reflectors. The stratigraphy observed in the core verifies the seismic stratigraphy. The upper, homogenous mad layer is followed downcore by alternations of muddy and sandy layers (Figures 12.3.29 and 12.3.30).

GC 12 North of M0078

GC12 is located ~1.5 nm northwest to IODP borehole M0078 in the eastern part of the Gulf. The seismic stratigraphy in the Parasound profile (Figure 12.3.31) and the sediment stratigraphy observed in the core (Figures 12.3.32 and 12.3.33) are similar to ones in the GC11 site, with muddy and sandy layers. The core penetrated 2.63 m below the seabed.

GC 13 South to the Center of M0078/ M0079

The seismic stratigraphy in the Parasound profile (Figure 12.3.34) and the sediment stratigraphy (Figures 12.3.35 and 12.3.36) observed in the core are similar to the ones in GC12 site. The core penetrated 3.40 m below the seabed. Turbidites have been found at ~116 and ~246 cm depth.

Table 5.3.1 Overview of GCs taken at research cruise M196

GC	Station	date	Lat	Lon	depth [m]	Info	Sample	Sample length [cm]
GC1	5-1	07.12.	38° 08,111	22° 46,911	854	close to M0078	porewater, sediment	353
GC2	14-2	08.12.	38° 14,235	22° 18,530	733	prelim. Dimitris	empty, no sample	-
GC3	14-3	08.12.	38° 14,235	22° 18,564	732	prelim. Dimitris	porewater, sediment, sediment 14-C	367
GC4	16-1	10.12.	38° 09,045	22° 43,636	854	between M0078 and M0079	porewater, sediment	321
GC5_1	19-1	11.12.	38° 16,163	22° 39,162	274	Bay of Antikyra, interface marine/ lacustrine sediments	no samples, processed at University of Patras	200
GC5_2	19-2	11.12.	38° 16,161	22° 39,168	247	Bay of Antikyra, interface marine/ lacustrine sediments	porewater, sediment	235
GC5_3	19-3	11.12.	38° 16,163	22° 39,165	248	Bay of Antikyra, interface marine/ lacustrine sediments	porewater, sediment	203
GC6	23-1	12.12.	38° 10,110	22° 40,884	848	west of M0079	porewater, sediment	364
GC6-1	23-2	12.12.	38° 10,110	22° 40,868	848	west of M0079	archive for Univestiy of Patras	343
GC6-2	23-3	12.12.	38° 10,110	22° 40,868	856	west of M0079	samples for noble gas analysis EAWAG	350
GC7-1	26-1	14.12.	38° 18,265	22° 28,365	209	Bay of Itea, marine/ lacustrine interface	foil (only observation)	300
GC7-2	26-2	14.12.	38° 18,265	22° 28,365	220	Bay of Itea, marine/ lacustrine interface	porewater, sediment	307
GC7-3	26-3	14.12.	38° 18,266	22° 28,365	218	Bay of Itea, marine/ lacustrine interface	samples for noble gas analysis EAWAG	300
GC8	26-4	14.12.	38° 19,193	22° 25,219	283	Bay of Itea, Sinkhole structure	porewater, sediment	449
GC9-1	28-1	15.12.	38° 11,935	22° 33,762	850	central Gulf, along CSEM Line 1	porewater, sediment	229
GC9-2	28-2	15.12.	38° 11,933	22° 33,760	850	central Gulf, along CSEM Line 1	archive for University of Patras	230
GC10	31-1	16.12.	38° 14,639	22° 24,465	802	central Gulf, western end of CSEM Line 1	porewater, sediment	314
GC11	32-1	16.12.	38° 08,886	22° 41,526	855	south to M0079	porewater, sediment	264
GC12-1	43-1	19.12.	38° 10,208	22° 44,849	859	north to M0078	porewater, sediment	269
GC13	44-1	19.12.	38° 08,208	22° 43,439	859	south to center between M0078 and M0079	porewater, sediment	340

5.3.3 Preliminary Results

Summary of Sedimentology Description

The gravity cores that are recovered from the deep basin of the Gulf of Corinth (GC-1, -3, -4, -6, -9, -10, -11, -12, -13) are roughly 3 – 3.5 m long and display similar stratigraphy. Mud/silt deposits

prevail in the first 1 – 1.5 m below the seafloor, while the lower part of the cores is characterized by alternations of mud/silt, silty sand and fine to medium sand layers. The coarse grain deposits (silty sand, fine and medium sand) represent mass transport deposits derived from the upper northern and southern slopes of the basin. In many cases the gravity flow layers display gradual decrease of the grain size upwards (from silty/fine sand to silt/mud).
GC-5 in the Bay Antikyra and GC-7 in the Bay of Itea are the only ones that penetrated below the marine mud and reached the lacustrine sediments at roughly 1.5 m below the seafloor. The lake deposits are distinguished from the marine ones due to the change in the colour of the sediments. No varves have been observed in the lacustrine section the cores.

GC-8 is recovered from the bottom of a circular depression in the Bay of Itea that was initially interpreted as a potential pockmark. The core displays mass transport deposits and slumping throughout its entire length. Turbidites as already described or the deep areas of the Gulf were observed in GC1, 4 and 13.

Porewater Salinity

Decreasing porewater salinities in the upper 3m have been observed in GC's 4, 5, 6, 7, 9, 10 and 11 (Figure 5.3.7), thus confirming observations of IODP 381. A more detailed analysis will be possible after laboratory measurements.

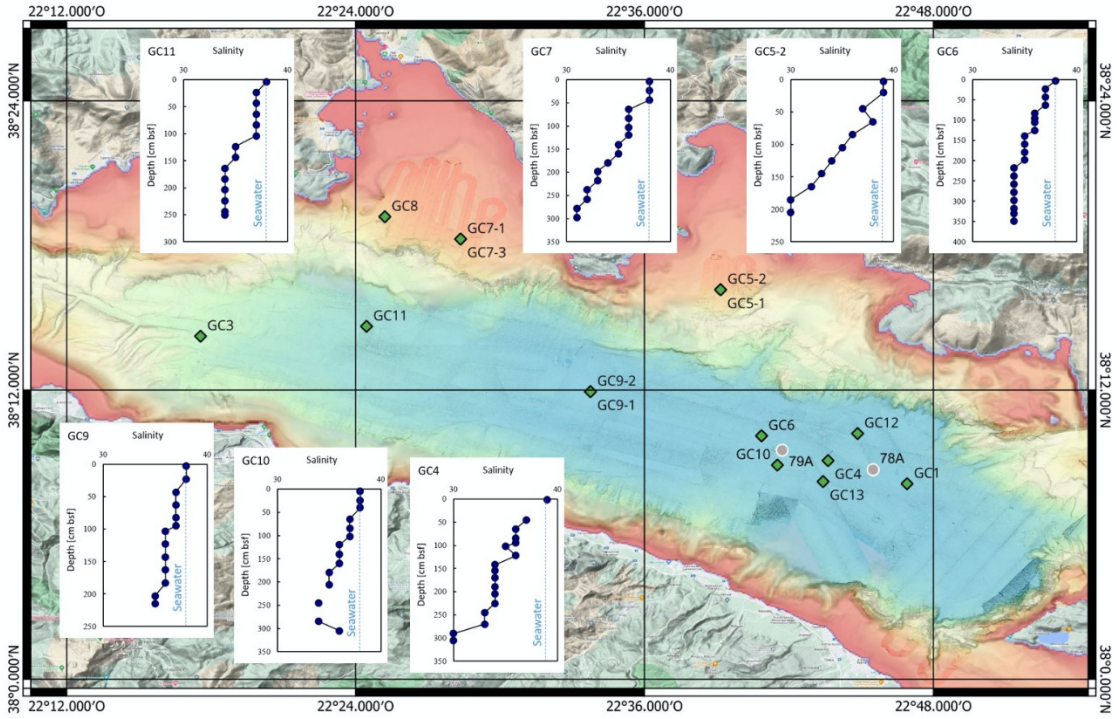

Fig. 5.3.7 GCs showing decreasing salinity profiles in the GoC.

Home-Based Laboratory Analyses

The samples are due to arrive in Kiel at the end of February/beginning of March. They will then be distributed to the respective laboratories (Table 5.3.2). Results for major ions and stable isotopes should be available in Q1 and Q2 2024, noble gases and ^{14}C measurements in Q3 2024.

Table 5.3.2 Planned sediment and porewater analysis of the GCs from M196.

Gravity Core	porosity/ TCNS (GEOMAR)	ICP/ ICP-OES (GEOMAR)	δ^2H/ $\delta^{18}O$ (GZN Erlangen)	noble gases (EAWAG Zürich)	^{14}C (HCMR Anavyssos)
1	x	x	x	-	-
3	x	x	x	-	x
4	x	x	x	-	-
5	x	x	x	-	-
6	x	x	x	x	-
7	x	x	x	x	-
8	x	x	x	-	-
9	x	x	x	-	-
10	x	x	x	-	-
11	x	x	x	-	-
12	x	x	x	-	-
13	x	x	x	-	-

5.4 Hydro Acoustics

(Bruna T. Pandolpho, Monica G. Bucci, Senay Horozal)

5.4.1 Multibeam System Overview and Data Processing

RV METEOR is equipped with two hull-mounted multibeam echosounders from Kongsberg Maritime: the Simrad EM122 operating at 12 kHz which covers water depths from 20 meters below the transducer up to full ocean depth; and the EM710 operating between 40 and 100 kHz for water depths between 3 m and 2000 m below the transducer. The transducers of both multibeam echosounder systems of RV METEOR are mounted in a so-called Mills cross array, where the transmit array is mounted along the length of the ship, and the receive array is mounted across the ship. For RV METEOR the EM122 system is a 1° x 2° design, while the EM710 system is of a 1° x 1° design and has smaller transducers. The system works by detecting echo signals from the seafloor that go through a transceiver unit (Kongsberg Seapath) into the data acquisition computer or operator station into the acquisition software Seafloor Information System (SIS). To determine the point on the seafloor where the acoustic echo is coming from, information about the ship's position, movement, and heading, as well as the sound velocity profile in the water column is required. Positioning is implemented onboard RV METEOR with conventional GPS/GLONASS plus differential GPS (DGPS) by using either DGPS satellites or DGPS land stations resulting in quasi-permanent DGPS positioning of the vessel. Both the ship’s position and its motion also go through the transceiver unit (Seapath) to the operator station where the latter is compensated within the Seapath and SIS. Last, correction regarding the beamforming, which requires sound speed data at the transducer head, is made via a sound velocity probe.

During cruise M196, both the EM122 and EM710 were used throughout the entire cruise to record bathymetric, backscatter and water column data. Data acquisition was set to high-density equidistant and automatic ping mode with the FM (chirp-modulated) pulse enabled for both sounders. In high-density equidistant mode, the EM122 produces 400 beams and the EM710produces 432 beams, regardless of the swath width. During the acquisition, the total swath width on both systems was set between 120° and 140° and survey speed varied between 6 and 8

knots, both settings aimed to prioritize sounding density and quality over coverage. The survey grid was initially set to 40 m for EM122 and 30 m for EM710 but was later altered to 10 m and 12.6 m respectively. Several sound velocity profiles were obtained using an Applied Microsystems (SVPlus V2) sound velocity probe (SVP 1 to 9) and additional sound velocity profiles were converted from the Seabird CTD measurements (CTD 1 to 5) (Figure 5.4.1). Weather conditions allowed for good-quality data. However, the simultaneous use of Parasound and EM710 resulted in interference and therefore deterioration of data quality for the latter, leaving only the EM122 as the final bathymetric product processed on board (Figure 5.4.1).

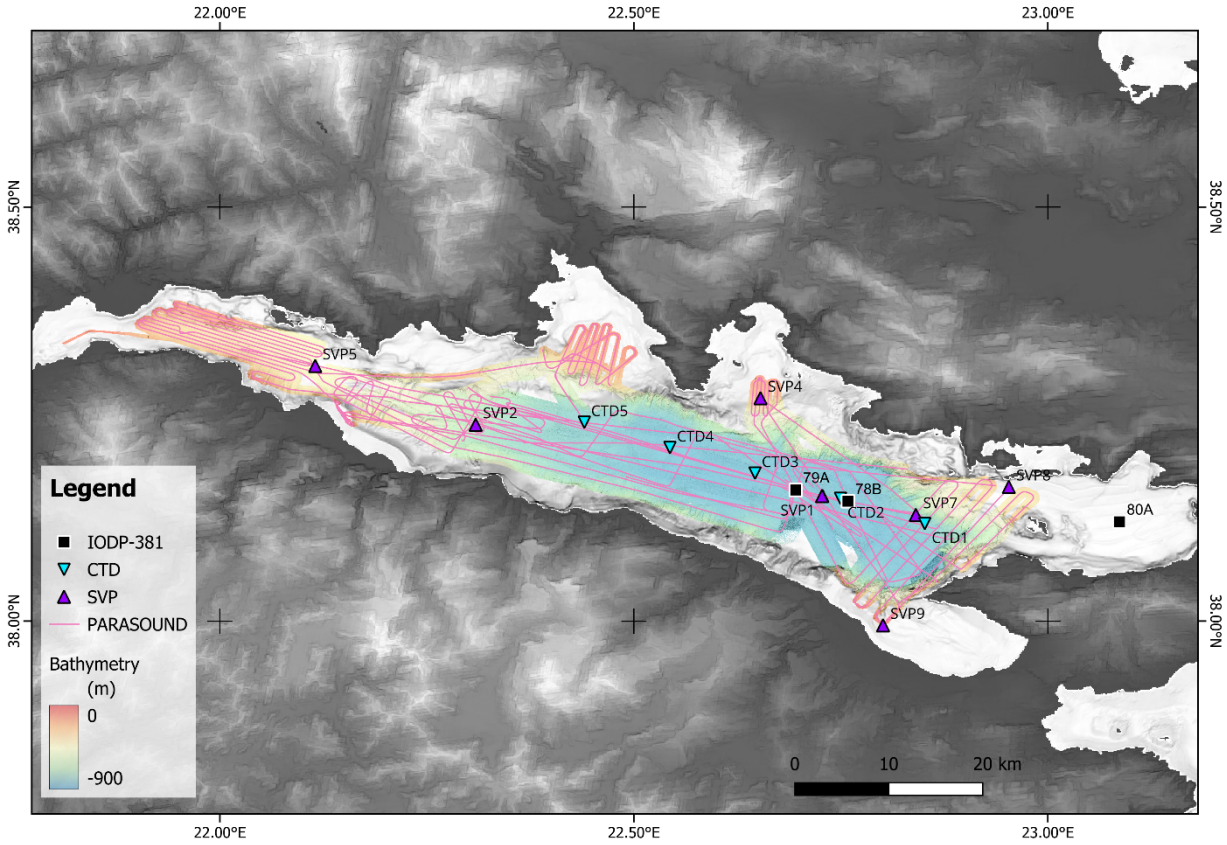

Fig. 5.4.1 Overview map of the total area covered by ship multibeam mapping during M196 (color-coded) including the profiles covered with Parasound and the sound velocity measurements from the SVP (sound velocity profile) probe and CTD. The background shaded relief is EMODNET 2022.

5.4.2 EM122 and EM710 Data Acquisition and Preliminary Results

A total area of approximately 1135 km^2 was mapped during the cruise (Figure 5.4.2a), resulting in 45% coverage of the entire Gulf of Corinth and extending previous bathymetric mapping both to the West and the East of the Gulf. Data processing was carried out onboard using QPS software (Qimera 2.8.4 for bathymetry, FMGT for backscatter data, and Fledermaus Midwater tool for water column data). After loading the raw data (.all files) and the correct sound velocity profile, a dynamic surface was created showing the ship's track and the raw data. The automatic elimination of major erratic data points was done using a spline filter. Furthermore, several tools for the detailed elimination of other erratic data points were used such as the swath editor, 2D editor, and a 3D editor, which enable the operator to process each single beam stepwise. After data cleaning,

a static surface was generated from the dynamic surface creating a .sd file, which was loaded in the QPS Fledermaus software, allowing 3D visualization of the cleaned data. In addition, the data was imported into FMGT to generate backscatter grids. Here, radiometric corrections, filtering, angle-varying gain, anti-aliasing filters and topographic corrections were applied to the backscatter data before outputting a georeferenced mosaic.

During the expedition M196, the processing of the bathymetric data focused on the EM122 data, as the EM710 suffered great interference with the Parasound. The final gridded surfaces in Qimera were exported as a geotiff raster for use with other GIS-related software. The exported soundings were gridded at 10 m resolution, using WGS84 Zone 34N as a coordinate system.

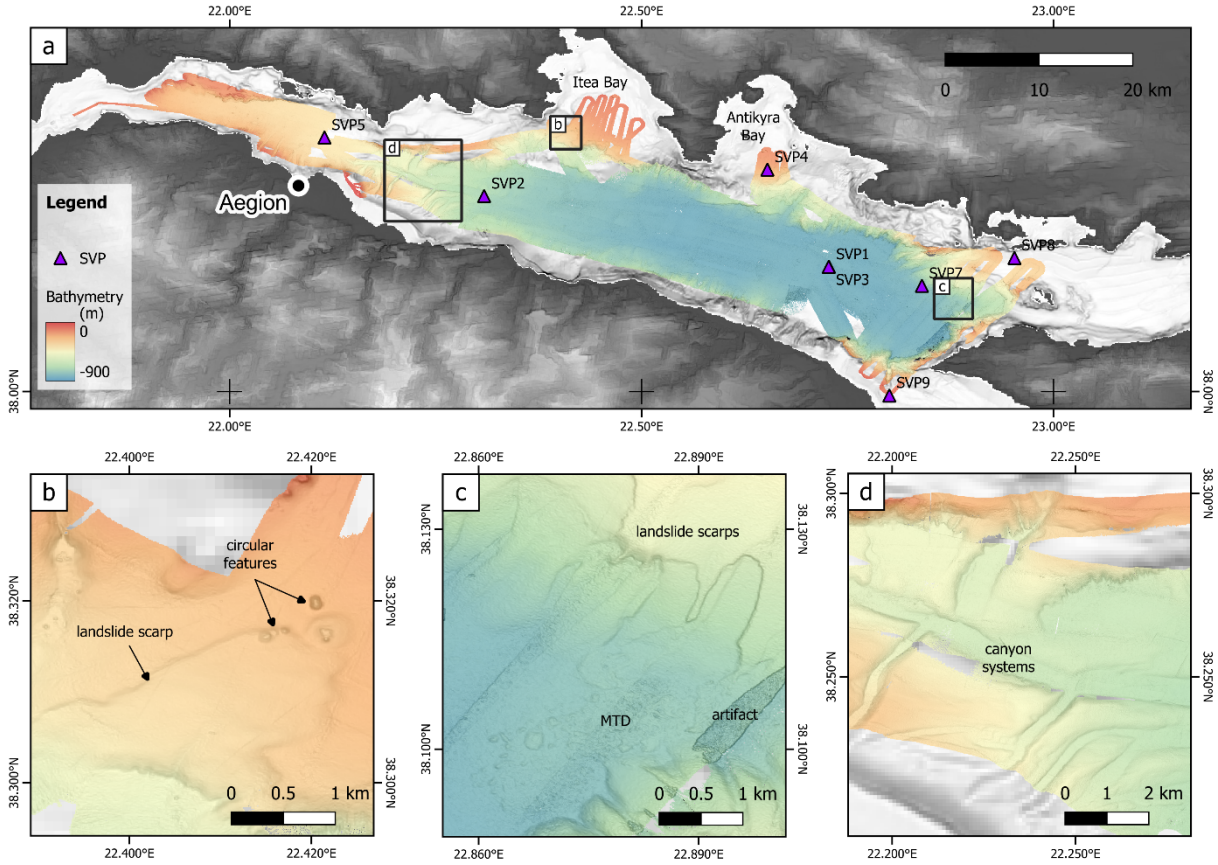

Fig. 5.4.2 (a) Bathymetry map obtained during M196 along with SVP locations used for processing the EM122 (10m grid). (b) Example of landslide scarp and circular features within the headscarp. (c) Examples of landslide scarps and landslide deposit/mass transport deposit (MTD). (d) Example of channels along the slope.

Preliminary interpretation of the mapped area of the Gulf of Corinth shows several landslides scarps, landslide deposits, and erosive channels and gullies along the slope (Figure 5.4.2b). New circular features were identified inside mass failure head scarps within Itea Bay suggesting the potential presence of pockmarks (Figure 5.4.2b). However, upon further investigation, these features were reinterpreted as deep circular-shaped moats formed likely by bottom currents (Figure 5.4.3). Parasound profiles showed drift sediments/contourites (various unconformable curvy beddings that are partially imaged due to repeated erosion and fill). These deposits are seen on the flanks of the deep erosive channels known as moats. The absence of a fluid flow indicator (i.e.,

seismic chimney/pipe) below these circular structures and repeated erosion observed clearly on seismic profiles are evidence that those features are not pockmarks.

5.4.3 Water Column Data Acquisition and Preliminary Results

Water column data was continuously acquired with both EM122 and EM710 sounders, except for the Video-CTD Survey which only EM710 was used aiming at higher resolutions of the water column along the transects upon the pockmark field near the Aegion continental margin (at approximately 20 m water depth). The data was scanned for the occurrences of gas flares using the FMMidwater tool (Version 7.9.4). Analysis was conducted mainly on the areas of known presence of pockmarks near the Aegion continental shelf (Figure 5.4.4) but no presence of gas flares was identified (Figure 5.4.4c). Post-cruise analyses will be undertaken to process all the data to further conclude the occurrences of gas flares and, if possible, define their physical extent (projected seafloor location, height in the water column).

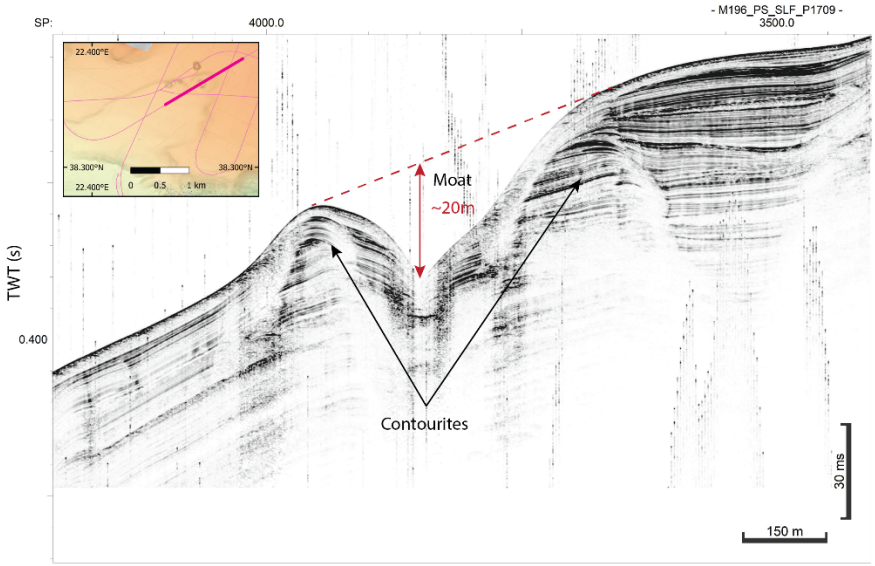

Fig. 5.4.3 Cross-section along one of the circular features seen in the bathymetry reinterpreted as moats. Line P1709.

5.4.4 Parasound Data Acquisition and Preliminary Results

RV METEOR is equipped with an ATLAS Parasound P70 sediment echo-sounding system. Sediment echo-sounding systems (or sub-bottom profilers) are used to image sub-seafloor geological structures such as marine sediment successions, for example. Within the survey area, the system was mainly used for the analysis of sedimentary processes, like the identification of mass transport deposits, background sedimentation, and the presence of pockmarks.

The Parasound on board the RV METEOR utilizes the parametric effect based on the nonlinear relation of pressure and density during sonar wave propagation, meaning that it can generate additional (secondary) low-frequency and high-frequency signals through the interference of its primary frequencies. Hence, the first primary low frequency (PLF) was fixed at 18 kHz whereas the primary high frequency (PHF) can be varied between 18.5 and 24 kHz, resulting in secondary

low frequencies (SLF) between 0.5 – 6 kHz and secondary high frequencies (SHF) between 36.5 – 42 kHz. Essentially, the superposition of the primary frequencies, radiated simultaneously into the water column at very high energy levels, generates the desired secondary signal frequencies. The secondary frequencies can be calculated as the sum (→ SHF) and the difference (→ SLF) of the two primary frequencies and can be optimized to achieve optimum penetration and resolution of the sub-bottom layer (Grant & Schreiber, 1990; Rostek et al., 1991; Wunderlich and Müller, 2003). During M196, PLF & PHF were set as 18 kHz and 22 kHz resulting in SLF & SHF of 4 kHz and 40 kHz, respectively. For sediment penetration, the SLF is of particular interest. However, as both PHF and SHF may also be used for imaging of the water column, this information was also stored.

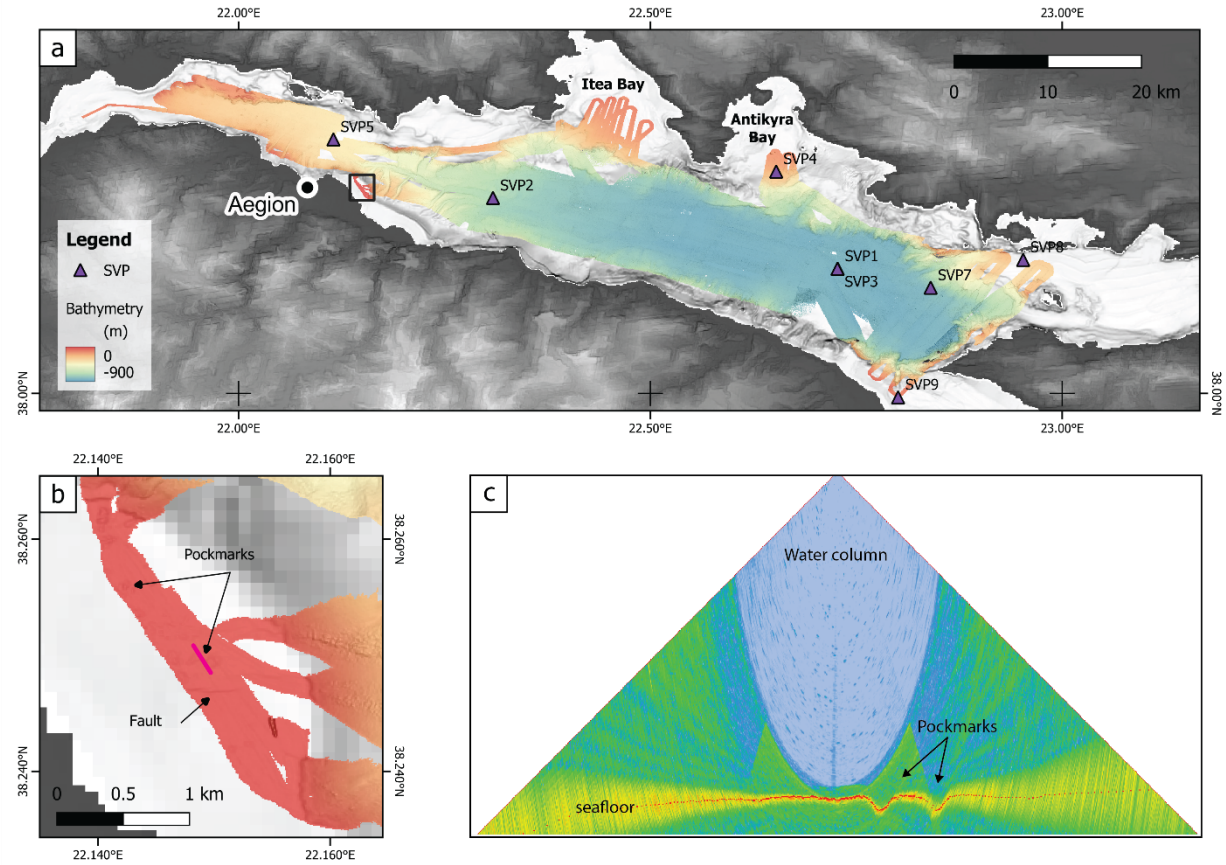

Fig. 5.4.4 (a) Bathymetry map obtained during M196 along with SVP locations used for processing the EM122 (10m grid). (b) Zoom in at the bathymetry along the Video-CTD lines. (c) Water column data (swath view) obtained with EM710 along the Video-CTD lines (pink profile in b). No evidence of seepage (File 0311_20231211_084029_M196_2023.wcd).

To achieve the best results for the study area, different settings were tested at the beginning of the cruise (surveys P100 to P700, Table 5.4.1) including the usage of the external trigger box aiming to avoid interference between EM710 and the Parasound. Unfortunately, the trigger box did not work properly and the data from survey P300-P500 had low sampling and quality and therefore not used. These surveys were later repeated (survey P2500 and P2700). In addition, P600 and P700 were acquired using the carrier frequency mode; however, they could not be opened in the software CodaOctopus from the Greek partners. To ensure good quality and workflow for all on board the final setting was set to use a Quasi-Equidistant Transmission sequence with a PHF

of 22 kHz and SLF of 4 kHz with a minimum pulse rate of 200 ms, and receiver amplification of 35 dB gain for the PHF and 20 dB for the SLF. The water velocity was set to 1500 ms^{-1}. The Oversample Ratio was set to 1 for the PHF and 3.1 for the SLF as a way to improve the data imaging quality. Additionally, an external system depth source (i.e. EM122) was used to maintain a semi-automatic track of the Parasound acquisition window of 200 m starting at 10% of the seafloor depth. Data storage was set to record position as Lat/Lon (ArcSec) and Envelope mode throughout the acquisition, except for survey lines P600/P6001 and P700 which were stored in Carrier Frequency mode. All data was recorded in PS3 and SEG-Y formats. Unfortunately, the software package ps32sgy (Hanno Keil, Uni Bremen) did not work during the cruise and the SEG-Y data was used instead. The SEG-Y files were merged into their respective survey profiles using the software Seaview-Moga and loaded into the seismic interpretation software IHS Kingdom.

While the PHF can be used to image gas bubbles, plankton, or fish in the water column, for the purpose of expedition M196, we primarily focused on the SLF for imaging the subsurface, further geologic interpretation, and choosing the Gravity Core locations. In total, nearly 1541 km of generally high-quality Parasound data were acquired continuously along pre-set profiles or transits between stations. Yet, no data was collected while the vessel was under 1-knot speed (e.g. during CSEM transects or Video-CTD), stationary (e.g. during coring, CTD measurements, or ROV work), or during OBEM deployment, recovery, and triangulation.

Table 5.4.1 Parasound settings used during M196. For all the surveys, PHF was set at 22 kHz and SLF at 4 kHz.

Survey	PS Setting		PS Storage			
	Transmission	Pulse Rate	Storage mode	Position	Window Length	Oversample Ratio
P100-200	Quasi-Equidistant	200 ms	Envelope	Lat/Long	200 ms	1 (PHF and SLF)
P300-500	Trigger box on – no data collected					
P600-700	Quasi-Equidistant	200 ms	Carrier Frequency	Lat/Long	300 ms	1 (PHF and SLF)
P800-4000	Quasi-Equidistant	200 ms	Envelope	Lat/Long	200 ms	1 (PHF) and 3.1 (SLF)

Parasound preliminary interpretation in the Gulf of Corinth was able to reveal several mass transport deposits (MTDs) close to the slope (Figure 5.4.5), plan-parallel stratification in the basin, and normal faults within the eastern deep basin (Figure 5.4.6). Several channels along the western basin and landslide scars along the slope were imaged (Figure 5.4.7).

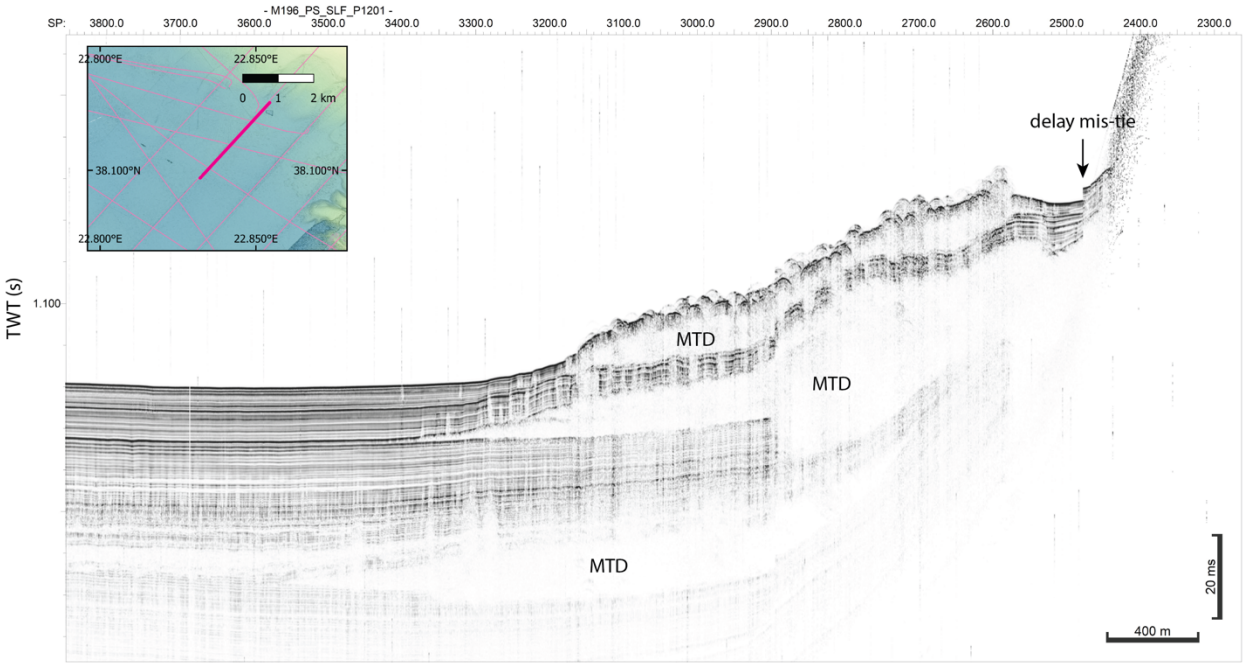

Fig. 5.4.5 Mass transport deposits (MTDs) within the eastern basin. Line P1201.

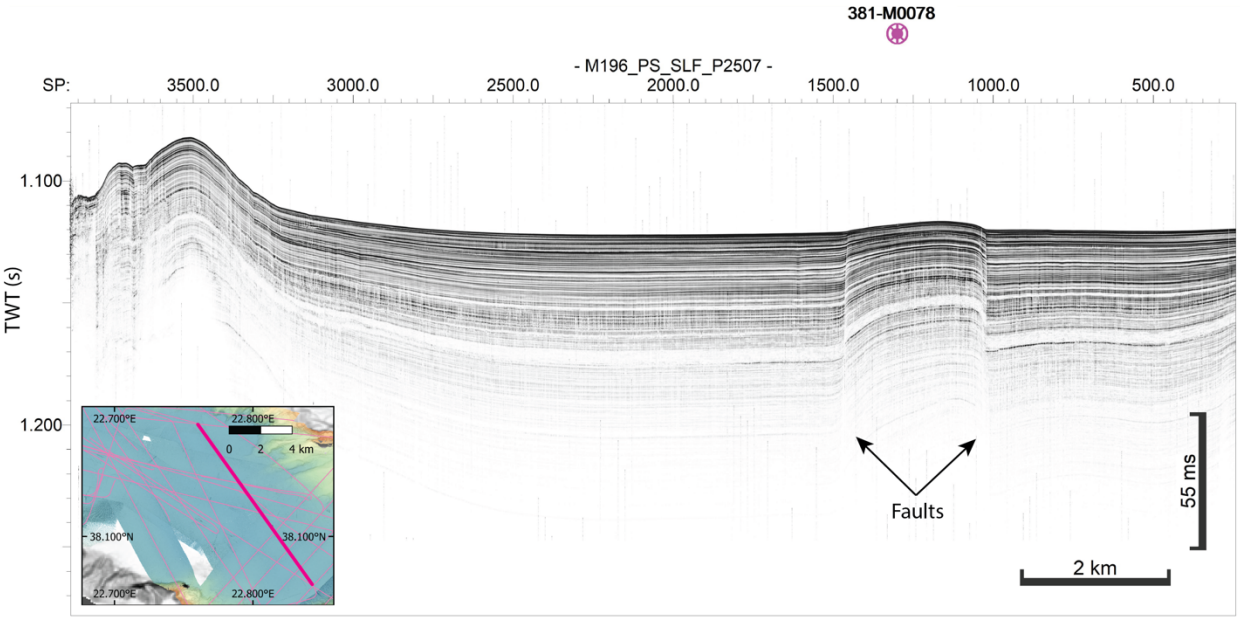

Fig. 5.4.6 Plan-parallel stratigraphy at the deep basin. IODP well from expedition 381 positioned between the faults. Line P2507.

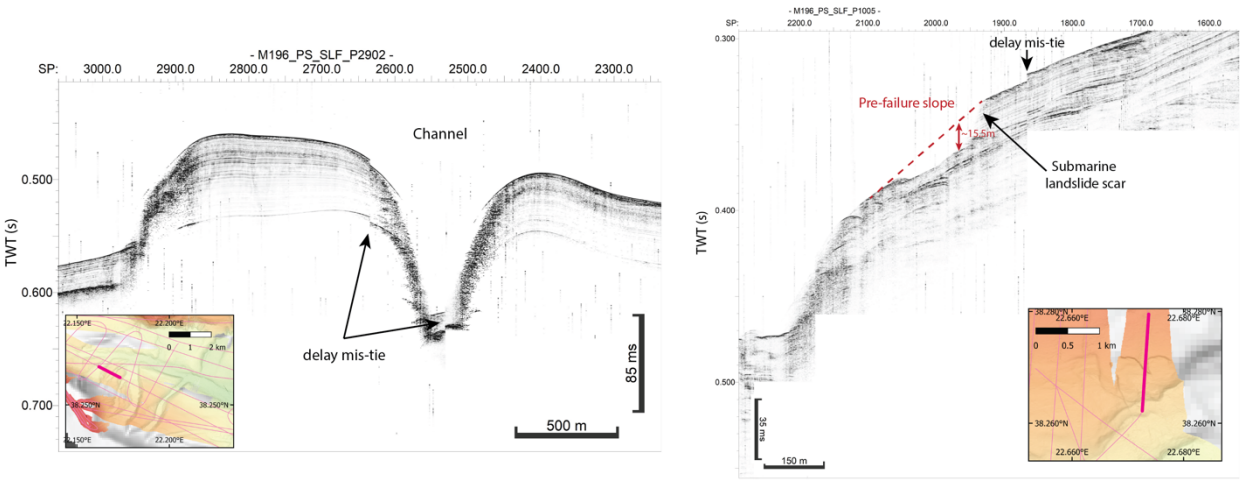

Fig. 5.4.7 Channel feature within the western basin (Line P2902 on the left). Landslide scar on the right (Line P1005).

6 Ship's Meteorological Station

(Michael Mertens, DWD)

The M196 research cruise was generally characterised by windy weather and frequent changes between high and low pressure systems dominating the Gulf of Corinth.

We left the port of Piraeus on 05.12.23 with sunshine and light winds of around 3 Bft. However, clouds increased in the evening and showers and thunderstorms developed overnight. The wind increased significantly to 5 to 7 Bft and gale force wind gusts of up to 39 knots (Bft 8) were recorded in the vicinity of thunderstorms. The sea increased to 1.5 to 2 metres, with a swell of around 1 to 1.5 metres from the west to southwest, with a period of 6 to 7 seconds. During the afternoon on the 6th of December, wind and swell eased quickly in the lee of the Ionian Islands.

For most of the rest of the research cruise, winds in the Gulf were blowing from two prevailing wind directions, easterly winds and westerly winds (see Figure 6.1). The winds in the Gulf of Corinth are dominated by local, mesoscale effects, particularly by the local topography. The highest wind speeds recorded were from northwest to west. However, this does not apply to the easternmost Gulf, where northeasterly winds can blow similarly strong. This is also due to the local topography there.

The atmospheric models that were available were not able to correctly forecast these wind systems and proved to be of little use for most of the research cruise. To provide useful and accurate weather forecast for the ship and scientific leadership on board, expert meteorological knowledge was required, together with the use of modelled pressure gradients, the observed local characteristics of the wind and the local knowledge of the Greek scientists on board.

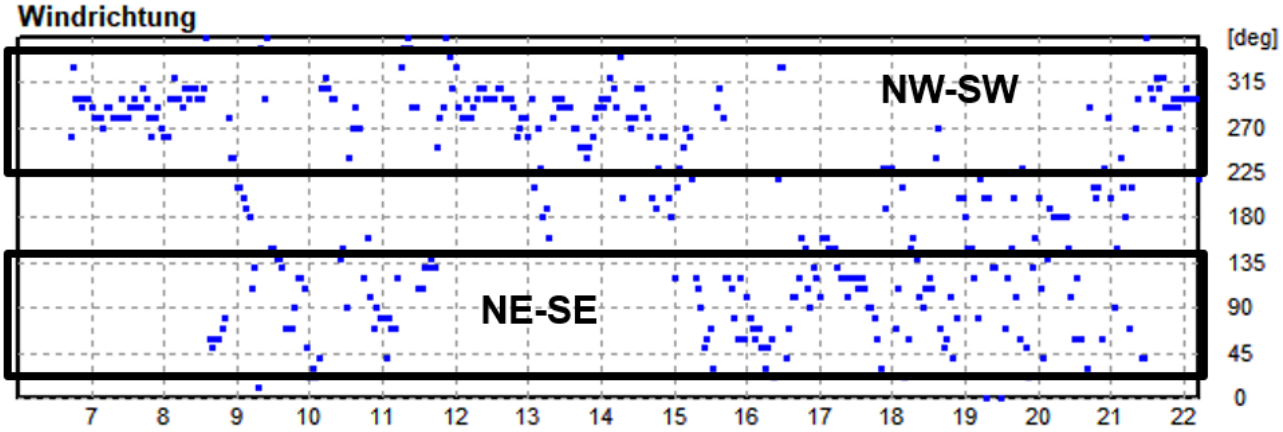

Fig. 6.1 Observed wind directions in the Gulf of Corinth (x-axis date, y-axis wind direction)

Overall, the following correlation between air pressure and wind distribution was observed: When there is high pressure over the Ionian Sea/the Ionian Islands, the wind over the Gulf blows from westerly directions; when there is high pressure in the Aegean Sea, the wind blows from northeasterly to easterly directions.

Strong winds of ≥ 6 Bft from west to northwest were observed on 07.12., 08.12. (however, in the evening from NE in the easternmost Gulf), 12.12., 13.12. and 14.12.

Strong winds of ≥ 6 Bft from easterly directions were observed on 08.12. (in the evening in the easternmost Gulf), 17.12. and 18.12.

Particularly noteworthy are 12.12., 14.12. and 16.12., when the wind reached 8 Bft at times, and the sea in the Gulf rose to 1.5 m to 2 m. Otherwise, waves were not significant, because the fetch in the Gulf, in most situations, is not long enough for a significant sea and swell to build. The strongest wind gusts were also recorded on the days mentioned above (with the exception of the 6th of December). We observed 36 kt (Bft 8) on the 12th of December, 41 kt (Bft 9) on the 14th of December and 40 kt (8 Bft) on the 16th of December.

Particularly light winds were recorded on the 10th of December, 19th of December and 20th of December, when winds were ≤ 3 Bft for long periods and the sea was smooth at times.

On 14.12., a southerly wind advected Saharan dust into the region. This caused the general visibility to dip to 10 km at times without precipitation and the sunset to be milky white.

Noteworthy precipitation was only recorded during the night from 10.12. to 11.12. with some rain, on 16.12. with showers during cold air advection (snow fell down to around 900 m) and from 20.12. in the evening to 22.12. in the afternoon, again with some showers.

The transit from Patras to Limassol was mostly fine. Only initially we observed seas of up to 2.5 m, with a westerly swell of around 2 m, a period of 6 to 8 s and westerly to northwesterly winds of 5 to 6 Bft. Further east and later on during the transit, seas, swells and winds eased gradually so that the sea became smooth at times.

I would like to take this opportunity to express my particular gratitude to the ship's command and chief scientist on board. The close and productive collaboration and the open, collegial and frequent communication contributed to the success of the research cruise.

Fig. 6.2 Gulf of Corinth, 08.12.23.

7 Station List M196

7.1 Overall Station List

Station	Date	Device	Time UTC	Action	Latitude N	Longitude E	Depth (m)	Comment
M196_1-1	06/12/2023	Sound Velocity Profiler	20:10	in the water	38° 14,971'	022° 22,674'	0	
M196_1-1	06/12/2023	Sound Velocity Profiler	20:28	max depth/on ground	38° 14,970'	022° 22,675'	0	SLmax = 700m
M196_1-1	06/12/2023	Sound Velocity Profiler	21:31	on deck	38° 14,971'	022° 22,678'	0	
M196_2-1	06/12/2023	Ocean bottom electro-magnetic receiver	23:20	in the water	38° 14,973'	022° 22,676'	0	W10, Posidonia Kalibrierung mit OBEM
M196_2-1	06/12/2023	Ocean bottom electro-magnetic receiver	23:30	information	38° 14,973'	022° 22,676'	0	Posidonia zu Wasser
M196_2-1	06/12/2023	Ocean bottom electro-magnetic receiver	23:55	max depth/on ground	38° 14,973'	022° 22,676'	0	SLmax = 100m
M196_2-1	07/12/2023	Ocean bottom electro-magnetic receiver	00:18	on deck	38° 14,973'	022° 22,676'	0	OBEM wieder an Deck, Test abgebrochen
M196_3-1	07/12/2023	Deep-sea Multibeam Echosounder	01:25	profile start	38° 16,382'	022° 18,440'	621	
M196_3-1	07/12/2023	Deep-sea Multibeam Echosounder	06:03	profile end	38° 06,681'	022° 51,827'	808	
M196_3-2	07/12/2023	Shallow-water Multibeam Echosounder	01:25	profile start	38° 16,377'	022° 18,448'	625	
M196_3-2	07/12/2023	Shallow-water Multibeam Echosounder	06:03	profile end	38° 06,679'	022° 51,837'	807	

M196_3-3	07/12/2023	P-70 Parasound	01:54	profile start	38° 15,328'	022° 22,081'	761	
M196_3-3	07/12/2023	P-70 Parasound	06:03	profile end	38° 06,677'	022° 51,855'	808	
M196_4-1	07/12/2023	Sound Velocity Profiler	07:20	in the water	38° 09,085'	022° 43,646'	845	W11
M196_4-1	07/12/2023	Sound Velocity Profiler	07:39	max depth/on ground	38° 09,086'	022° 43,648'	841	SLmax = 750m, SZmax = 15,0kN
M196_4-1	07/12/2023	Sound Velocity Profiler	07:58	on deck	38° 09,087'	022° 43,648'	844	
M196_5-1	07/12/2023	Gravity Corer	08:53	in the water	38° 08,110'	022° 46,908'	862	W11
M196_5-1	07/12/2023	Gravity Corer	09:14	max depth/on ground	38° 08,112'	022° 46,911'	0	SLmax = 864m, SZmax = 40,5kN
M196_5-1	07/12/2023	Gravity Corer	09:37	on deck	38° 08,110'	022° 46,908'	857	
M196_6-1	07/12/2023	Ocean bottom electro-magnetic receiver	12:27	in the water	38° 08,048'	022° 47,618'	864	W11, OBEM 6
M196_6-1	07/12/2023	Ocean bottom electro-magnetic receiver	13:08	max depth/on ground	38° 08,049'	022° 47,618'	0	SLmax = 800,6 m
M196_6-1	07/12/2023	Ocean bottom electro-magnetic receiver	13:26	on deck	38° 08,049'	022° 47,618'	0	
M196_7-1	07/12/2023	Ocean bottom electro-magnetic receiver	14:42	in the water	38° 09,852'	022° 39,883'	861	W11, OBEM 5
M196_7-1	07/12/2023	Ocean bottom electro-magnetic receiver	15:14	max depth/on ground	38° 09,852'	022° 39,883'	862	SLmax = 800m, released
M196_7-1	07/12/2023	Ocean bottom electro-magnetic receiver	15:31	on deck	38° 09,853'	022° 39,884'	861	
M196_8-1	07/12/2023	Ocean bottom electro-magnetic receiver	16:35	in the water	38° 11,386'	022° 33,432'	865	W11, OBEM 4
M196_8-1	07/12/2023	Ocean bottom electro-magnetic receiver	17:07	max depth/on ground	38° 11,398'	022° 33,382'	865	W11, released
M196_8-1	07/12/2023	Ocean bottom electro-magnetic receiver	17:28	on deck	38° 11,399'	022° 33,384'	863	Releaser geöffnet, OBEM verhakt und wieder bis zur Oberfläche gehievt, OBEM an Oberfläche auf Tiefe gegangen
M196_9-1	07/12/2023	Ocean bottom electro-magnetic receiver	18:36	in the water	38° 13,308'	022° 27,270'	827	
M196_10-1	07/12/2023	Ocean bottom electro-magnetic receiver	19:47	in the water	38° 14,850'	022° 23,023'	798	
M196_11-1	07/12/2023	Ocean bottom electro-magnetic receiver	20:14	in the water	38° 14,972'	022° 22,675'	795	

M196_11-1	07/12/2023	Ocean bottom electro-magnetic receiver	20:44	max depth/on ground	38° 14,976'	022° 22,677'	794	SLmax = 750m, SZmax = 11,4kN
M196_11-1	07/12/2023	Ocean bottom electro-magnetic receiver	21:51	information	38° 14,970'	022° 22,707'	0	Beginn Kalibrierung
M196_11-1	08/12/2023	Ocean bottom electro-magnetic receiver	05:05	information	38° 14,718'	022° 23,136'	791	released
M196_11-1	08/12/2023	Ocean bottom electro-magnetic receiver	05:34	on deck	38° 14,932'	022° 22,787'	0	
M196_12-1	08/12/2023	Deep-sea Multibeam Echosounder	00:52	profile start	38° 14,848'	022° 16,323'	698	
M196_12-1	08/12/2023	Deep-sea Multibeam Echosounder	04:20	profile end	38° 15,363'	022° 21,208'	754	
M196_12-2	08/12/2023	Shallow-water Multibeam Echosounder	00:52	profile start	38° 14,842'	022° 16,340'	698	
M196_12-2	08/12/2023	Shallow-water Multibeam Echosounder	04:00	profile end	38° 14,808'	022° 21,950'	782	
M196_12-3	08/12/2023	P-70 Parasound	00:52	profile start	38° 14,831'	022° 16,369'	698	
M196_12-3	08/12/2023	P-70 Parasound	04:20	profile end	38° 15,370'	022° 21,203'	753	
M196_13-1	08/12/2023	Ocean bottom electro-magnetic receiver	07:37	in the water	38° 16,399'	022° 18,377'	630	
M196_14-1	08/12/2023	Sound Velocity Profiler	08:29	in the water	38° 14,236'	022° 18,530'	732	W11
M196_14-1	08/12/2023	Sound Velocity Profiler	08:49	max depth/on ground	38° 14,235'	022° 18,529'	732	
M196_14-1	08/12/2023	Sound Velocity Profiler	09:06	on deck	38° 14,235'	022° 18,529'	732	
M196_14-2	08/12/2023	Gravity Corer	09:23	in the water	38° 14,235'	022° 18,529'	733	
M196_14-2	08/12/2023	Gravity Corer	09:37	max depth/on ground	38° 14,235'	022° 18,529'	732	
M196_14-2	08/12/2023	Gravity Corer	09:56	on deck	38° 14,234'	022° 18,529'	732	
M196_14-3	08/12/2023	Gravity Corer	10:27	in the water	38° 14,235'	022° 18,565'	734	W11
M196_14-3	08/12/2023	Gravity Corer	10:42	max depth/on ground	38° 14,233'	022° 18,561'	733	SLmax = 737m, SZmax = 39,6kN
M196_14-3	08/12/2023	Gravity Corer	11:00	on deck	38° 14,235'	022° 18,561'	732	
M196_15-1	08/12/2023	Controlled Source Electromagnetics	15:52	in the water	38° 06,594'	022° 52,742'	786	Kettenvorlauf
M196_15-1	08/12/2023	Controlled Source Electromagnetics	15:52	in the water	38° 06,601'	022° 52,712'	791	Receiver 4
M196_15-1	08/12/2023	Controlled Source Electromagnetics	16:22	in the water	38° 06,744'	022° 52,097'	0	Receiver 3
M196_15-1	08/12/2023	Controlled Source Electromagnetics	16:41	in the water	38° 06,842'	022° 51,860'	0	Receiver 2
M196_15-1	08/12/2023	Controlled Source Electromagnetics	17:06	in the water	38° 06,948'	022° 51,472'	0	Receiver 1
M196_15-1	08/12/2023	Controlled Source Electromagnetics	17:22	in the water	38° 07,026'	022° 51,235'	0	Elektrode 1
M196_15-1	08/12/2023	Controlled Source Electromagnetics	17:34	in the water	38° 07,081'	022° 51,081'	0	Elektrode 2
M196_15-1	08/12/2023	Controlled Source Electromagnetics	18:02	in the water	38° 07,176'	022° 50,720'	0	Schwein

M196_15-1	08/12/2023	Controlled Source Electromagnetics	19:30	profile start	38° 07,404'	022° 49,979'	0	
M196_15-1	10/12/2023	Controlled Source Electromagnetics	04:31	profile end	38° 16,034'	022° 21,076'	0	
M196_15-1	10/12/2023	Controlled Source Electromagnetics	06:18	on deck	38° 16,466'	022° 19,580'	0	Schwein
M196_15-1	10/12/2023	Controlled Source Electromagnetics	06:35	on deck	38° 16,532'	022° 19,346'	0	Elektronde 2
M196_15-1	10/12/2023	Controlled Source Electromagnetics	06:48	on deck	38° 16,584'	022° 19,169'	0	Elektrode 1
M196_15-1	10/12/2023	Controlled Source Electromagnetics	07:04	on deck	38° 16,650'	022° 18,941'	0	Receiver 1
M196_15-1	10/12/2023	Controlled Source Electromagnetics	07:26	on deck	38° 16,739'	022° 18,644'	0	Receiver 2
M196_15-1	10/12/2023	Controlled Source Electromagnetics	07:50	on deck	38° 16,842'	022° 18,306'	0	Receiver 3
M196_15-1	10/12/2023	Controlled Source Electromagnetics	07:57	on deck	38° 16,871'	022° 18,211'	0	Receiver 4
M196_15-1	10/12/2023	Controlled Source Electromagnetics	07:58	on deck	38° 16,875'	022° 18,198'	0	Kettenvorlauf
M196_16-1	10/12/2023	Gravity Corer	11:05	in the water	38° 09,068'	022° 43,631'	853	
M196_16-1	10/12/2023	Gravity Corer	11:23	max depth/on ground	38° 09,071'	022° 43,630'	858	SLmax = 869m, SZmax = 41kN
M196_16-1	10/12/2023	Gravity Corer	11:43	on deck	38° 09,071'	022° 43,630'	0	
M196_16-2	10/12/2023	Sound Velocity Profiler	12:23	in the water	38° 09,071'	022° 43,629'	0	
M196_16-2	10/12/2023	Sound Velocity Profiler	12:42	max depth/on ground	38° 09,071'	022° 43,628'	0	SLmax = 751m
M196_16-2	10/12/2023	Sound Velocity Profiler	12:59	on deck	38° 09,070'	022° 43,629'	0	
M196_17-1	10/12/2023	Deep-sea Multibeam Echosounder	14:07	profile start	38° 14,630'	022° 38,710'	549	
M196_17-1	10/12/2023	Deep-sea Multibeam Echosounder	16:58	profile end	38° 15,825'	022° 40,363'	369	
M196_17-2	10/12/2023	Shallow-water Multibeam Echosounder	14:07	profile start	38° 14,638'	022° 38,710'	538	
M196_17-2	10/12/2023	Shallow-water Multibeam Echosounder	16:58	profile end	38° 15,800'	022° 40,362'	372	
M196_17-3	10/12/2023	P-70 Parasound	14:07	profile start	38° 14,657'	022° 38,710'	542	
M196_17-3	10/12/2023	P-70 Parasound	16:58	profile end	38° 15,776'	022° 40,360'	370	
M196_18-1	10/12/2023	Deep-sea Multibeam Echosounder	17:00	profile start	38° 15,668'	022° 40,322'	401	
M196_18-1	11/12/2023	Deep-sea Multibeam Echosounder	03:00	information	38° 01,221'	022° 48,181'	369	
M196_18-1	11/12/2023	Deep-sea Multibeam Echosounder	03:35	profile end	38° 00,768'	022° 49,037'	204	
M196_18-2	10/12/2023	Shallow-water Multibeam Echosounder	17:00	profile start	38° 15,632'	022° 40,296'	403	
M196_18-2	11/12/2023	Shallow-water Multibeam Echosounder	03:35	profile end	38° 00,775'	022° 49,044'	205	
M196_18-3	10/12/2023	P-70 Parasound	17:00	profile start	38° 15,605'	022° 40,272'	396	
M196_18-3	11/12/2023	P-70 Parasound	03:35	profile end	38° 00,782'	022° 49,050'	208	

M196_19-1	11/12/2023	Gravity Corer	06:29	in the water	38° 16,163'	022° 39,163'	249	
M196_19-1	11/12/2023	Gravity Corer	06:35	max depth/on ground	38° 16,163'	022° 39,163'	249	SLmax = 254m, SZmax = 28.2kN
M196_19-1	11/12/2023	Gravity Corer	06:47	on deck	38° 16,162'	022° 39,167'	248	
M196_19-2	11/12/2023	Gravity Corer	07:16	in the water	38° 16,161'	022° 39,167'	246	
M196_19-2	11/12/2023	Gravity Corer	07:21	max depth/on ground	38° 16,162'	022° 39,168'	246	SLmax = 258m, SZmax = 27,0kN
M196_19-2	11/12/2023	Gravity Corer	07:33	on deck	38° 16,162'	022° 39,166'	248	
M196_19-3	11/12/2023	Gravity Corer	08:26	in the water	38° 16,163'	022° 39,167'	246	
M196_19-3	11/12/2023	Gravity Corer	08:32	max depth/on ground	38° 16,163'	022° 39,166'	247	SLmax = 262m, SZmax = 28,7kN
M196_19-3	11/12/2023	Gravity Corer	08:44	on deck	38° 16,163'	022° 39,166'	248	
M196_19-4	11/12/2023	Sound Velocity Profiler	09:15	in the water	38° 16,162'	022° 39,166'	248	
M196_19-4	11/12/2023	Sound Velocity Profiler	09:33	on deck	38° 16,163'	022° 39,165'	246	
M196_20-1	11/12/2023	CTD	11:53	in the water	38° 07,073'	022° 51,071'	825	clean ship
M196_20-1	11/12/2023	CTD	12:16	max depth/on ground	38° 07,072'	022° 51,070'	825	SLmax = 830m
M196_20-1	11/12/2023	CTD	12:44	on deck	38° 07,073'	022° 51,071'	822	
M196_20-2	11/12/2023	CTD	13:50	in the water	38° 08,897'	022° 44,956'	856	clean ship
M196_20-2	11/12/2023	CTD	14:12	max depth/on ground	38° 08,898'	022° 44,966'	855	
M196_20-2	11/12/2023	CTD	14:31	on deck	38° 08,900'	022° 44,965'	853	
M196_20-3	11/12/2023	CTD	15:29	in the water	38° 10,727'	022° 38,774'	858	clean ship
M196_20-3	11/12/2023	CTD	15:51	max depth/on ground	38° 10,727'	022° 38,771'	870	
M196_20-3	11/12/2023	CTD	16:08	on deck	38° 10,742'	022° 38,762'	857	
M196_20-4	11/12/2023	CTD	17:06	in the water	38° 12,580'	022° 32,579'	855	clean ship
M196_20-4	11/12/2023	CTD	17:29	max depth/on ground	38° 12,572'	022° 32,606'	855	
M196_20-4	11/12/2023	CTD	17:49	on deck	38° 12,593'	022° 32,587'	854	
M196_20-5	11/12/2023	CTD	18:49	in the water	38° 14,411'	022° 26,411'	815	
M196_20-5	11/12/2023	CTD	19:09	max depth/on ground	38° 14,414'	022° 26,405'	816	SLmax = 819m
M196_20-5	11/12/2023	CTD	19:26	on deck	38° 14,413'	022° 26,405'	816	
M196_21-1	11/12/2023	Deep-sea Multibeam Echosounder	20:07	profile start	38° 17,755'	022° 24,275'	533	
M196_21-1	12/12/2023	Deep-sea Multibeam Echosounder	03:44	profile end	38° 19,672'	022° 23,411'	254	

M196_21-2	11/12/2023	Shallow-water Multibeam Echosounder	20:07	profile start	38° 17,767'	022° 24,274'	530	
M196_21-2	12/12/2023	Shallow-water Multibeam Echosounder	03:44	profile end	38° 19,682'	022° 23,420'	255	
M196_21-3	11/12/2023	P-70 Parasound	20:07	profile start	38° 17,782'	022° 24,274'	526	
M196_21-3	12/12/2023	P-70 Parasound	03:44	profile end	38° 19,685'	022° 23,423'	253	
M196_22-1	12/12/2023	Deep-sea Multibeam Echosounder	03:53	profile start	38° 19,278'	022° 24,257'	281	
M196_22-1	12/12/2023	Deep-sea Multibeam Echosounder	07:00	profile end	38° 06,586'	022° 46,178'	860	
M196_22-2	12/12/2023	Shallow-water Multibeam Echosounder	03:53	profile start	38° 19,264'	022° 24,286'	281	
M196_22-2	12/12/2023	Shallow-water Multibeam Echosounder	07:00	profile end	38° 06,579'	022° 46,187'	858	
M196_22-3	12/12/2023	P-70 Parasound	03:53	profile start	38° 19,250'	022° 24,315'	290	
M196_22-3	12/12/2023	P-70 Parasound	07:00	profile end	38° 06,571'	022° 46,200'	858	
M196_23-1	12/12/2023	Gravity Corer	08:30	in the water	38° 10,104'	022° 40,873'	856	
M196_23-1	12/12/2023	Gravity Corer	08:45	max depth/on ground	38° 10,100'	022° 40,869'	858	SLmax = 872m, SZmax = 38,9kN
M196_23-1	12/12/2023	Gravity Corer	09:06	on deck	38° 10,100'	022° 40,868'	857	
M196_23-2	12/12/2023	Gravity Corer	10:21	in the water	38° 10,100'	022° 40,868'	855	
M196_23-2	12/12/2023	Gravity Corer	10:40	max depth/on ground	38° 10,100'	022° 40,866'	857	SLmax = 874 m , SZmax = 39,9 kN
M196_23-2	12/12/2023	Gravity Corer	11:03	on deck	38° 10,100'	022° 40,867'	858	
M196_23-3	12/12/2023	Gravity Corer	11:51	in the water	38° 10,100'	022° 40,867'	857	
M196_23-3	12/12/2023	Gravity Corer	12:08	max depth/on ground	38° 10,100'	022° 40,867'	858	SLmax = 873 m, SZmax = 38,5 kN
M196_23-3	12/12/2023	Gravity Corer	12:30	on deck	38° 10,100'	022° 40,867'	857	
M196_24-1	12/12/2023	Controlled Source Electromagnetics	14:43	in the water	38° 02,862'	022° 51,783'	314	Kettenvorlauf
M196_24-1	12/12/2023	Controlled Source Electromagnetics	14:46	in the water	38° 02,872'	022° 51,766'	321	Receiver 4
M196_24-1	12/12/2023	Controlled Source Electromagnetics	14:55	in the water	38° 02,912'	022° 51,705'	352	Receiver 3
M196_24-1	12/12/2023	Controlled Source Electromagnetics	15:05	in the water	38° 02,954'	022° 51,641'	471	Receiver 2
M196_24-1	12/12/2023	Controlled Source Electromagnetics	15:13	in the water	38° 02,985'	022° 51,596'	528	Receiver 1
M196_24-1	12/12/2023	Controlled Source Electromagnetics	15:21	in the water	38° 03,019'	022° 51,543'	587	Elektrode 1
M196_24-1	12/12/2023	Controlled Source Electromagnetics	15:31	in the water	38° 03,059'	022° 51,485'	619	Elektrode 2
M196_24-1	12/12/2023	Controlled Source Electromagnetics	15:50	in the water	38° 03,142'	022° 51,359'	715	Schwein

M196_24-1	12/12/2023	Controlled Source Electromagnetics	16:50	profile start	38° 03,384'	022° 50,988'	834	
M196_24-1	13/12/2023	Controlled Source Electromagnetics	17:19	profile end	38° 13,234'	022° 36,162'	0	
M196_24-1	13/12/2023	Controlled Source Electromagnetics	18:36	on deck	38° 13,233'	022° 36,160'	0	Schwein
M196_24-1	13/12/2023	Controlled Source Electromagnetics	19:00	on deck	38° 13,257'	022° 36,128'	0	Elektrode 2
M196_24-1	13/12/2023	Controlled Source Electromagnetics	19:08	on deck	38° 13,301'	022° 36,059'	0	Elektrode 1
M196_24-1	13/12/2023	Controlled Source Electromagnetics	19:14	on deck	38° 13,342'	022° 36,020'	0	Receiver 1
M196_24-1	13/12/2023	Controlled Source Electromagnetics	19:30	on deck	38° 13,474'	022° 35,979'	0	Receiver 2
M196_24-1	13/12/2023	Controlled Source Electromagnetics	19:40	on deck	38° 13,546'	022° 35,946'	0	Receiver 3
M196_24-1	13/12/2023	Controlled Source Electromagnetics	19:43	on deck	38° 13,569'	022° 35,938'	0	alles an deck
M196_25-1	13/12/2023	Deep-sea Multibeam Echosounder	23:07	profile start	38° 16,933'	022° 04,650'	305	
M196_25-2	13/12/2023	Shallow-water Multibeam Echosounder	23:07	profile start	38° 16,933'	022° 04,650'	305	
M196_25-3	13/12/2023	P-70 Parasound	23:07	profile start	38° 16,933'	022° 04,650'	305	
M196_25-1	14/12/2023	Deep-sea Multibeam Echosounder	03:14	profile end	38° 18,331'	022° 05,801'	389	
M196_25-3	14/12/2023	P-70 Parasound	03:14	on deck	38° 18,317'	022° 05,848'	390	
M196_25-2	14/12/2023	Shallow-water Multibeam Echosounder	03:15	profile end	38° 18,287'	022° 05,961'	391	
M196_26-1	14/12/2023	Gravity Corer	06:17	in the water	38° 18,265'	022° 28,365'	218	
M196_26-1	14/12/2023	Gravity Corer	06:23	max depth/on ground	38° 18,266'	022° 28,365'	218	SLmax = 219m, SZmax = 27,8kN
M196_26-1	14/12/2023	Gravity Corer	06:34	on deck	38° 18,265'	022° 28,365'	213	
M196_26-2	14/12/2023	Gravity Corer	06:55	in the water	38° 18,266'	022° 28,365'	215	
M196_26-2	14/12/2023	Gravity Corer	07:01	max depth/on ground	38° 18,265'	022° 28,365'	216	SLmax = 227m, SZmax = 27,8kN
M196_26-2	14/12/2023	Gravity Corer	07:13	on deck	38° 18,265'	022° 28,365'	209	
M196_26-3	14/12/2023	Gravity Corer	07:38	in the water	38° 18,266'	022° 28,365'	219	
M196_26-3	14/12/2023	Gravity Corer	07:43	max depth/on ground	38° 18,266'	022° 28,365'	213	SLmax = 223m, SZmax = 28,1kN
M196_26-3	14/12/2023	Gravity Corer	07:55	on deck	38° 18,266'	022° 28,364'	217	
M196_26-4	14/12/2023	Gravity Corer	09:45	in the water	38° 19,193'	022° 25,219'	283	
M196_26-4	14/12/2023	Gravity Corer	09:51	max depth/on ground	38° 19,193'	022° 25,219'	279	SLmax = 310m, SZmax = 35,3kN

M196_26-4	14/12/2023	Gravity Corer	10:05	on deck	38° 19,193'	022° 25,219'	281	
M196_27-1	14/12/2023	Deep-sea Multibeam Echosounder	11:45	profile start	38° 14,943'	022° 16,166'	683	
M196_27-1	15/12/2023	Deep-sea Multibeam Echosounder	06:08	profile end	38° 15,720'	022° 20,762'	749	
M196_27-2	14/12/2023	Shallow-water Multibeam Echosounder	11:45	profile start	38° 14,925'	022° 16,223'	687	
M196_27-2	15/12/2023	Shallow-water Multibeam Echosounder	06:08	profile end	38° 15,776'	022° 20,760'	744	
M196_27-3	14/12/2023	Shallow-water Multibeam Echosounder	11:45	profile start	38° 14,900'	022° 16,303'	691	
M196_27-3	15/12/2023	Shallow-water Multibeam Echosounder	06:08	profile end	38° 15,754'	022° 20,755'	745	
M196_28-1	15/12/2023	Gravity Corer	07:49	in the water	38° 11,934'	022° 33,761'	859	
M196_28-1	15/12/2023	Gravity Corer	08:05	max depth/on ground	38° 11,933'	022° 33,760'	857	SLmax = 874m, SZmax = 30,7kN
M196_28-1	15/12/2023	Gravity Corer	08:26	on deck	38° 11,934'	022° 33,760'	857	
M196_28-2	15/12/2023	Gravity Corer	08:54	in the water	38° 11,933'	022° 33,760'	858	
M196_28-2	15/12/2023	Gravity Corer	09:10	max depth/on ground	38° 11,933'	022° 33,761'	859	SLmax = 880m, SZmax = 31,4kN
M196_28-2	15/12/2023	Gravity Corer	09:33	on deck	38° 11,933'	022° 33,761'	859	
M196_29-1	15/12/2023	Ocean bottom electro-magnetic receiver	11:33	information	38° 07,887'	022° 47,317'	857	OBEM 6, Ranging 1
M196_29-1	15/12/2023	Ocean bottom electro-magnetic receiver	12:04	information	38° 07,874'	022° 47,904'	0	OBEM 6, Ranging 2
M196_29-1	15/12/2023	Ocean bottom electro-magnetic receiver	12:23	information	38° 08,384'	022° 47,648'	0	OBEM 6, Ranging 3
M196_29-2	15/12/2023	Ocean bottom electro-magnetic receiver	13:39	information	38° 09,571'	022° 40,115'	0	OBEM 5, Ranging 1
M196_29-2	15/12/2023	Ocean bottom electro-magnetic receiver	14:03	information	38° 09,715'	022° 39,503'	0	OBEM 5, Ranging 2
M196_29-2	15/12/2023	Ocean bottom electro-magnetic receiver	14:30	information	38° 10,169'	022° 39,924'	0	OBEM 5, Ranging 3
M196_29-3	15/12/2023	Ocean bottom electro-magnetic receiver	15:31	information	38° 11,747'	022° 33,511'	0	OBEM 4 Ranging 1, keine Antwort
M196_29-3	15/12/2023	Ocean bottom electro-magnetic receiver	15:53	information	38° 11,184'	022° 33,126'	0	OBEM 4 Ranging 2, keine Antwort
M196_29-4	15/12/2023	Ocean bottom electro-magnetic receiver	16:58	information	38° 13,384'	022° 26,886'	0	OBEM 3 Ranging 1
M196_29-4	15/12/2023	Ocean bottom electro-magnetic receiver	17:16	information	38° 13,533'	022° 27,568'	0	OBEM 3 Ranging 2

M196_29-4	15/12/2023	Ocean bottom electro-magnetic receiver	17:34	information	38° 12,989'	022° 27,316'	0	OBEM 3 Ranging 3
M196_29-4	15/12/2023	Ocean bottom electro-magnetic receiver	18:12	information	38° 13,596'	022° 27,130'	0	OBEM 3 ausgelöst
M196_29-4	15/12/2023	Ocean bottom electro-magnetic receiver	19:15	on deck	38° 13,413'	022° 26,996'	0	OBEM 3
M196_29-5	15/12/2023	Ocean bottom electro-magnetic receiver	19:59	information	38° 14,923'	022° 23,324'	0	OBEM 2 Ranging 1
M196_29-5	15/12/2023	Ocean bottom electro-magnetic receiver	20:31	information	38° 14,616'	022° 22,949'	0	OBEM 2 Ranging 2
M196_29-5	15/12/2023	Ocean bottom electro-magnetic receiver	21:00	information	38° 15,033'	022° 22,757'	0	OBEM 2 Ranging 3
M196_29-6	15/12/2023	Ocean bottom electro-magnetic receiver	22:53	information	38° 16,097'	022° 18,536'	0	OBEM 1, Ranging 1
M196_29-6	15/12/2023	Ocean bottom electro-magnetic receiver	23:23	information	38° 16,242'	022° 18,244'	0	OBEM 1, Ranging 2
M196_29-6	15/12/2023	Ocean bottom electro-magnetic receiver	23:36	information	38° 16,267'	022° 17,902'	0	OBEM 1, Ranging 3
M196_29-6	15/12/2023	Ocean bottom electro-magnetic receiver	23:40	information	38° 16,264'	022° 17,951'	0	release
M196_29-6	16/12/2023	Ocean bottom electro-magnetic receiver	00:30	on deck	38° 16,595'	022° 18,266'	0	
M196_30-2	16/12/2023	Shallow-water Multibeam Echosounder	01:10	profile start	38° 15,639'	022° 20,907'	743	
M196_30-3	16/12/2023	P-70 Parasound	01:10	profile start	38° 15,639'	022° 20,907'	743	
M196_30-1	16/12/2023	Deep-sea Multibeam Echosounder	01:10	profile start	38° 15,639'	022° 20,907'	743	
M196_30-1	16/12/2023	Deep-sea Multibeam Echosounder	05:52	profile end	38° 14,604'	022° 24,353'	802	
M196_30-2	16/12/2023	Shallow-water Multibeam Echosounder	05:52	profile end	38° 14,597'	022° 24,360'	804	
M196_30-3	16/12/2023	P-70 Parasound	05:52	profile end	38° 14,591'	022° 24,367'	804	
M196_31-1	16/12/2023	Gravity Corer	06:23	in the water	38° 14,642'	022° 24,459'	802	W12
M196_31-1	16/12/2023	Gravity Corer	06:43	max depth/on ground	38° 14,644'	022° 24,458'	803	SLmax = 816m, SZmax = 35,4kN
M196_31-1	16/12/2023	Gravity Corer	07:03	on deck	38° 14,641'	022° 24,458'	802	
M196_32-1	16/12/2023	Gravity Corer	10:07	in the water	38° 08,890'	022° 41,522'	852	
M196_32-1	16/12/2023	Gravity Corer	10:37	max depth/on ground	38° 08,887'	022° 41,526'	852	SLmax = 870m, 34,1 kN
M196_32-1	16/12/2023	Gravity Corer	10:47	on deck	38° 08,889'	022° 41,525'	852	
M196_33-1	16/12/2023	Sound Velocity Profiler	15:50	in the water	38° 18,498'	022° 06,904'	405	W12
M196_33-1	16/12/2023	Sound Velocity Profiler	16:01	max depth/on ground	38° 18,498'	022° 06,905'	406	SLmax = 350m
M196_33-1	16/12/2023	Sound Velocity Profiler	16:14	on deck	38° 18,498'	022° 06,904'	405	
M196_34-1	16/12/2023	Deep-sea Multibeam Echosounder	16:45	profile start	38° 18,666'	022° 06,643'	403	
M196_34-1	17/12/2023	Deep-sea Multibeam Echosounder	05:45	profile end	38° 18,204'	022° 05,262'	378	

M196_34-2	16/12/2023	Shallow-water Multibeam Echosounder	16:54	profile start	38° 19,017'	022° 05,465'	383	
M196_34-2	17/12/2023	Shallow-water Multibeam Echosounder	05:45	profile end	38° 18,191'	022° 05,303'	379	
M196_34-3	16/12/2023	P-70 Parasound	16:54	profile start	38° 19,026'	022° 05,434'	382	
M196_34-3	17/12/2023	P-70 Parasound	05:45	profile end	38° 18,186'	022° 05,319'	379	
M196_35-2	17/12/2023	Deep-sea Multibeam Echosounder	06:44	profile end	38° 15,297'	022° 08,591'	49	
M196_35-2	17/12/2023	Deep-sea Multibeam Echosounder	06:59	profile start	38° 15,340'	022° 08,672'	54	
M196_35-1	17/12/2023	P-70 Parasound	06:44	profile end	38° 15,312'	022° 08,579'	50	
M196_35-1	17/12/2023	P-70 Parasound	06:59	profile start	38° 15,296'	022° 08,702'	53	
M196_35-3	17/12/2023	Shallow-water Multibeam Echosounder	06:44	profile end	38° 15,346'	022° 08,552'	49	
M196_35-3	17/12/2023	Shallow-water Multibeam Echosounder	06:59	profile start	38° 15,307'	022° 08,694'	53	
M196_35-4	17/12/2023	Video-CTD	07:33	in the water	38° 14,484'	022° 09,173'	51	
M196_35-4	17/12/2023	Video-CTD	08:00	recording start	38° 14,481'	022° 09,165'	51	
M196_35-4	17/12/2023	Video-CTD	11:02	on deck	38° 15,236'	022° 08,718'	52	
M196_35-4	17/12/2023	Video-CTD	11:55	in the water	38° 15,236'	022° 08,717'	52	
M196_35-4	17/12/2023	Video-CTD	12:09	on deck	38° 15,237'	022° 08,718'	52	
M196_35-4	17/12/2023	Video-CTD	12:54	in the water	38° 15,235'	022° 08,717'	52	
M196_35-4	17/12/2023	Video-CTD	13:06	on deck	38° 15,237'	022° 08,719'	52	
M196_35-4	17/12/2023	Video-CTD	13:19	in the water	38° 15,237'	022° 08,718'	52	
M196_35-4	17/12/2023	Video-CTD	13:32	recording start	38° 15,236'	022° 08,720'	52	
M196_35-4	17/12/2023	Video-CTD	14:57	information	38° 14,521'	022° 09,178'	51	Profil Ende
M196_35-4	17/12/2023	Video-CTD	15:05	on deck	38° 14,522'	022° 09,179'	51	
M196_36-1	17/12/2023	Video-CTD	16:07	in the water	38° 15,168'	022° 08,850'	53	W12, clean ship
M196_36-1	17/12/2023	Video-CTD	16:48	max depth/on ground	38° 15,163'	022° 08,848'	54	SLmax = 54m
M196_36-1	17/12/2023	Video-CTD	17:19	on deck	38° 15,160'	022° 08,823'	53	
M196_37-1	17/12/2023	Ocean bottom electro-magnetic receiver	21:21	in the water	38° 09,317'	022° 42,368'	0	OBEM 8
M196_37-1	17/12/2023	Ocean bottom electro-magnetic receiver	21:49	information	38° 09,315'	022° 42,369'	0	OBEM 8 released
M196_37-1	17/12/2023	Ocean bottom electro-magnetic receiver	22:09	on deck	38° 09,315'	022° 42,369'	0	
M196_37-2	17/12/2023	Ocean bottom electro-magnetic receiver	22:53	in the water	38° 08,750'	022° 45,030'	0	
M196_37-2	17/12/2023	Ocean bottom electro-magnetic receiver	23:26	information	38° 08,732'	022° 45,030'	0	Released
M196_37-2	17/12/2023	Ocean bottom electro-magnetic receiver	23:40	on deck	38° 08,732'	022° 45,029'	0	

M196_38-1	18/12/2023	Sound Velocity Profiler	00:44	in the water	38° 07,619'	022° 50,502'	815	
M196_38-1	18/12/2023	Sound Velocity Profiler	01:02	max depth/on ground	38° 07,618'	022° 50,501'	813	SLmax = 750m
M196_38-1	18/12/2023	Sound Velocity Profiler	01:21	on deck	38° 07,596'	022° 50,450'	823	
M196_39-1	18/12/2023	Deep-sea Multibeam Echosounder	01:35	profile start	38° 07,596'	022° 50,449'	823	
M196_39-1	18/12/2023	Deep-sea Multibeam Echosounder	06:28	profile end	38° 14,995'	022° 08,984'	0	
M196_39-2	18/12/2023	Shallow-water Multibeam Echosounder	01:35	profile start	38° 07,595'	022° 50,447'	827	
M196_39-2	18/12/2023	Shallow-water Multibeam Echosounder	06:28	profile end	38° 14,996'	022° 08,984'	0	
M196_39-3	18/12/2023	P-70 Parasound	01:35	profile start	38° 07,593'	022° 50,442'	829	
M196_39-3	18/12/2023	P-70 Parasound	06:28	profile end	38° 14,995'	022° 08,984'	0	
M196_40-1	18/12/2023	Remote Operated Vehicle	06:58	information	38° 14,987'	022° 08,955'	0	Meteorit zu Wasser
M196_40-1	18/12/2023	Remote Operated Vehicle	07:50	in the water	38° 14,981'	022° 08,932'	0	Mini-ROV
M196_40-1	18/12/2023	Remote Operated Vehicle	09:00	information	38° 15,000'	022° 09,007'	0	
M196_40-1	18/12/2023	Remote Operated Vehicle	09:12	on deck	38° 15,019'	022° 09,000'	0	
M196_40-1	18/12/2023	Remote Operated Vehicle	10:10	information	38° 15,041'	022° 08,989'	0	Boot mit ROV zurück an Bord
M196_41-1	18/12/2023	Sound Velocity Profiler	15:44	in the water	38° 07,706'	022° 50,429'	0	W12
M196_41-1	18/12/2023	Sound Velocity Profiler	16:02	max depth/on ground	38° 07,700'	022° 50,420'	0	SLmax = 675m
M196_41-1	18/12/2023	Sound Velocity Profiler	16:20	on deck	38° 07,697'	022° 50,412'	0	
M196_42-1	18/12/2023	Controlled Source Electromagnetics	16:29	in the water	38° 07,640'	022° 50,463'	0	Receiver 1
M196_42-1	18/12/2023	Controlled Source Electromagnetics	16:39	in the water	38° 07,660'	022° 50,373'	0	Receiver 2
M196_42-1	18/12/2023	Controlled Source Electromagnetics	16:46	in the water	38° 07,677'	022° 50,304'	0	Receiver 3
M196_42-1	18/12/2023	Controlled Source Electromagnetics	16:56	in the water	38° 07,698'	022° 50,199'	0	Elektrode 1
M196_42-1	18/12/2023	Controlled Source Electromagnetics	17:04	in the water	38° 07,714'	022° 50,124'	0	Elektrode 2
M196_42-1	18/12/2023	Controlled Source Electromagnetics	17:27	in the water	38° 07,749'	022° 49,939'	0	Schwein
M196_42-1	18/12/2023	Controlled Source Electromagnetics	18:20	profile start	38° 07,767'	022° 49,945'	0	
M196_42-1	19/12/2023	Controlled Source Electromagnetics	08:00	profile end	38° 10,287'	022° 38,224'	0	
M196_42-1	19/12/2023	Controlled Source Electromagnetics	08:49	on deck	38° 10,353'	022° 37,954'	0	Schwein
M196_42-1	19/12/2023	Controlled Source Electromagnetics	09:02	on deck	38° 10,371'	022° 37,876'	0	Elektrode 2
M196_42-1	19/12/2023	Controlled Source Electromagnetics	09:03	on deck	38° 10,371'	022° 37,875'	0	Elektrode 1
M196_42-1	19/12/2023	Controlled Source Electromagnetics	09:17	on deck	38° 10,375'	022° 37,841'	0	Receiver 3
M196_42-1	19/12/2023	Controlled Source Electromagnetics	09:29	on deck	38° 10,381'	022° 37,801'	0	Receiver 2

M196_42-1	19/12/2023	Controlled Source Electromagnetics	09:38	on deck	38° 10,386'	022° 37,771'	0	Receiver 1
M196_43-1	19/12/2023	Gravity Corer	10:42	in the water	38° 10,202'	022° 44,847'	0	
M196_43-1	19/12/2023	Gravity Corer	10:57	max depth/on ground	38° 10,196'	022° 44,857'	856	SLmax = 874m, SZmax = 35,1kN
M196_43-1	19/12/2023	Gravity Corer	11:20	on deck	38° 10,200'	022° 44,861'	858	
M196_44-1	19/12/2023	Gravity Corer	12:19	in the water	38° 08,207'	022° 43,435'	860	
M196_44-1	19/12/2023	Gravity Corer	12:34	max depth/on ground	38° 08,202'	022° 43,423'	856	SLmax = 872m, SZmax = 34,9kN
M196_44-1	19/12/2023	Gravity Corer	12:56	on deck	38° 08,214'	022° 43,449'	857	
M196_45-1	19/12/2023	Ocean bottom electro-magnetic receiver	14:27	information	38° 09,995'	022° 39,715'	0	Nr. 5, released
M196_45-1	19/12/2023	Ocean bottom electro-magnetic receiver	14:40	information	38° 10,020'	022° 39,743'	0	aufgetaucht
M196_45-1	19/12/2023	Ocean bottom electro-magnetic receiver	14:59	on deck	38° 09,862'	022° 40,149'	0	
M196_45-2	19/12/2023	Ocean bottom electro-magnetic receiver	15:45	information	38° 09,485'	022° 42,595'	0	Nr. 08, released
M196_45-2	19/12/2023	Ocean bottom electro-magnetic receiver	15:53	information	38° 09,470'	022° 42,571'	0	aufgetaucht
M196_45-2	19/12/2023	Ocean bottom electro-magnetic receiver	16:08	on deck	38° 09,306'	022° 42,565'	0	
M196_46-1	19/12/2023	Sound Velocity Profiler	17:19	in the water	38° 06,607'	022° 44,541'	0	W12
M196_46-1	19/12/2023	Sound Velocity Profiler	17:36	max depth/on ground	38° 06,644'	022° 44,537'	861	SLmax = 750m
M196_46-1	19/12/2023	Sound Velocity Profiler	17:54	on deck	38° 06,681'	022° 44,515'	858	
M196_47-1	19/12/2023	Deep-sea Multibeam Echosounder	18:16	profile start	38° 06,880'	022° 44,365'	863	
M196_47-1	19/12/2023	Deep-sea Multibeam Echosounder	20:38	profile end	38° 09,714'	022° 56,589'	294	
M196_47-2	19/12/2023	Shallow-water Multibeam Echosounder	18:16	profile start	38° 06,900'	022° 44,360'	861	
M196_47-2	19/12/2023	Shallow-water Multibeam Echosounder	20:38	profile end	38° 09,721'	022° 56,569'	291	
M196_47-3	19/12/2023	P-70 Parasound	18:16	profile start	38° 06,901'	022° 44,359'	861	
M196_47-3	19/12/2023	P-70 Parasound	20:38	profile end	38° 09,732'	022° 56,539'	292	
M196_48-1	19/12/2023	Sound Velocity Profiler	21:00	in the water	38° 09,723'	022° 57,161'	292	
M196_48-1	19/12/2023	Sound Velocity Profiler	21:05	max depth/on ground	38° 09,723'	022° 57,160'	293	SLmax = 250m
M196_48-1	19/12/2023	Sound Velocity Profiler	21:19	on deck	38° 09,739'	022° 57,178'	290	
M196_49-2	19/12/2023	Shallow-water Multibeam Echosounder	21:40	profile start	38° 09,503'	022° 57,034'	310	
M196_49-2	20/12/2023	Shallow-water Multibeam Echosounder	03:30	profile end	38° 04,553'	022° 52,399'	746	

M196_49-1	19/12/2023	Deep-sea Multibeam Echosounder	21:40	profile start	38° 09,458'	022° 56,992'	315	
M196_49-1	20/12/2023	Deep-sea Multibeam Echosounder	03:30	profile end	38° 04,563'	022° 52,381'	755	
M196_49-3	19/12/2023	P-70 Parasound	21:40	profile start	38° 09,441'	022° 56,975'	315	
M196_49-3	20/12/2023	P-70 Parasound	03:31	profile end	38° 04,576'	022° 52,360'	768	
M196_50-1	19/12/2023	Sound Velocity Profiler	23:26	in the water	37° 59,705'	022° 48,047'	117	
M196_50-1	19/12/2023	Sound Velocity Profiler	23:32	max depth/on ground	37° 59,705'	022° 48,047'	121	SLmax = 100m
M196_50-1	19/12/2023	Sound Velocity Profiler	23:39	on deck	37° 59,705'	022° 48,047'	114	
M196_51-1	20/12/2023	Ocean bottom electro-magnetic receiver	05:59	information	38° 08,231'	022° 47,645'	0	OBEM 6 released
M196_51-1	20/12/2023	Ocean bottom electro-magnetic receiver	06:30	information	38° 08,259'	022° 47,698'	0	aufgetaucht
M196_51-1	20/12/2023	Ocean bottom electro-magnetic receiver	07:00	on deck	38° 08,248'	022° 47,940'	0	
M196_52-1	20/12/2023	Ocean bottom electro-magnetic receiver	09:30	information	38° 08,445'	022° 47,237'	0	OBEM 7 aufgetaucht
M196_52-1	20/12/2023	Ocean bottom electro-magnetic receiver	10:06	on deck	38° 07,046'	022° 49,707'	0	
M196_53-1	20/12/2023	Video Multi Corer	13:23	in the water	38° 14,884'	022° 22,842'	0	W12
M196_53-1	20/12/2023	Video Multi Corer	13:24	information	38° 14,885'	022° 22,841'	0	Ausgelöst
M196_53-1	20/12/2023	Video Multi Corer	13:57	max depth/on ground	38° 14,881'	022° 22,838'	0	SLmax = 820m
M196_53-1	20/12/2023	Video Multi Corer	14:34	on deck	38° 14,899'	022° 22,890'	0	
M196_53-1	20/12/2023	Video Multi Corer	14:52	in the water	38° 14,898'	022° 22,831'	0	
M196_53-1	20/12/2023	Video Multi Corer	17:04	on deck	38° 14,896'	022° 22,824'	792	
M196_54-1	20/12/2023	Ocean bottom electro-magnetic receiver	18:04	on deck	38° 14,699'	022° 16,029'	684	
M196_55-1	20/12/2023	Deep-sea Multibeam Echosounder	20:04	profile start	38° 13,580'	022° 17,707'	725	
M196_55-1	21/12/2023	Deep-sea Multibeam Echosounder	05:11	profile end	38° 16,806'	022° 12,161'	518	
M196_55-2	20/12/2023	Shallow-water Multibeam Echosounder	20:04	profile start	38° 13,630'	022° 17,680'	724	
M196_55-2	21/12/2023	Shallow-water Multibeam Echosounder	05:11	profile end	38° 16,849'	022° 12,185'	521	
M196_55-3	20/12/2023	P-70 Parasound	20:05	profile start	38° 13,654'	022° 17,666'	723	
M196_55-3	21/12/2023	P-70 Parasound	05:11	profile end	38° 16,803'	022° 12,159'	526	
M196_56-1	21/12/2023	Remote Operated Vehicle	07:52	in the water	38° 14,836'	022° 08,964'	53	
M196_56-1	21/12/2023	Remote Operated Vehicle	09:56	information	38° 14,834'	022° 08,965'	54	aufgetaucht
M196_56-1	21/12/2023	Remote Operated Vehicle	10:00	on deck	38° 14,835'	022° 08,964'	53	

8 Data and Sample Storage and Availability

The data were collected within the SMART project. These data gathered during M196 are stored in facilities of GEOMAR Helmholtz-Zentrum für Ozeanforschung Kiel and visible within the Ocean Science Information System (OSIS-Kiel). All metadata are immediately available publicly via the following link pointing to OSIS-Kiel in the GEOMAR data management portal (https://osis.geomar.de/app/expeditions/363627). In addition, the portal provides a single downloadable KML formatted file (https://osis.geomar.de/app/expeditions/363627), which retrieves and combines up-to-date cruise (M196) related information, links to restricted data and published data for visualization e.g. in GoogleEarth.

After a three-year moratorium, the GEOMAR data management will assist in publishing these data by dissemination to national and international data archives, i.e. the data will be submitted to PANGAEA no later January 2027. Sediment and rock samples will be stored at the Core and Rock Repository at GEOMAR in Kiel (responsible: Dr. Mark Schmidt).

Type	Data Base	Available	Free Access	Contact
Hydrographic Data	PANGAEA	07/2024	01/2027	gdy@geomar.de
Towed CSEM Data	OSIS/PANGAEA	07/2024	01/2027	gdy@geomar.de
Magnetotelluric Data	OSIS/PANGAEA	07/2024	01/2027	gdy@geomar.de
CTD Video Data	OSIS/PANGAEA	07/2024	01/2027	gdy@geomar.de
Gravity Cores	OSIS/PANGAEA	07/2024	01/2027	gdy@geomar.de
Mini-ROV Data	OSIS/PANGAEA	07/2024	01/2027	gdy@geomar.de

Table 8.1: Overview of data availability

9 Acknowledgements

We thank Captain Derk Apetz of RV METEOR and his crew for relentless support throughout the entire cruise and the collegial and constructive working atmosphere. Particular thanks go to our partners at the University of Malta, our Greek collaboration partners of HMCR, the University of Patras and Dr Katrin Schwalenberg of the Federal German Institute for Geosciences and Natural Resources. We like to thank the Greek Ministry of Foreign Affairs for granting work permits and the German embassy in Athens for their support and visit to the vessel. The cruise would not have been possible without financial support from the Helmholtz Association for the SMART project through the Helmholtz European Partnering program.

10 References

Bell, R. E., L. C. McNeill, J. M. Bull, T. J. Henstock, R. E. L. Collier, and M. R. Leeder (2009), Fault architecture, basin structure and evolution of the Gulf of Corinth Rift, central Greece, Basin Res., 21(6), 824–855, doi:10.1111/j.1365-2117.2009.00401.x.

Brennwald, M. S., Hofer, M., Peeters, F., Aeschbach-Hertig, W., Strassmann, K., Kipfer, R., et al. (2003), Analysis of dissolved noble gases in the pore water of lacustrine sediments. Limnology and Oceanography: Methods, 1(1), 51–62.

Bernard, P., et al. (2006), Seismicity, deformation and seismic hazard in the western rift of Corinth: New insights from the Corinth Rift Laboratory (CRL), Tectonophysics, 426(1-2), 7–30, doi:10.1016/j.tecto.2006.02.012

Clarke, P. J., et al. (1998), Crustal strain in central Greece from repeated GPS measurements

in the interval 1989–1997, Geophys. J. Int., 135(1),195–214, doi:10.1046/j.1365-246X.1998.00633.x.

Ford, M., E. A. Williams, F. Malartre, and S.-M. Popescu (2008), Stratigraphic architecture, sedimentology and structure of the Vouraikos Gilbert-type fan delta, Gulf of Corinth, Greece, Int. Assoc. Sediment. Spec. Publ., 38, 49–90.

Ford, M., S. Rohais, E. A. Williams, S. Bourlange, D. Jousselin, N. Backert, and F. Malartre (2013), Tectono-sedimentary evolution of the western Corinth Rift (Central Greece), Basin Res., 25(1), 3–25, doi:10.1111/j.1365-2117.2012.00550.x

Grant, J.A. & Schreiber, R. (1990), Modern Swathe Sounding and sub-bottom Profiling Technology for Research Applications: The Atlas Hydrosweep and PARASOUND Systems. Marine Geophysical Researches, 12, 9 – 19.

Grasshoff K., Ehrhardt M., Kremling K. (1999), Methods of Seawater Analysis. Wiley VCH,Weinheim, 600 pages. ISBN: 978-3527295890.

Heezen, B., M. Ewing & G.L. Johnson (1966), The Gulf of Corinth floor, Deep-Sea Research, 13, 381-411.

Kershaw, S., Guo, L., Braga, J.C. (2005), A Holocene coral–algal reef at Mavra Litharia, Gulf of Corinth, Greece. Structure, history, and applications in relative sea-level change. Mar Geol. 215, 171-192.

Leeder, M. R., D. F. Mark, R. L. Gawthorpe, H. Kranis, S. Loveless, N. Pedentchouk, E. Skourtsos, J. Turner, J. E. Andrews, and M. Stamatakis (2012), A “Great Deepening”: Chronology of rift climax, Corinth Rift, Greece, Geology, 40(11), 999–1002, doi:10.1130/G33360.1.

Linke P., Schmidt M., Rohleder M., Al-Barakati A., Al-Farawati R. (2015), Novel online digital video and high-speed data broadcasting via standard coaxial cable onboard marine operating vessels. Marine Technology Society Journal 49(1), 7-18.

McNeill L. C., D. Shillington, Carter, and the Expedition 381 Participants (2019), Proceedings of the International Ocean Discovery Program Volume 381 publications.iodp.org

Moretti, I., V. Lykousis, D. Sakellariou, J. Y. Reynaud, B. Benziane, and A. Prinzhoffer (2004), Sedimentation and subsidence rate in the Gulf of Corinth: What we learn from the Marion Dufresne’s long-piston coring, C. R. Geosci., 336(4-5), 291–299, doi:10.1016/j.crte.2003.11.011.

Poulos, S.E., Collins, M.B., Pattiaratchi, C., Cramp, A., Gull, W., Tsimplis, M., Papatheodorou, G. (1996), Oceanography and sedimentation in the semi-enclosed, deep-water Gulf of Corinth (Greece). Marine Geology, Volume 134, Issues 3–4, 213-235. https://doi.org/10.1016/0025-3227(96)00028-X.

Nixon, C. W., L.C. McNeill, J. M. Bull, R. E. Bell, R. L.Gawthorpe , T. J. Henstock, D. Christodoulou, M. Ford, B. Taylor, D. Sakellariou, G. Ferentinos, G. Papatheodorou, M. R. Leeder, R. E. L. Collier, A. M. Goodliffe, M. Sachpazi, and H. Kranis (2016), Rapid spatiotemporal variations in rift structure during development of the Corinth Rift, central Greece, Tectonics, 35, 1225–1248, doi:10.1002/2015TC004026.

Perissoratis C., D. J. W. Piper and V. Lykousis (2000), Alternating marine and lacustrine sedimentation during late Quaternary in the Gulf of Corinth rift basin, central Greece, Marine Geology, 167, 391-411.

Rostek, F., Spiess, V. and Bleil, U. (1991), PARASOUND echosounding: Comparison of analogue and digital echosounder records and physical properties of sediments from the Equatorial South Atlantic. Marine Geology, 99, 118.

Rubi, R., Hubert-Ferrari, A., Fakiris, E., Christodoulou, D., Dimas, X., Geraga, M., Papatheodorou, G., Caterina, B. (2022), Hydrodynamics and sedimentary processes in the modern Rion strait (Greece): interplay between tidal currents and internal tides. Mar. Geol. 446, Article 106771. 10.1016/j.margeo.2022.106771.

Sakellariou, D., V. Lykousis, S. Alexandri, H. Kaberi, G. Rousakis, P. Nomikou, P.

Georgiou, and D. Ballas (2007), Faulting, seismic-stratigraphic architecture and Late Quaternary evolution of the Gulf of Alkyonides Basin-East Gulf of Corinth, Central Greece, Basin Res., 19(2), 273–295, doi:10.1111/j.1365-2117.2007.00322.x.

Schwalenberg, K., R.S. Gehrmann, J. Bialas and D. Rippe (2020), Analysis of marine controlled source electromagnetic data for the assessment of gas hydrates in the Danube deep-sea fan, Black Sea, Marine and Petroleum Geology, 122.

Seeberg-Elverfeldt, J., Schlüter, M., Feseker, T., Kölling, M. (2005), Rhizon sampling of porewaters near the sediment-water interface of aquatic systems. Limnology and Oceanography: Methods, 3(8), 361–371.

Skourtsos, E., and H. Kranis (2009), Structure and evolution of the western Corinth Rift, through new field data from the Northern Peloponnesus, Geol. Soc. London Spec. Publ., 321(1), 119–138, doi:10.1144/SP321.6.

Sommer, S., Linke, P., Pfannkuche, O., Schleicher, T., Schneider von Deimling, J., Reitz, A., et al. (2009), Seabed methane emissions and the habitat of frenulate tubeworms on the Captain Arutyunov mud volcano (Gulf of Cadiz). Marine Ecology Progress Series, 382, 69–86. https://doi.org/10.3354/meps07956.

Taylor, B., J. R. Weiss, A. M. Goodliffe, M. Sachpazi, M. Laigle, and A. Hirn (2011), The structures, stratigraphy and evolution of the Gulf ofCorinth Rift, Greece, Geophys. J. Int., 185(3), 1189–1219, doi:10.1111/j.1365-246X.2011.05014.x.

Tomonaga, Y., Brennwald, M.S., Kipfer, R. (2011), An improved method for the analysis of dissolved noble gases in the porewater of unconsolidated sediments: Noble-gas analysis in sediment pore water. Limnol. Oceanogr. Methods 9, 42–49. https://doi.org/10.4319/lom.2011.9.42.

Wunderlich, J. & Möller, S., 2003. High-resolution sub-bottom profiling using parametric acoustics. International Ocean Systems, Vol. 7 No. 4, S. 611.

Zygouri, V., Verroios, S., Kokkalas, S., Xypolias, P., Koukouvelas, I.K. (2008), Scaling properties within the Gulf of Corinth, Greece; comparison between offshore and onshore active faults. Tectonophysics 453, 193-210.

11 Abbreviations

CSEM	controlled source electromagnetics
ctd	conductivity-temperature-depth sensor
GC	gravity core
GoC	Gulf od Corinth
h	hour
Hz	Hertz (1/s)
kn	knots
MT	Magnetotellurics
nm	nautical mile
OBEM	ocean bottom electromagnetic receiver
OFG	offshore freshened groundwater

12 Appendices

12.1 Overview Magnetotelluric Raw Data

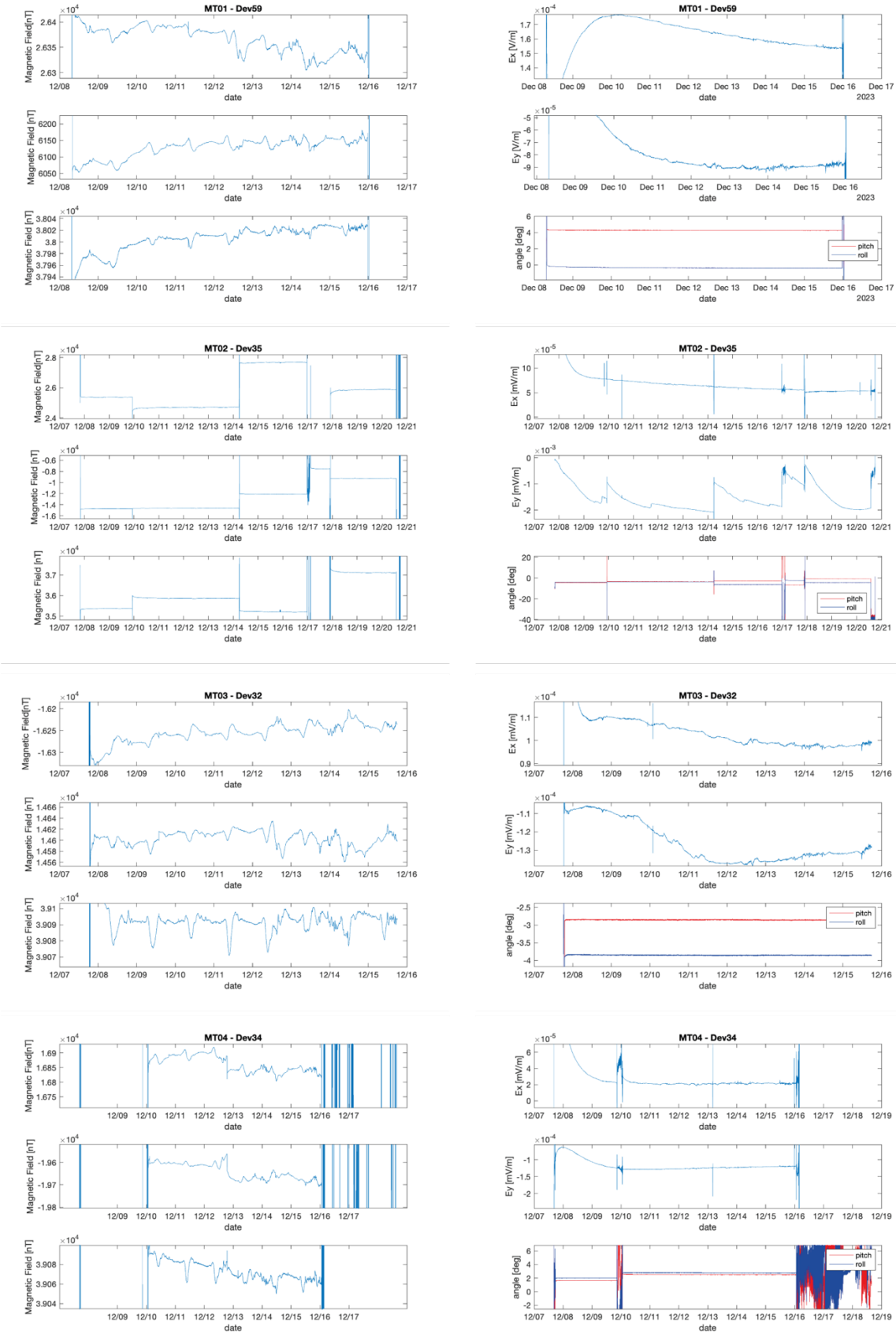

Fig. 12.1.1 OBEM Raw data stations 1 to 4, showing the recorded 3 component magnetic fields, 2 horizontal component electric fields and pitch and roll variations.

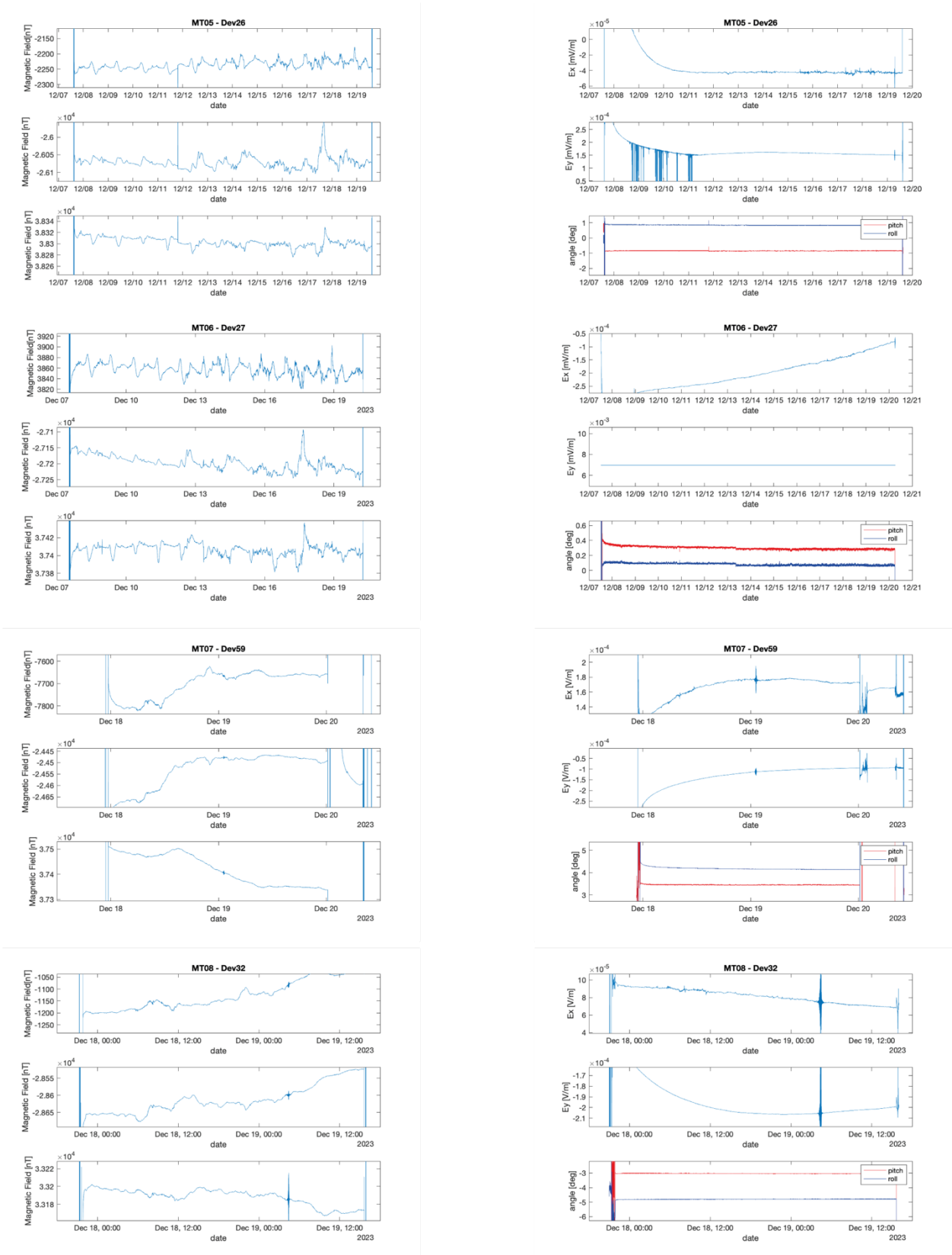

Fig. 12.1.2 OBEM Raw data stations 5 to 8, showing the recorded 3 component magnetic fields, 2 horizontal component electric fields and pitch and roll variations.

12.2 Details on Recorded Video-CTD Files

Table 12.2.1 Details of recorded Video-CTD files.

Video file ID	Duration	UTC of start	UTC of stop	Comment 1	Comment 2
11	0:11:34	17.12.2023 07:59	17.12.2023 08:10	VCTD1 recording start	transect 1
12	0:11:25	17.12.2023 08:10	17.12.2023 08:21		transect 1
13	0:11:23	17.12.2023 08:21	17.12.2023 08:33		transect 1
14	0:11:23	17.12.2023 08:33	17.12.2023 08:44	Egion fault cliff	transect 1
15	0:11:23	17.12.2023 08:44	17.12.2023 08:56		transect 1
16	0:09:48	17.12.2023 08:56	17.12.2023 09:06		transect 1
17	0:11:35	17.12.2023 09:22	17.12.2023 09:33		transect 1
18	0:05:26	17.12.2023 09:33	17.12.2023 09:38	VCTD1 recording stop	transect 1
19	0:10:23	17.12.2023 10:25	17.12.2023 10:35	bottom contact due to delayed streaming	transect 2 terminated
20	0:09:59	17.12.2023 13:37	17.12.2023 13:47	VCTD2 recording start	transect 2
21	0:11:35	17.12.2023 14:13	17.12.2023 14:27		transect 2
22	0:01:54	17.12.2023 14:27	17.12.2023 14:28	VCTD2 recording stop	transect 2
23	0:11:29	17.12.2023 16:20	17.12.2023 16:31	VCTD3 recording start	hydrocast 3
24	0:11:29	17.12.2023 16:31	17.12.2023 16:42	Egion fault pockmark	hydrocast 3
25	0:11:23	17.12.2023 16:42	17.12.2023 16:54		hydrocast 3
26	0:11:23	17.12.2023 16:54	17.12.2023 17:05		hydrocast 3
27	0:00:44	17.12.2023 17:05	17.12.2023 17:06	VCTD3 recording stop	hydrocast 3

12.3 Details on Sediment Cores

GC 1 - Eastern GoC

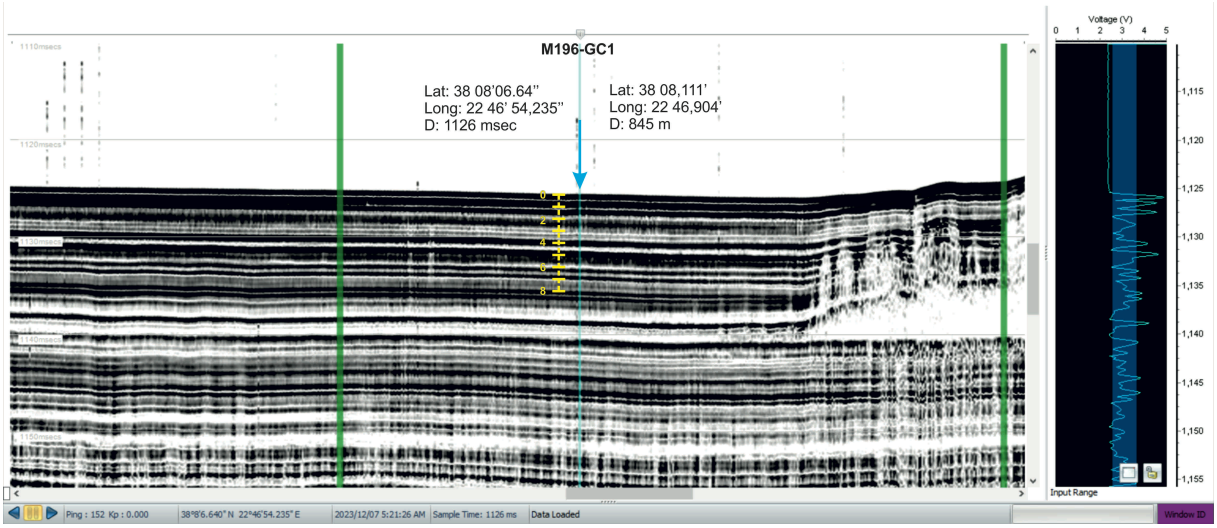

Fig. 12.3.1 GC 1 location of GC1 on a parasound profile in the eastern part of the basin

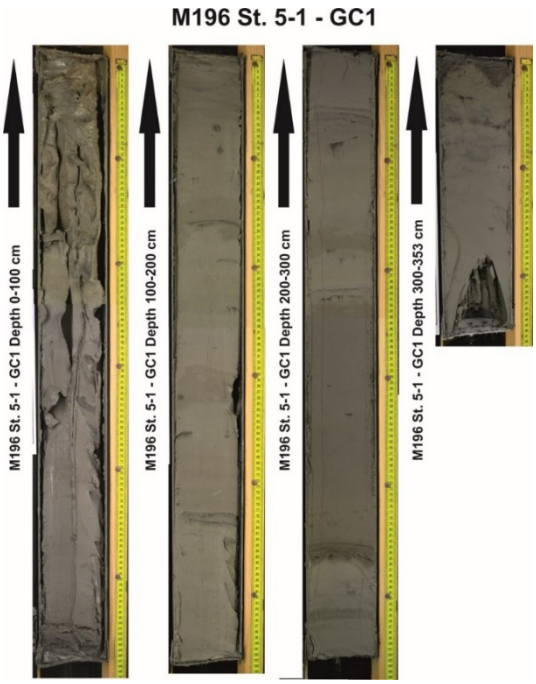

Fig. 12.3.2 Photographs of sediment sections of GC 1.

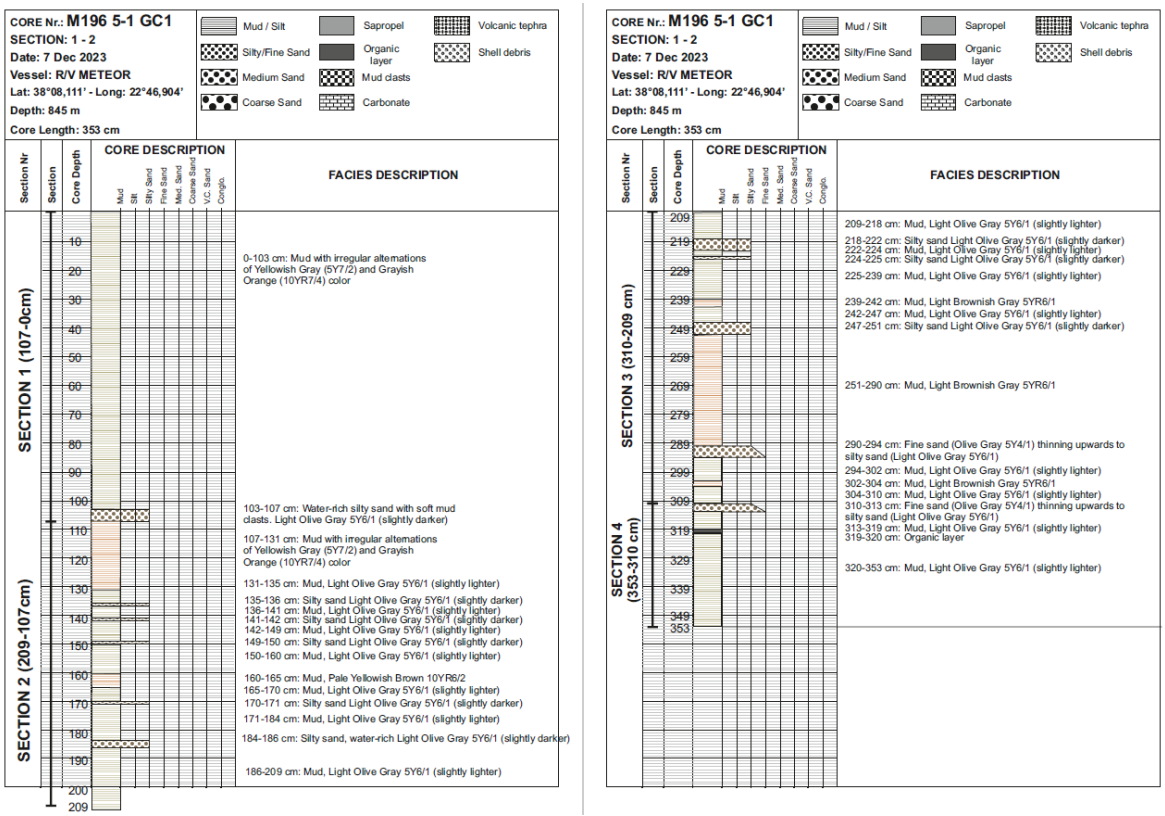

Fig. 12.3.3 Sedimentological description of GC 1.

GC 2 and GC 3 - Central to Western Part of GoC, North of Akrata

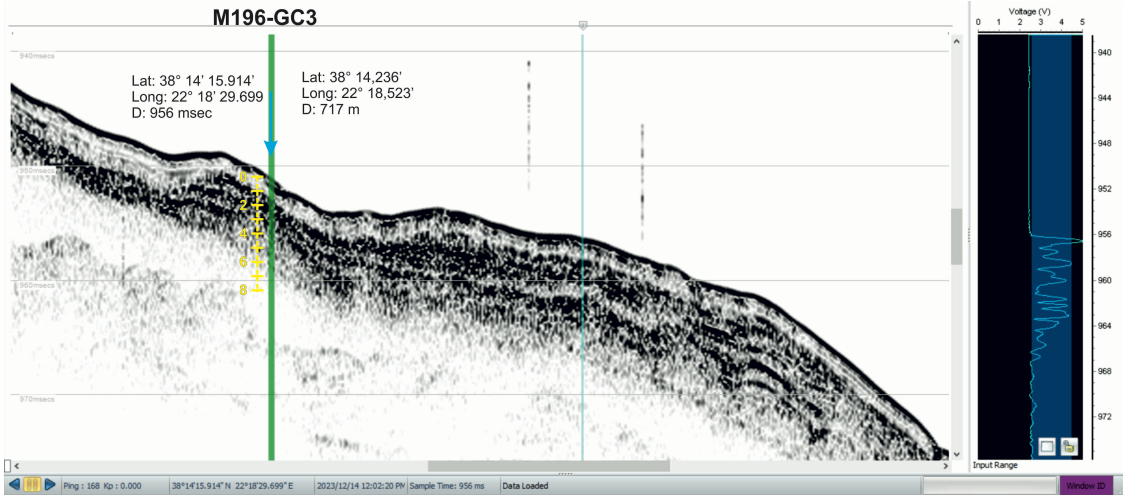

Fig. 12.3.4 GC 3 location on a parasound profile, in the western part of the basin.

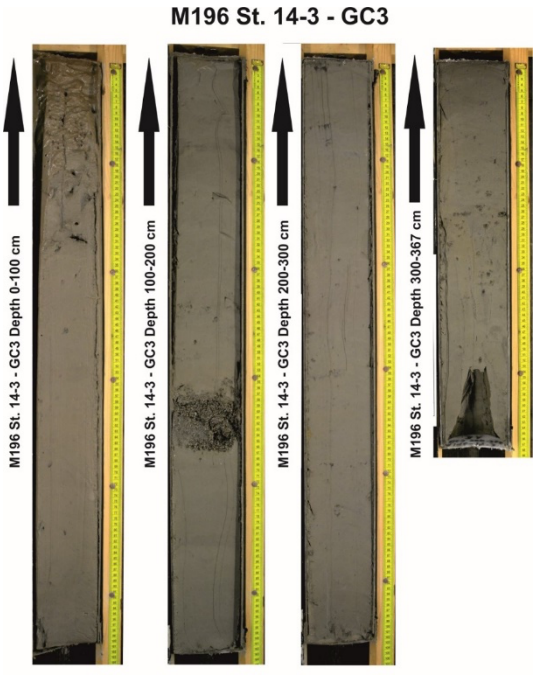

Fig. 12.3.5 Photographs of sediment sections of GC 3.

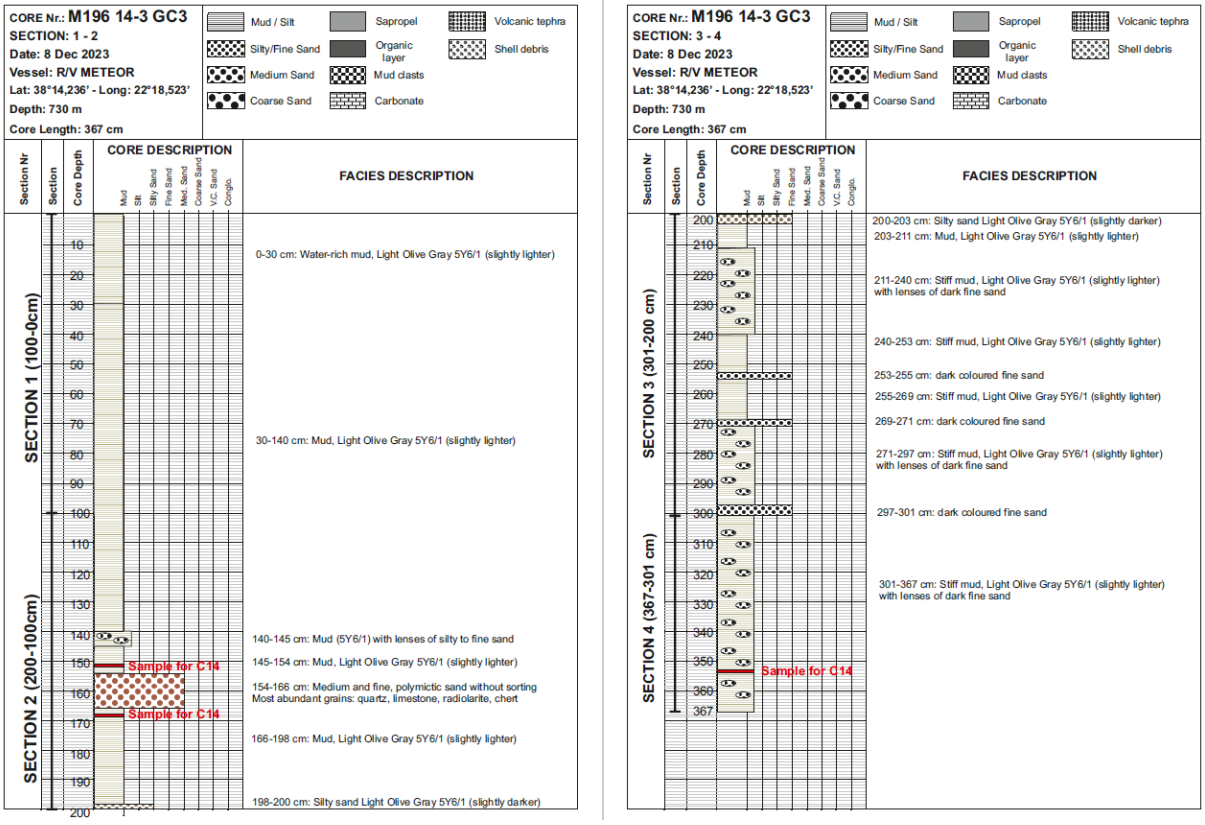

Fig. 12.3.6 Sedimentological description of GC 3.

GC 4 - Eastern GoC, Between M0078 and M0079

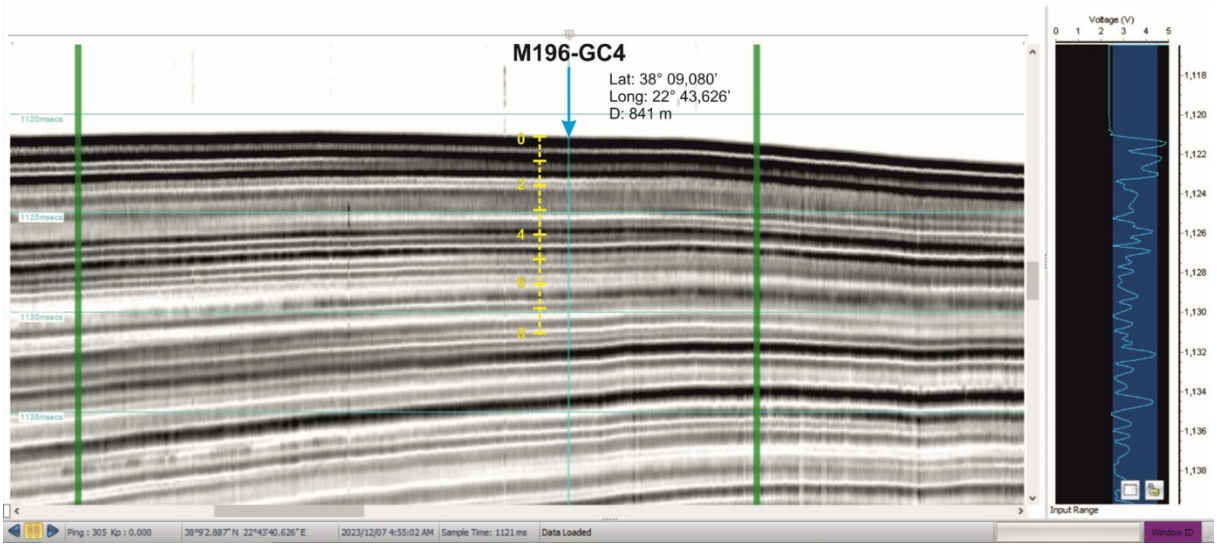

Fig. 12.3.7 Parasound profile in the area of GC4.

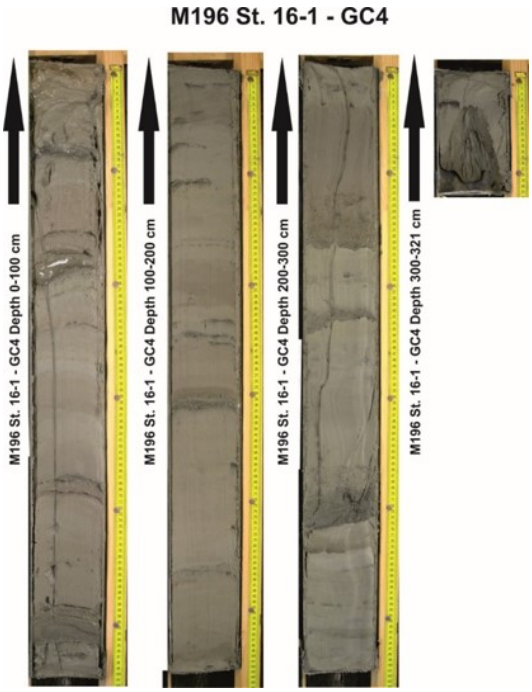

Fig. 12.3.8 Photographs of sediment sections of GC 4.

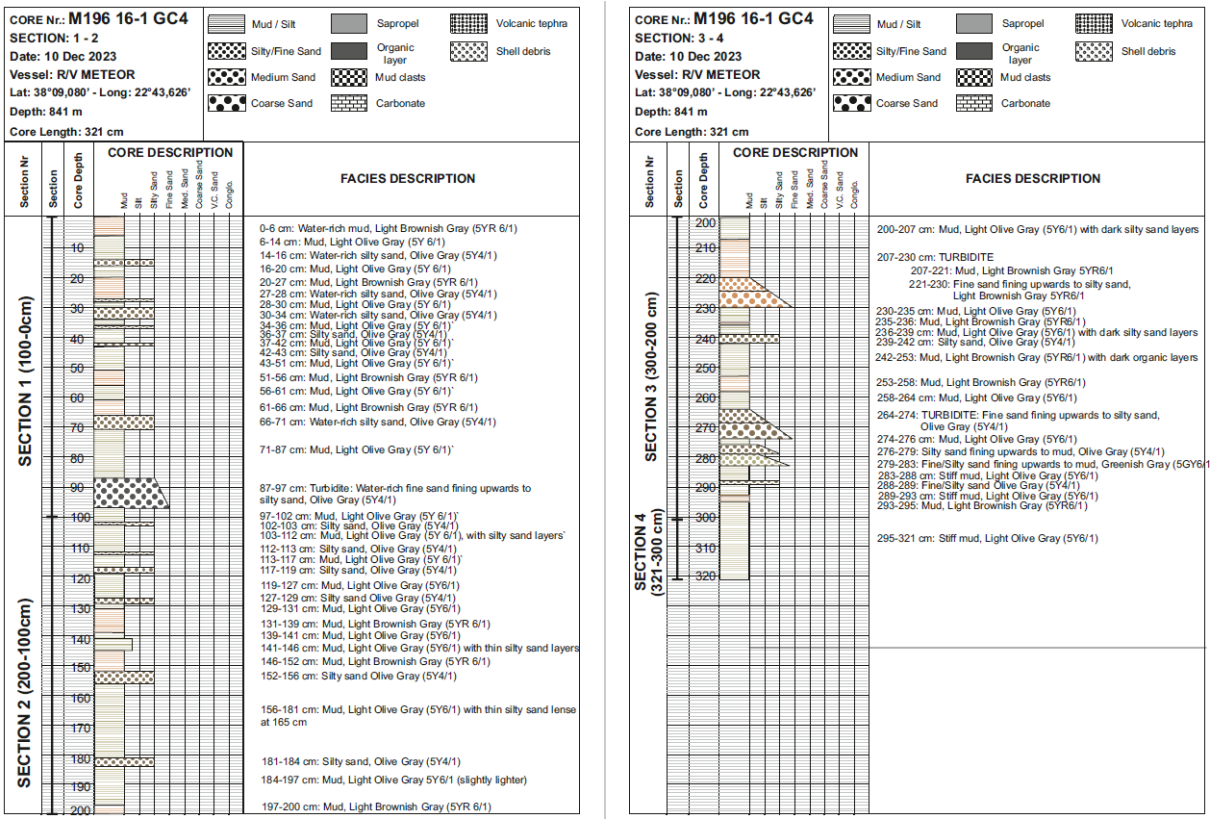

Fig. 12.3.9 Sedimentological description of GC 4.

GC 5 - Bay of Antikyra

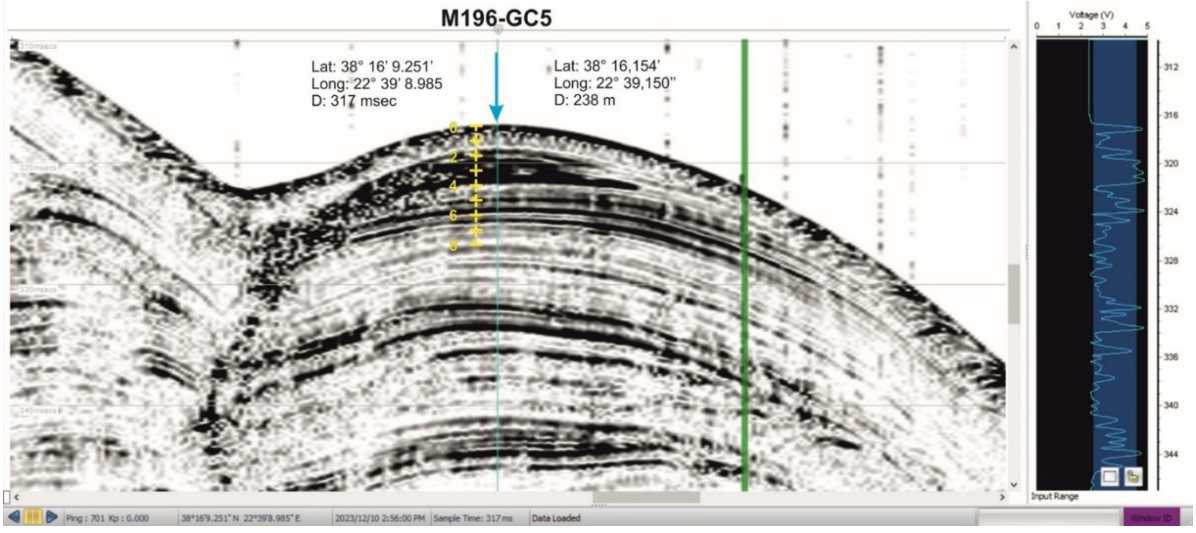

Fig. 12.3.10 Parasound profile in the area of GC 5.

Fig. 12.3.11 Photographs of sediment sections of GC 5.

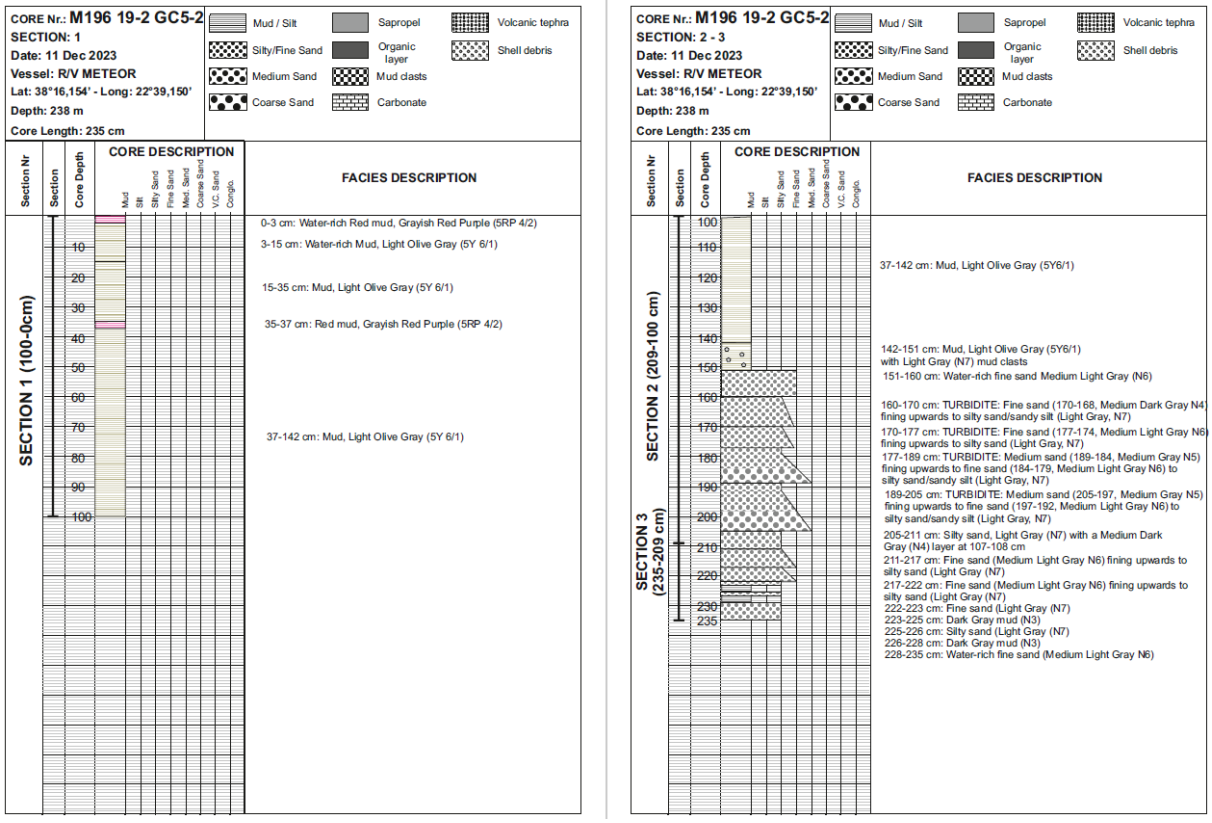

Fig. 12.3.12 Sedimentological description of GC 5.

GC 6 - West of M0079

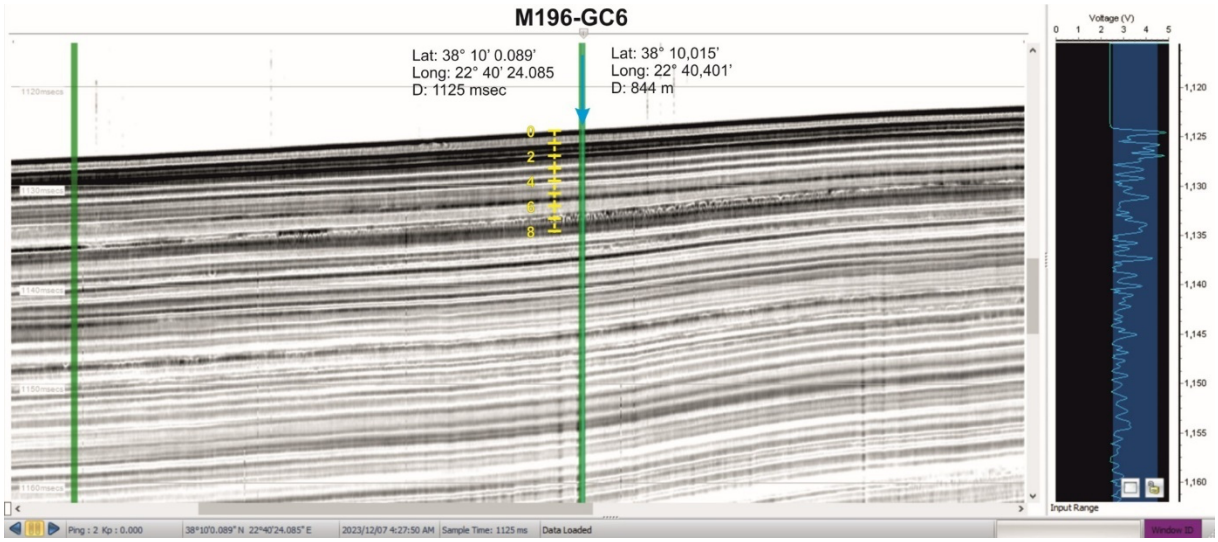

Fig. 12.3.13 Parasound profile along GC6.

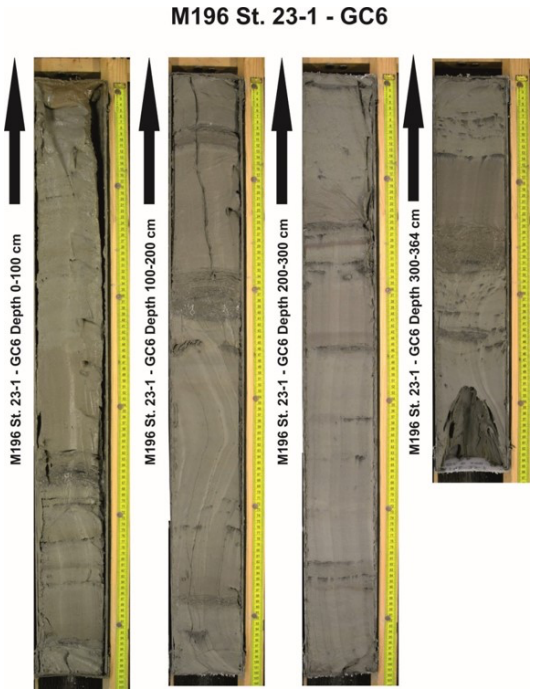

Fig. 12.3.14 Photographs of sediment sections of GC 6.

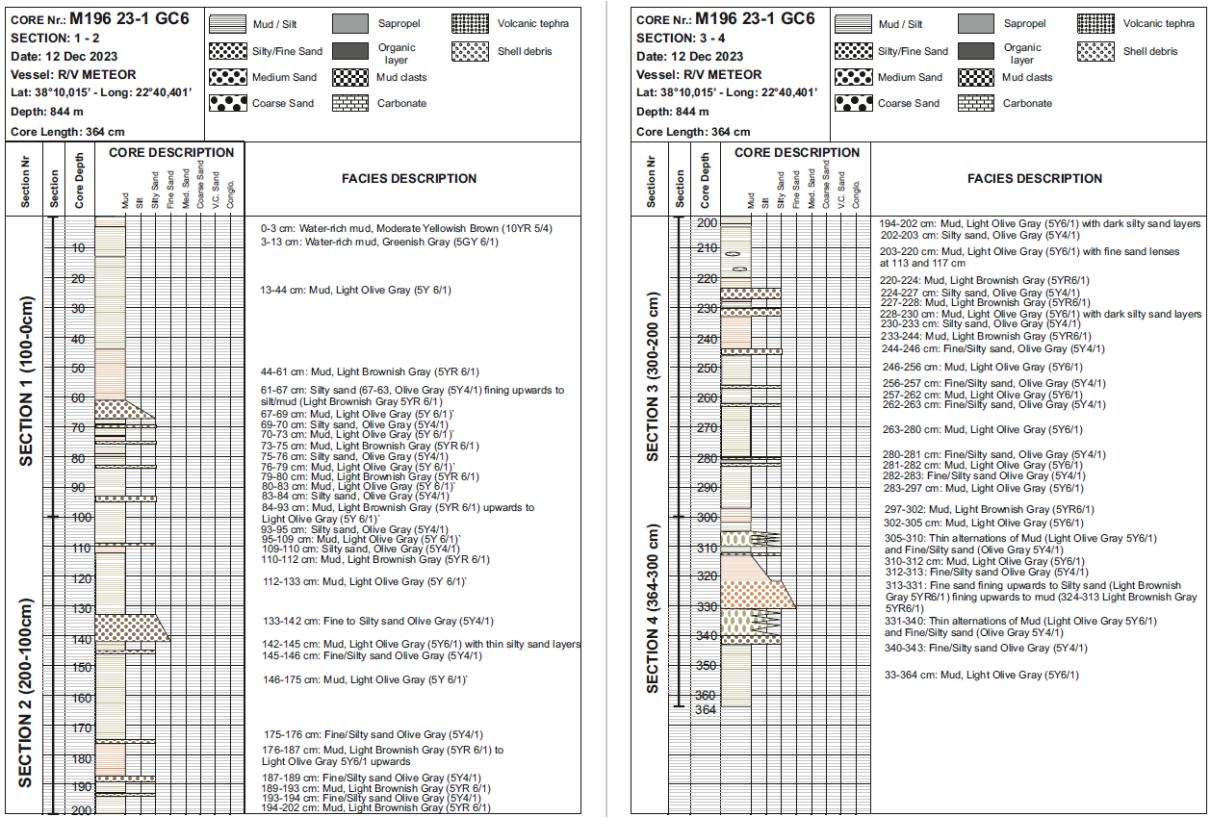

Fig. 12.3.15 Sedimentological description of GC 6.

GC 7 - Bay of Itea

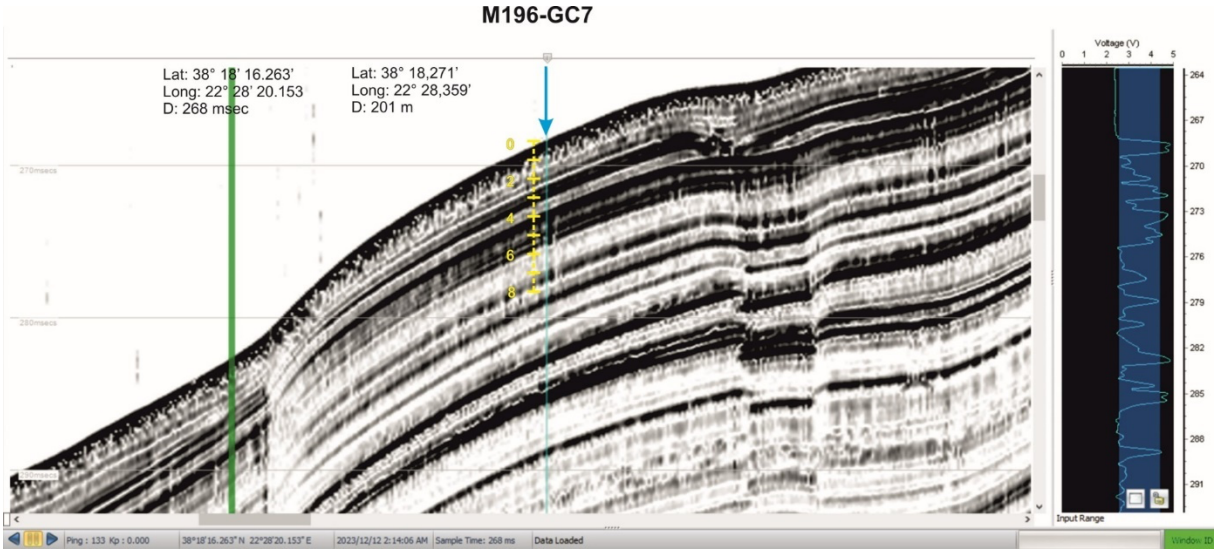

Fig. 12.3.16 Parasound profile along GC7.

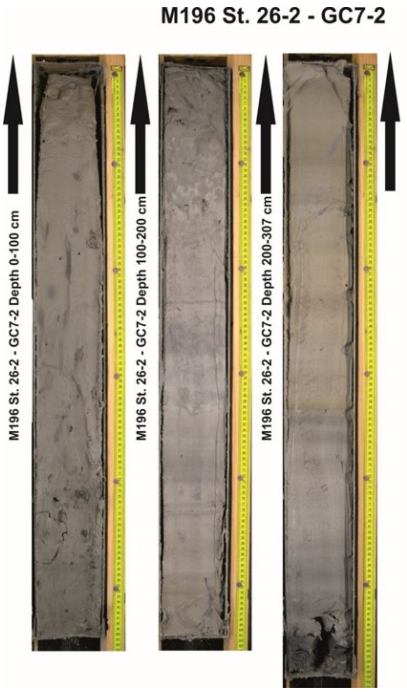

Fig. 12.3.17 Photographs of sediment sections of GC 7.

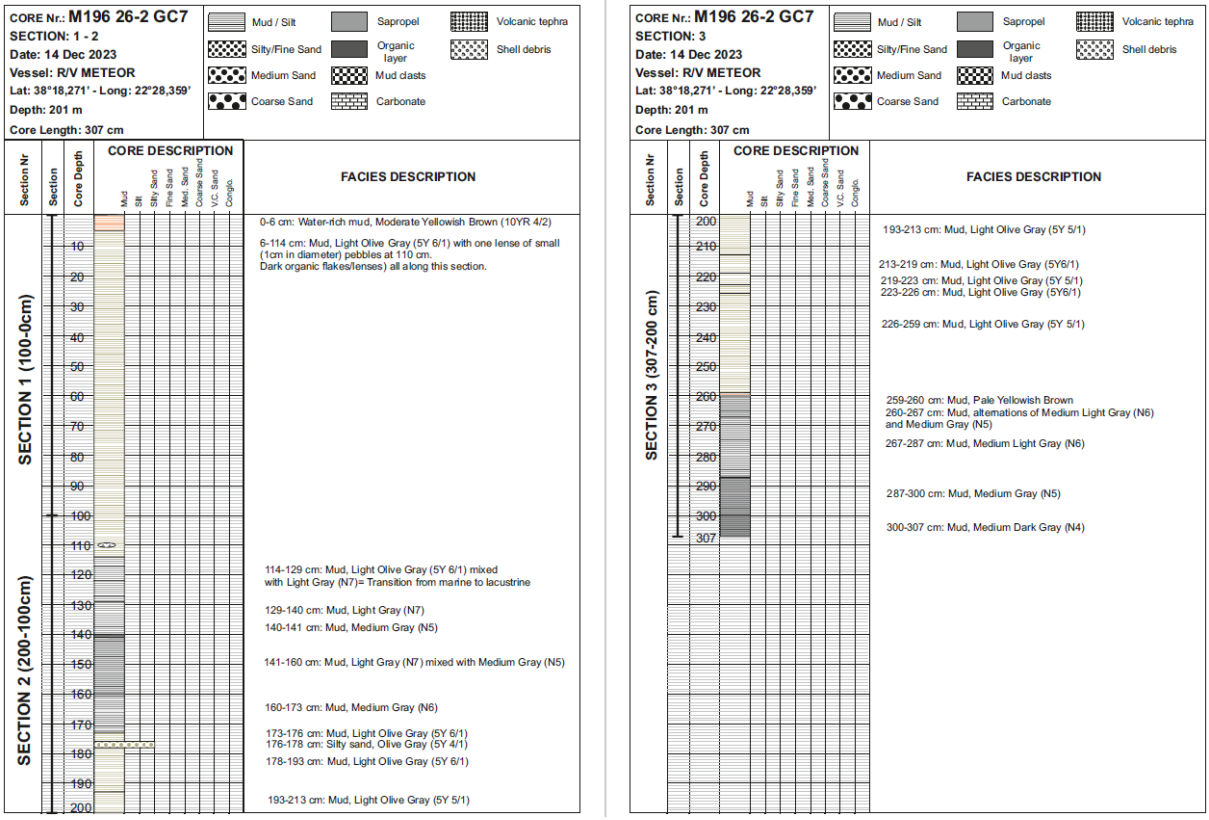

Fig. 12.3.18 Sedimentological description of GC 7.

GC 8 – Circular Depression at Bay of Itea

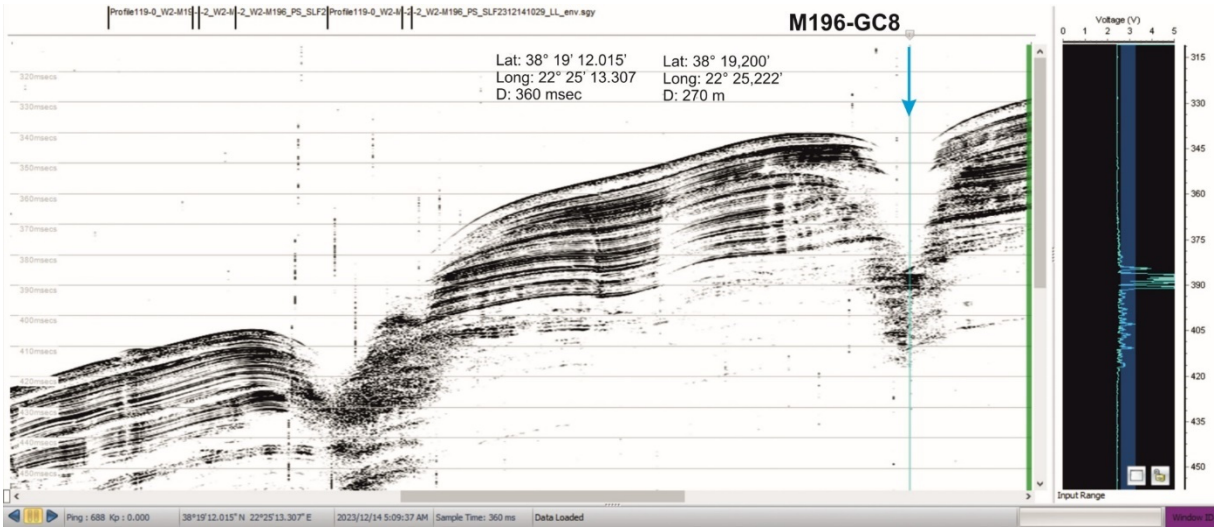

Fig. 12.3.19 Parasound profile along GC8.

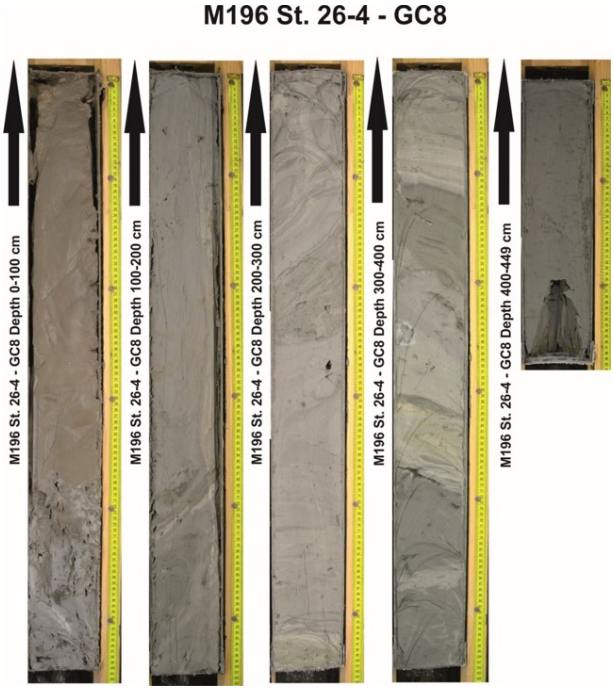

Fig. 12.3.20 Photographs of sediment sections of GC8.

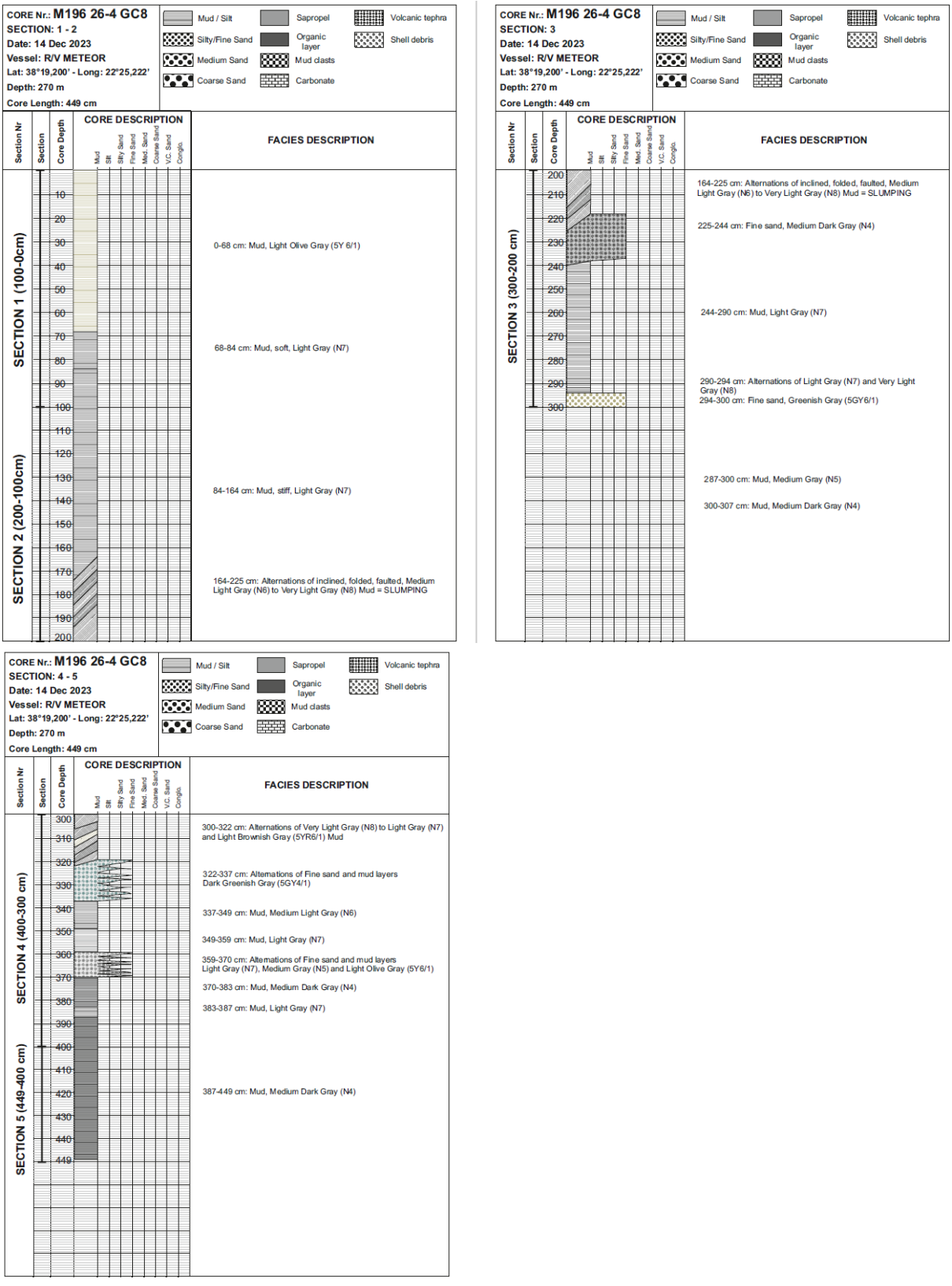

Fig. 12.3.21 Sedimentological description of GC 8.

GC 9 Central GoC

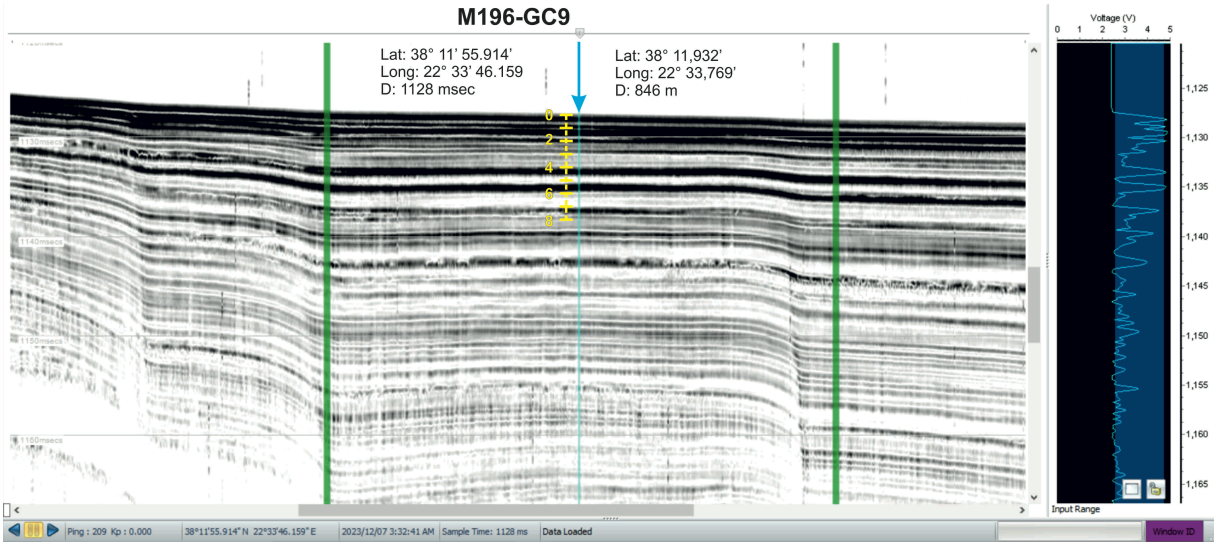

Fig. 12.3.22 Parasound profile along GC9.

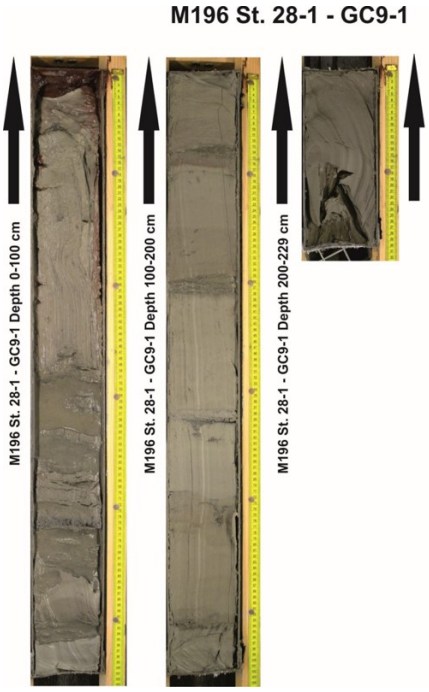

Fig. 12.3.23 Photographs of sediment sections of GC9.

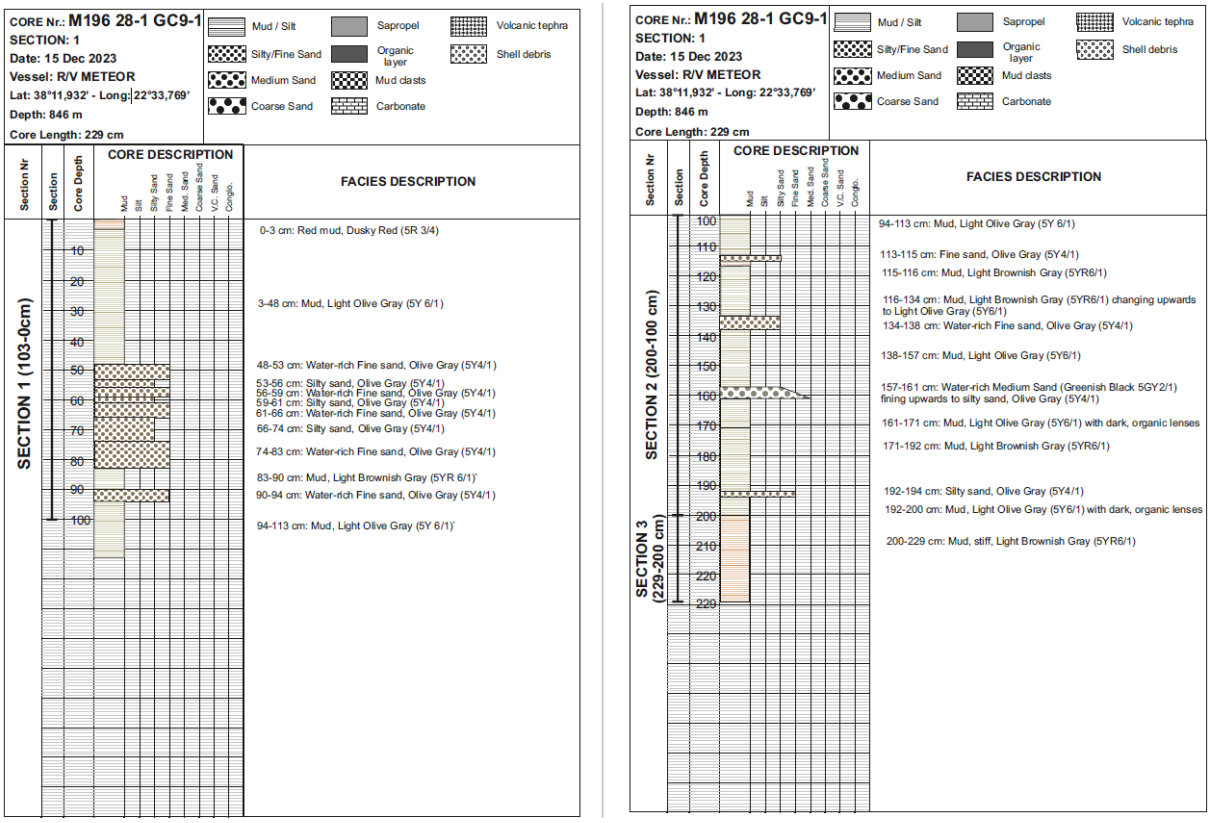

Fig. 12.3.24 Sedimentological description of GC 9

GC 10 Central GoC, the Western End of CSEM Line 1

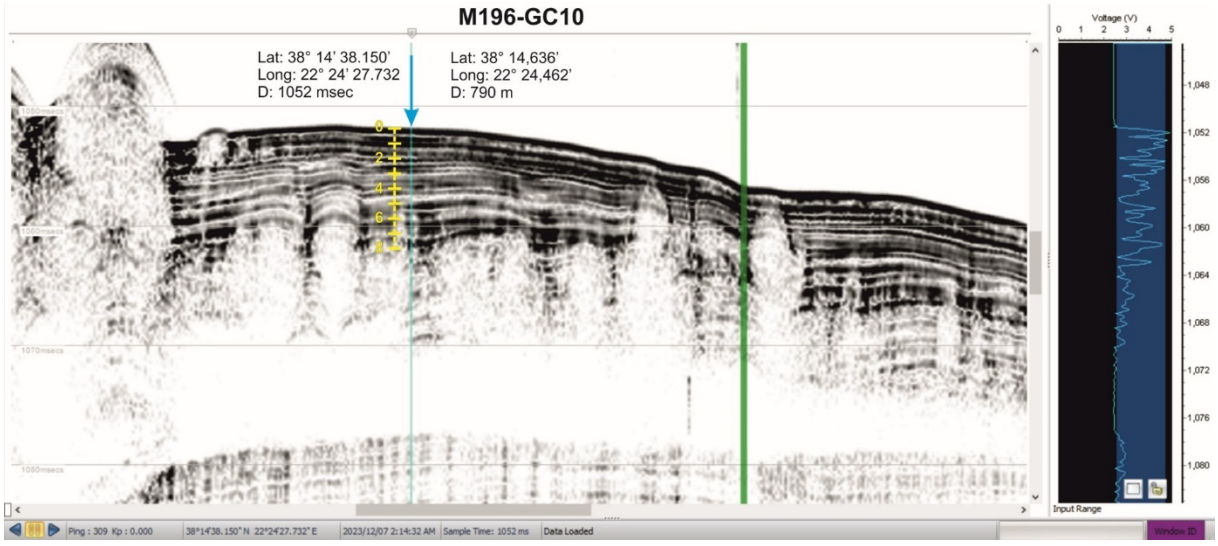

Fig. 12.3.25 Parasound profile along GC10.

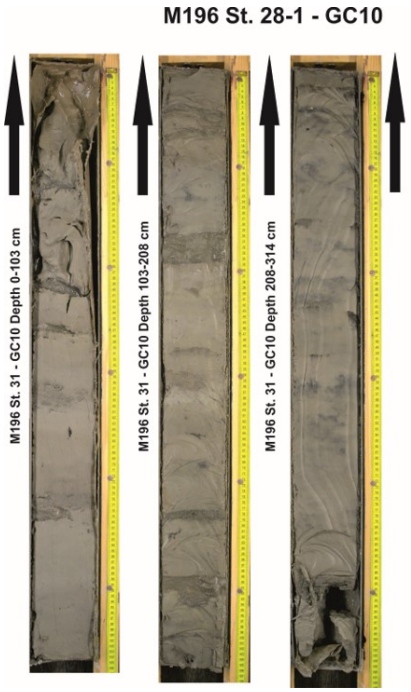

Fig. 12.3.26 Photographs of sediment sections of GC10.

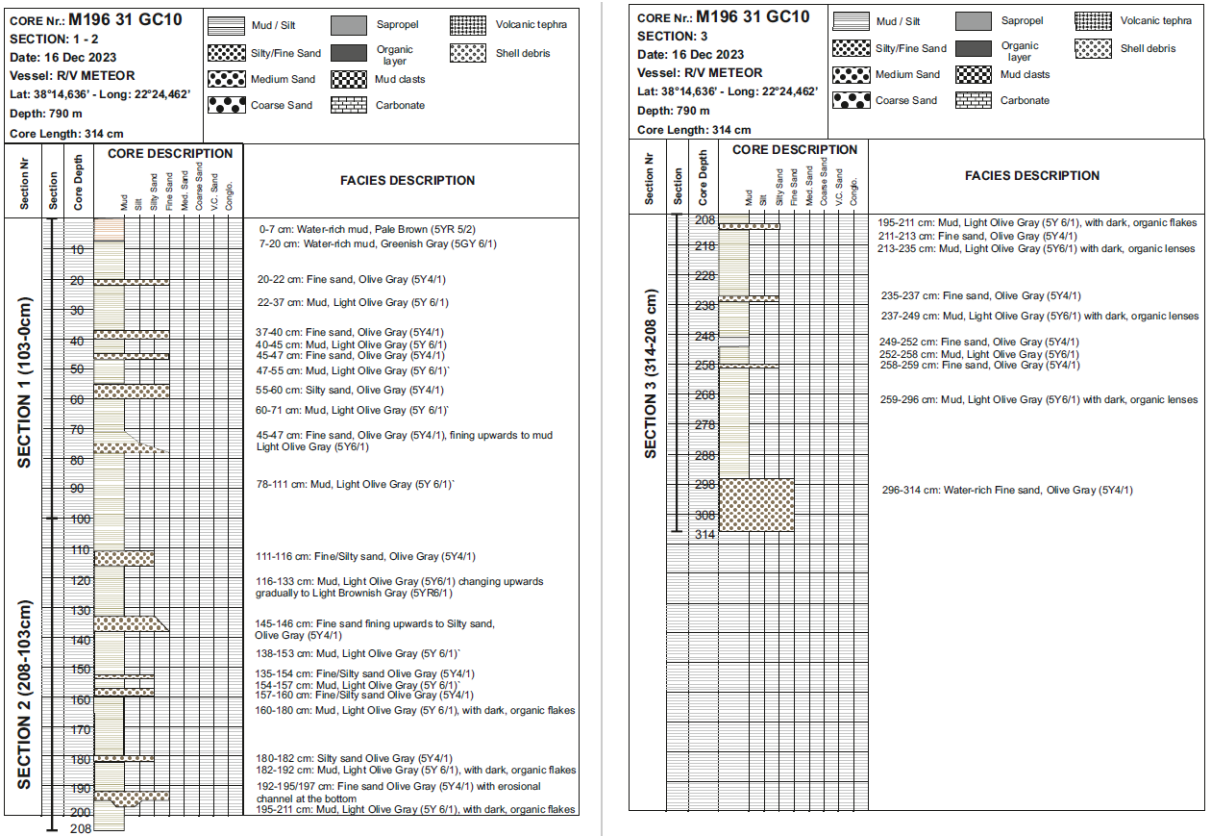

Fig. 12.3.27 Sedimentological description of GC 10.

GC 11 South of M0079

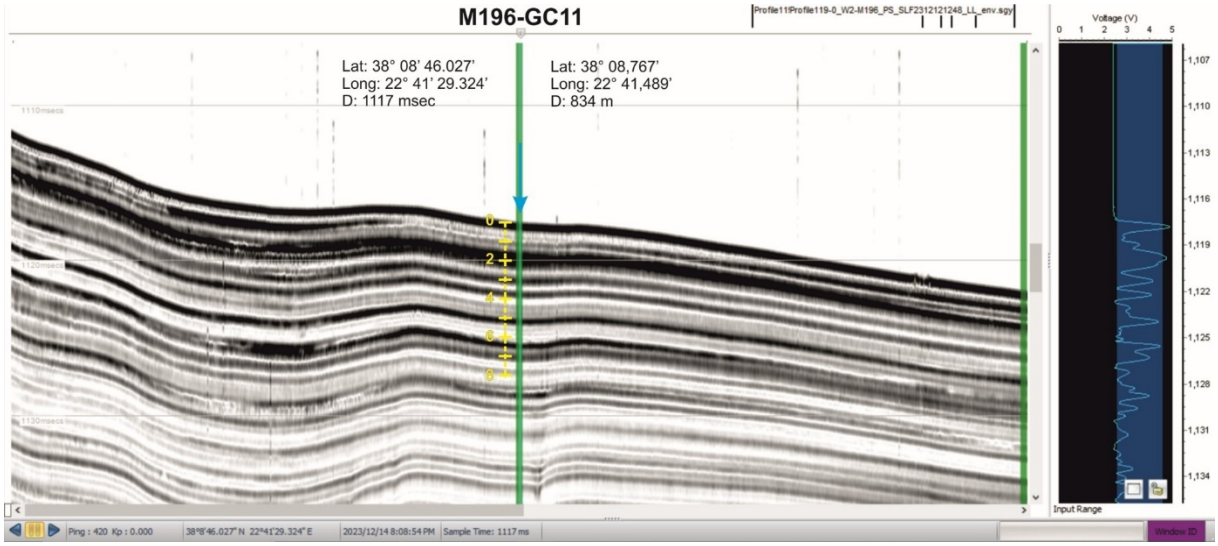

Fig. 12.3.28 Parasound profile along GC11.

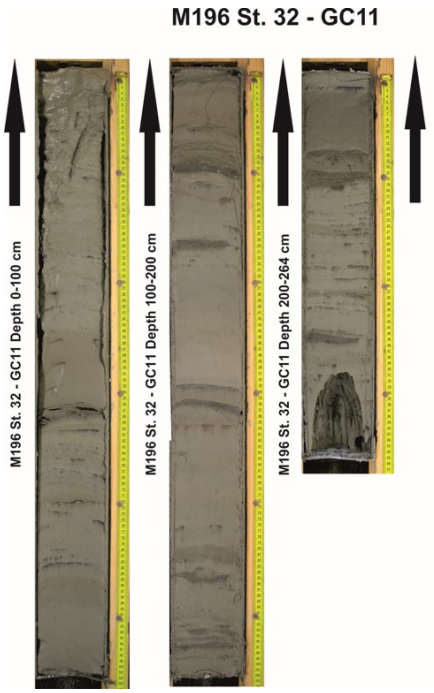

Fig. 12.3.29 Photograph of sediment sections of GC11.

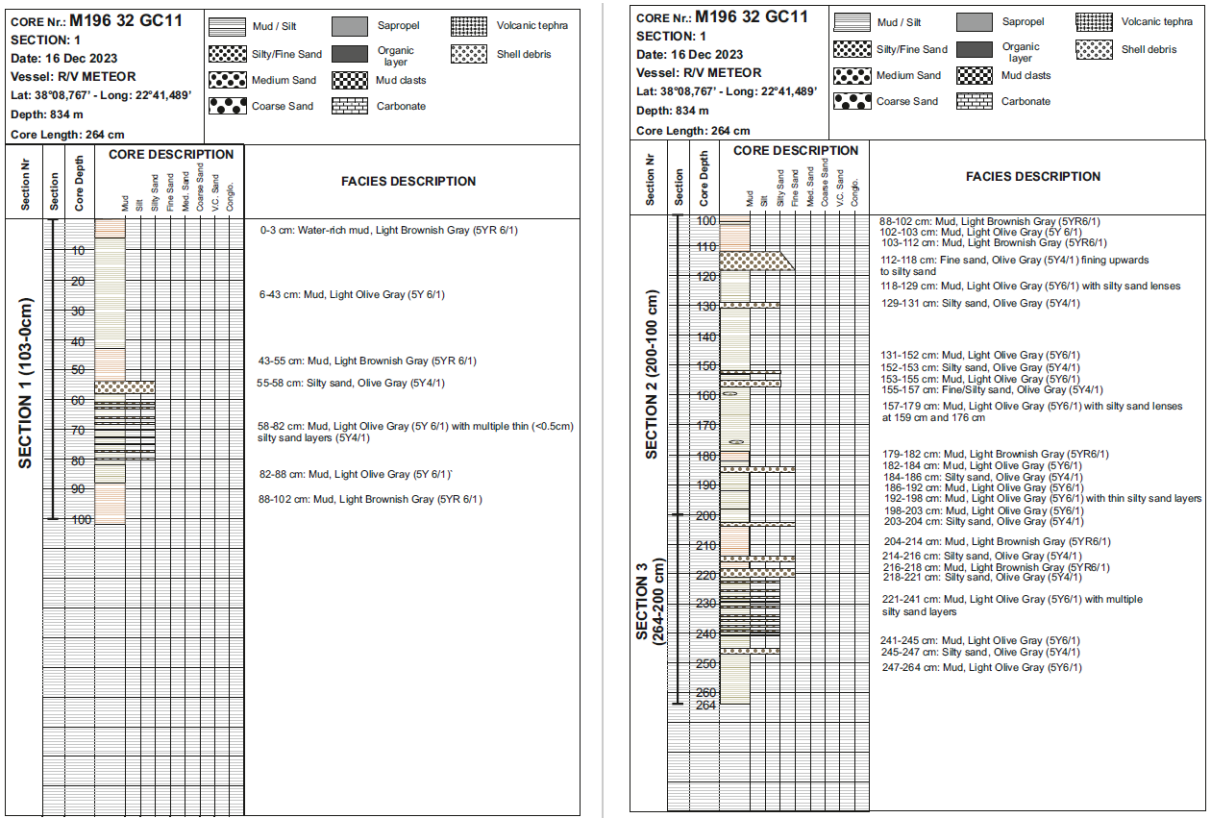

Fig. 12.3.30 Sedimentological description of GC 11.

GC 12 North of M0078

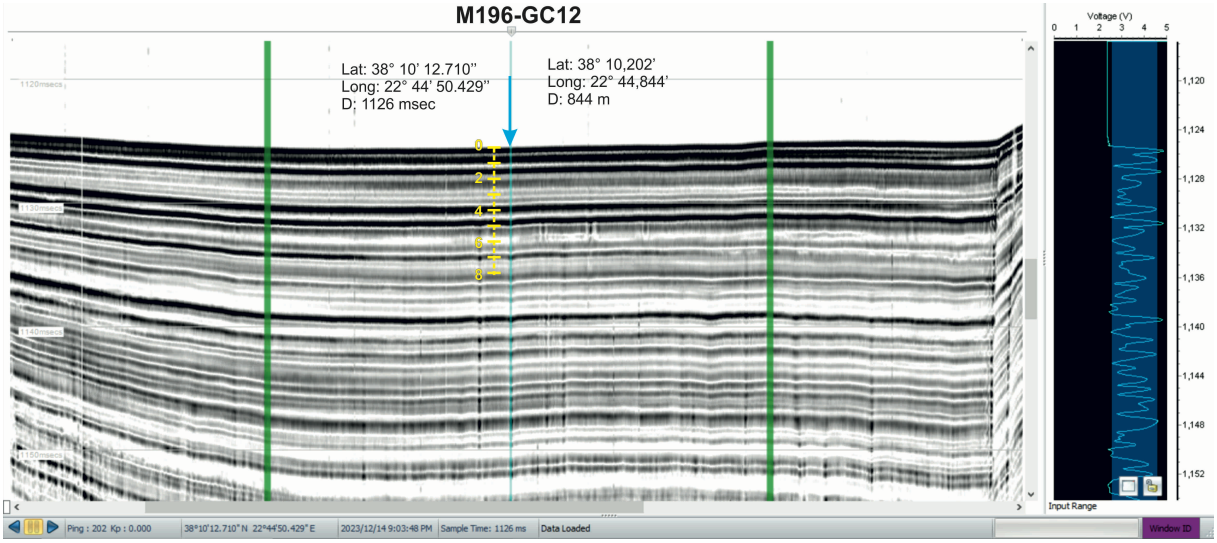

Fig. 12.3.31 Parasound profile along GC11.

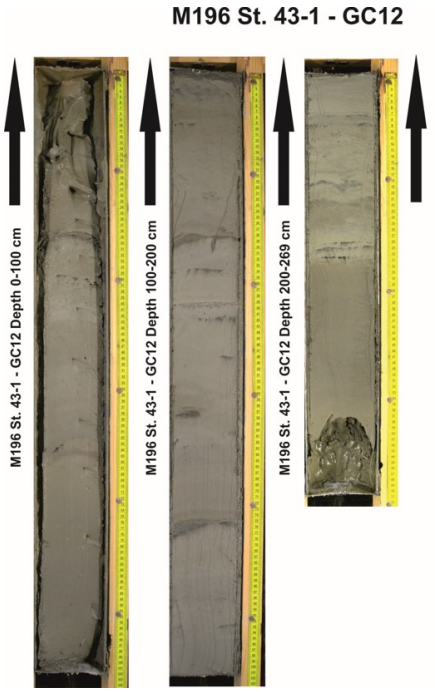

Fig. 12.3.32 Photographs of sediment sections of GC12.

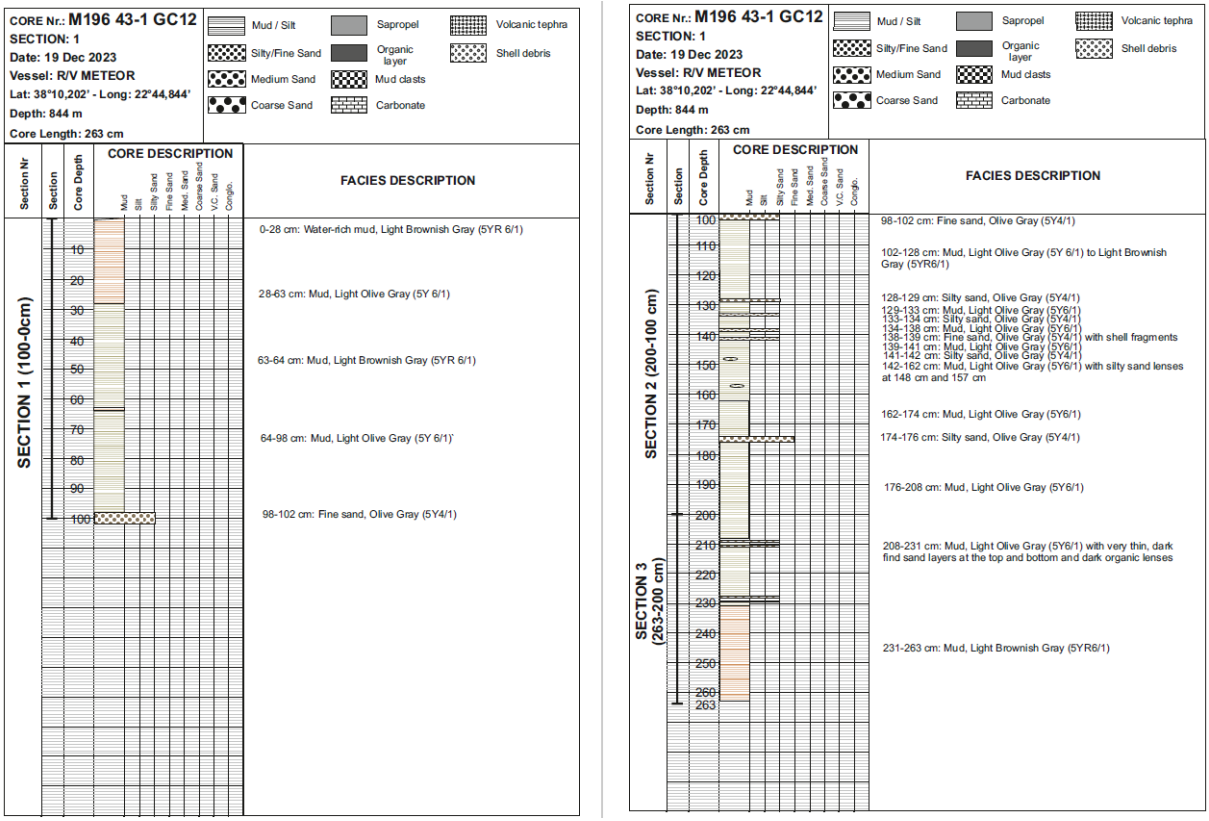

Fig. 12.3.33 Sedimentological description of GC12.

GC 13 South to the Center of M0078/ M0079

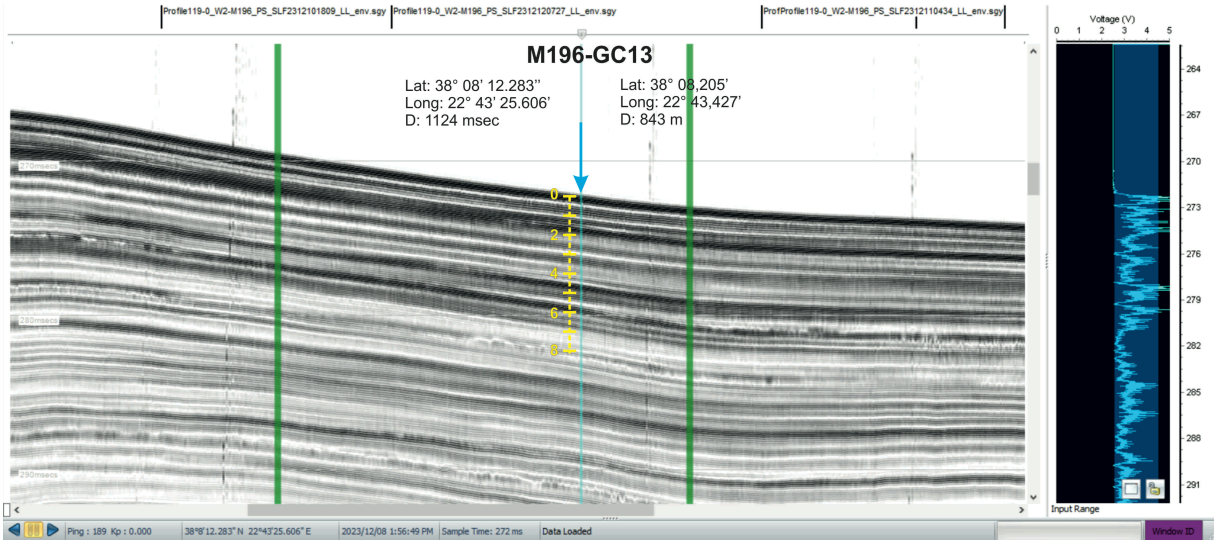

Fig. 12.3.34 Parasound profile along GC13.

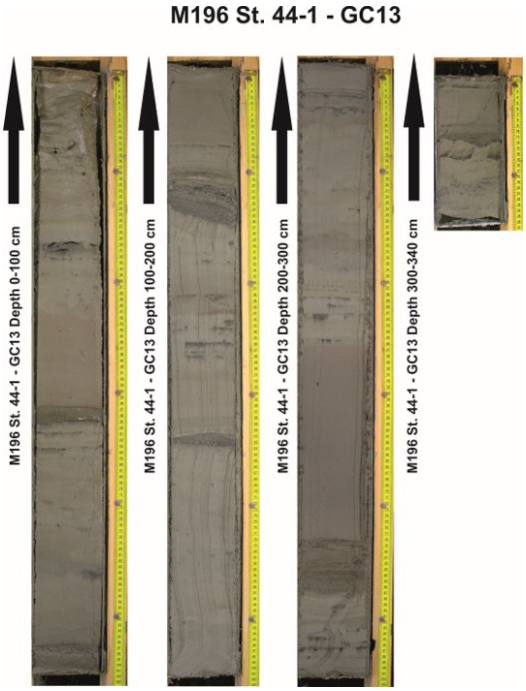

Fig. 12.3.35 Photographs of sediment sections of GC13.

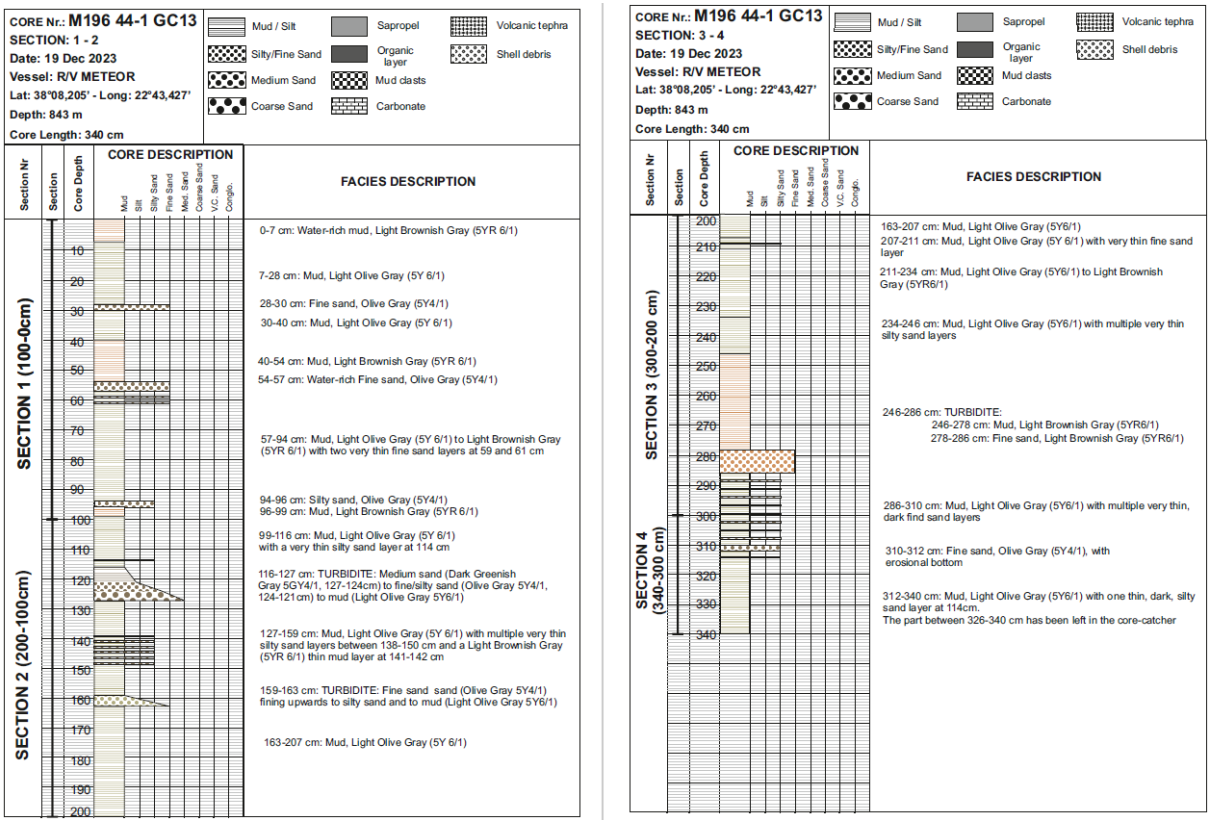

Fig. 12.3.36 Sedimentological description of GC12.

12.4 Selected Pictures and Videos of Shipboard Operations

On M196, professional videos were recorded by the film maker Hannes Schuler. 13 episodes of 3 min to 5 min lengths have been cut together from the material, featuring episodes on our scientific goals, on marine data acquisition with various methods and other activities on the ship. The videos are published on GEOMAR's youtube channel (Link to First Episode).

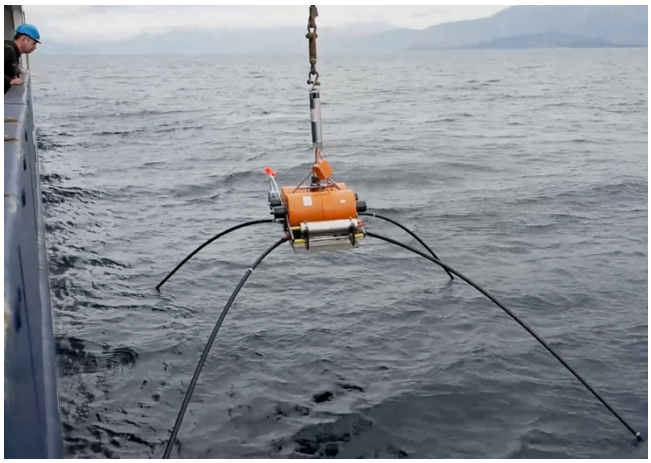

Fig. 12.4.1 Deployment of OBEM station

Fig. 12.4.2 Investigation of gravity core

Fig. 12.4.3 Deployment of the head of CSEM streamer

Fig. 12.4.4 Deployment of gravity core